Development of a combined In-Cell ELISA and flow cytometry method for quantification of uptake of PEGylated nanoparticles by Raw264.7 and HepG2 cells

EVELINA FOLKESSON

MASTER'S DEGREE PROJECT, 30 CREDITS
APPLIED BIOCHEMISTRY
DEPARTMENT OF PURE AND APPLIED BIOCHEMISTRY | LUNDS TEKNISKA HÖGSKOLA

LUNDS UNIVERSITET
Lunds Tekniska Högskola

Supervisors:

Dr. Sania Bäckström
Spago Nanomedical AB

Dr. Tove Sivik
Spago Nanomedical AB

Prof. Anette Gjörloff Wingren
Malmö University

September 2016

Table of contents

Abstract

Cancer is one of today's most common causes of human mortality. For long, chemotherapeutics has been a conventional treatment of the disease, but due to its low precision and high frequency of side effects, this treatment has been highly debated. Nanosized particles, so called nanoparticles (NPs), have emerged as a promising tool for cancer treatment, due to their ability of selectively reaching tumor sites. Developing biocompatible NPs has turned out to be challenging, due to the particles' tendency of interacting with proteins and immune cells present throughout the blood, interactions further leading to removal of the NPs from the bloodstream. This removal strongly reduces the circulation half-life of NPs in the blood, something that in turn reduces the therapeutic efficacy of the particles. Coating of NPs is often used as a tool for increasing the half-life of the particles in the blood. By attaching coating molecules to the surface of the NPs, protein interaction and subsequent removal of the particles from the bloodstream can be reduced. Polyethylene glycol (PEG) is one of the most common polymers used for coating of NPs.

The main goal of this project was to study whether coating degree and PEG length of NPs had an impact on the uptake of these particles by Raw264.7 (macrophage cell line) and HepG2 (hepatocyte cell line) cells. To study the impact of coating on cellular uptake, organosilicophosphonate core NPs were coated with PEG of three different lengths, each at two different coating degrees. The coated NPs were characterized with respect to size, pH, charge, coating degree and tendency to aggregate in culture media. Analytical techniques such as gel permeation chromatography (GPC), dynamic light scattering (DLS), zeta potential measurements and inductively coupled plasma optical emission spectroscopy (ICP-OES) were used for characterization of the particles. Uptake of PEG coated as well as bare NPs by Raw264.7 and HepG2 cells was quantified by developing and using a combined method constituting In-Cell enzyme-linked immunosorbent assay (In-Cell ELISA), ELISA and flow cytometry. Finally, the intracellular distribution of NPs in Raw264.7 cells was studied using fluorescence microscopy. Indicatively, coating degree as well as PEG length had an impact on the cellular uptake of NPs. NPs coated with long-length PEG showed a lower uptake, compared to NPs coated with short-length PEG. In addition, NPs coated with a high amount of PEG showed a lower uptake than NPs coated with a low amount of PEG. Preliminary indications of differences in intracellular distribution of PEG coated NPs in Raw264.7 cells were seen.

List of abbreviations

BSA	Bovine serum albumin
Ca	Calcium
CA	Contrast agent
CC	Control coating
DAPI	4’,6-diamidino-2-phenylindole
d_H	Hydrodynamic diameter
DLS	Dynamic light scattering
DMEM	Dulbecco’s modified eagle medium
EE	Early endosome
ELISA	Enzyme-linked immunosorbent assay
ELSD	Evaporative light scattering detector
EPR	Enhanced permeability and retention
FACS	Fluorescence-activated cell sorting
FBS	Fetal bovine serum
FDA	Food and drug administration
FITC	Fluorescein isothiocyanate
FL	Fluorescence
FSC	Forward scatter
GPC	Gel permeation chromatography
HRP	Horseradish peroxidase
ICE	In-Cell ELISA
ICP-OES	Inductively coupled plasma optical emission spectroscopy
LE	Late endosome
LOQ	Limit of quantification
Mn	Manganese
MPS	Mononuclear phagocyte system
MQ	Milli-Q
MRI	Magnetic resonance imaging
NFF	Normal flow filtration

NPs	Nanoparticles
P	Phosphorus
PBS	Phosphate buffered saline
PEG	Polyethylene glycol
PEG6-9	mPEG6-9-trimethoxysilane
PEG21	mPEG21-triethoxysilane
PEG44	mPEG44-triethoxysilane
R_H	Hydrodynamic radius
RPMI	Roswell Park Memorial Institute
Si	Silicon
SOP	Standard operational procedure
SSC	Side scatter
$t_{1/2}$	Circulation half-life
TMB	3,3',5,5'-Tetramethylbenzidine
TFF	Tangential flow filtration
WHO	World Health Organization
ζ	Zeta potential

1. INTRODUCTION

1.1 Nanoparticles as a tool for cancer diagnosis and therapy

Cancer is one of the biggest threats against human health and it remains one of the most common causes of human mortality. According to the World Health Organization (WHO) 13% of global deaths in 2012 were attributed to cancer and worldwide incidences of cancer are expected to increase by 70% within the next two decades [1]. For many years chemotherapeutics has been a conventional treatment of cancer, with elimination of malignant cells as its primary purpose. With this cancer treatment, tumor elimination efficacy is high, but the precision of the treatment is low and side effects are frequent [2]. Due to its lack of selectivity, the systemic exposure is high and therefore doses have to be limited in order to avoid toxic side effects. Restricting the doses, however, limits the therapeutic effects that are needed in order to treat the cancer. To overcome problems with lack of selectivity, researchers worldwide are searching for treatments that selectively target the cancer cells, without affecting the surrounding healthy tissue. The possibility of using nanosized particles, so called nanoparticles (NPs), as the mediator of such a selective targeting is a major goal and is currently under intense investigation. Due to the unique properties of the NPs and to the ease by which they can be precisely engineered, these particles can be used for both active and passive targeting of a broad range of diseases [4]. Interestingly, by conjugating drugs to NPs, circulation half-life and *in vivo* stability of the drugs can be increased [3].

1.1.1 Different types of nanoparticles

The development of a broad range of NPs has provided a significant resource for nanomedicine, with NP applications ranging from drug delivery to diagnosis [5]. Broadly speaking, NPs are nanosized materials (1-100 nm), classified in any of the platforms organic, inorganic or hybrid NPs, of which organic NPs are the ones that have been the most thoroughly explored. Organic polymer systems, copolymers, dendrimers and lipid-based NPs (micelles and liposomes) all belong to the organic platform (see **a-c** in Figure 1.1) [5]. Particles commonly classified as inorganic NPs include quantum dots, silica and gold particles, as well as magnetic and carbon-based materials (see **d-h** in Figure 1.1) [5]. NPs of the inorganic platform can be engineered to express properties (e.g. conductivity, magnetism) that are not possible with NPs from the organic platform. Hybrid NPs are composed of both organic and inorganic components. Constructs such as magnetic NPs enclosed by liposomes exemplify such a hybrid material [5].

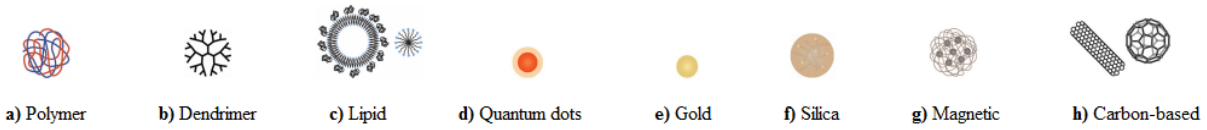

Figure 1.1. Different types of NPs belonging to the organic (**a-c**) and inorganic (**d-h**) platforms. **a)** Organic polymers (e.g. synthetic and natural polymers), **b)** Dendrimers, **c)** Lipid-based NPs, including liposomes (big) and micelles (small), **d)** Quantum dots, composed of semi conductive material, **e)** Gold particles, **f)** Silica particles, **g)** Magnetic particles, useful in magnetic resonance imaging (MRI) applications. **h)** Carbon-based particles. (Image modified from [5])

The company Spago Nanomedical AB, located in Lund, performs research and development of new polymeric nanomaterials; Spago Pix and Tumorad. Both materials are based on organosilicophosphonate core NPs which are coated with polyethylene glycol (PEG). The Spago Pix NPs are loaded with manganese (Mn) and have an intended use as a contrast agent (CA) for magnetic resonance imaging (MRI). The Tumorad particles are loaded with radionuclides and are intended to be used for radiotherapy. By using a clinically relevant animal model, studies on Spago Pix have demonstrated a selectively enhanced MR tumor contrast, which makes this CA a promising tool in the early detection of tumors [6].

1.1.2 The enhanced permeability and retention effect

One of the largest strengths of NPs is that they have the possibility to passively, yet selectively, target cancer sites [7]. This selective targeting is based on the characteristics of the environment close to the cancer tumor, an environment that arises due to the fast growth rate of the tumor. As a tumor grows in size, the formation of new blood vessels becomes essential in order for the tumor to be supplied with nutrients and oxygen. New blood vessels are formed, but due to imbalance between the factors responsible for this formation, the blood vessels become highly disorganized and leaky. This allows particles with a diameter of several hundreds of nm to leak out from the vessels (see Figure 1.2), whereas the corresponding leakage from vessels surrounding healthy tissues is restricted to particles with a diameter of 2-4 nm [3]. In this way, the particles selectively target the cancer tumor. At the tumor site, the lymphatic drainage is impaired (compared to healthy tissue which has well-functioning drainage) and this will lead to retention of NPs close to the tumor. This effect is called the enhanced permeability and retention (EPR) effect.

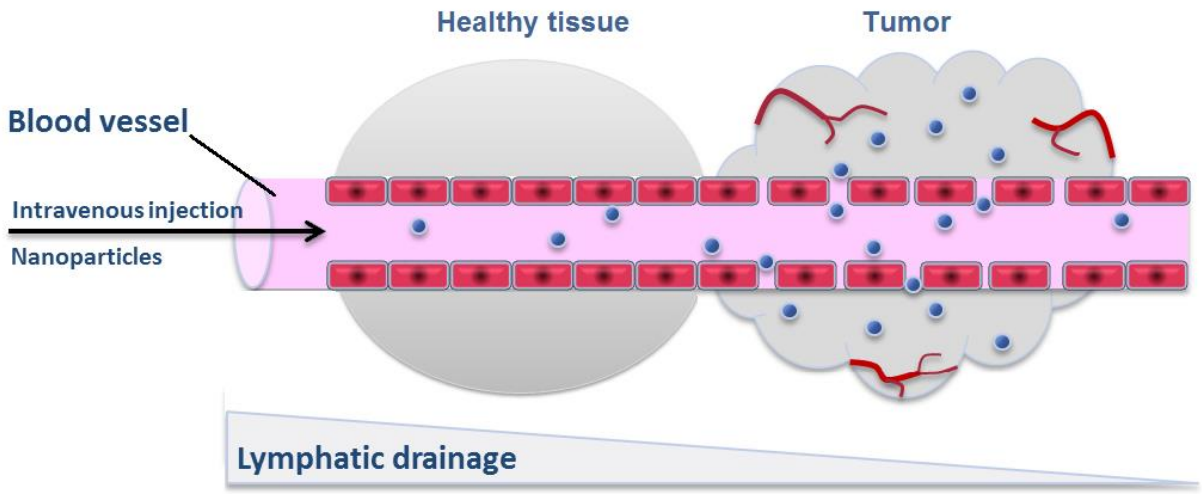

Figure 1.2. NPs accumulate at the tumor site through the EPR effect. Leaky vasculature close to the tumor and impaired lymphatic drainage enable this accumulation. (Image modified from [8])

1.2 Nanoparticle – protein interactions

Intravenous injection is the intended route of delivery for many NP drug candidates. In order to be safe and successful, these NPs have to be compatible with the blood, which contains a broad range of proteins. As NPs are injected into the blood they will encounter these proteins [9]. If the NPs are not bioinert, some of the proteins will be adsorbed onto their surface [10]. The adsorbed proteins are called opsonins and the process by which they are adsorbed is called opsonization (see Figure 1.3).

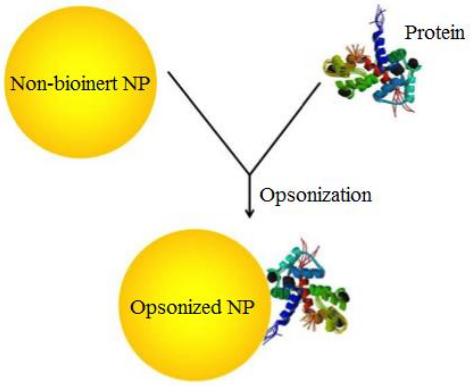

Figure 1.3. Proteins are adsorbed onto the surface of non-bioinert NPs through a process called opsonization. The proteins adsorbed onto the NPs are called opsonins. (Image modified from [11])

Opsonization starts immediately upon administration of non-bioinert NPs to the blood and is thought to occur through random Brownian motion of NPs and proteins [12]. Attractive forces such as van der Waals, electrostatic and ionic forces could possibly also be involved. For example, studies have demonstrated that charged NPs are opsonized faster and to a larger extent than neutral particles [10] and that different types of proteins are adsorbed onto the NPs depending on whether the particles are positively or negatively charged [12]. Opsonization has also been shown to be affected by the hydrophobicity of the NPs, with proteins generally being adsorbed faster onto hydrophobic, than onto hydrophilic NPs [12]. Size and curvature of the surface of the NPs are other factors that are believed to affect adsorption of proteins [12].

The proteins that are adsorbed onto the non-bioinert NPs will form a protein "corona", which is regarded as being composed of two different layers [9]. The layer closest to the NP surface is called the "hard" layer and consists of proteins irreversibly adsorbed onto the NP surface. The second layer, composed of proteins adsorbed onto the "hard" layer, is called the "soft" layer. These proteins are reversibly adsorbed and can be exchanged [9]. The protein corona is highly complex and variable, due to the large number of different proteins present in the blood. Studies [12] have demonstrated that biodistribution of NPs is affected by the number, as well as by the identities of the proteins adsorbed to the NPs.

Much effort has been put into identifying the proteins commonly adsorbed onto non-bioinert NPs. These studies have revealed that the profile of the soft protein corona changes over time [12], something that could be attributed to differences in kinetic properties of the proteins present in the blood. Some proteins, like albumin, immunoglobulin G (IgG) and apolipoproteins are found in the protein corona of most non-bioinert NPs [12]. Most likely, the high frequency of these proteins is due to their large abundance in blood.

1.3 Nanoparticle – cell interactions

1.3.1 Circulation half-life

Therapeutic and diagnostic NPs need a certain circulation time in the blood in order to reach the tumor site. In addition, the NPs must be able to remain at the tumor site for at least as long as it takes for an image to be captured (diagnostic NPs) or therapy to be delivered (therapeutic NPs) [13]. Circulation half-life ($t_{1/2}$) is often used as a measure of the NPs' circulation time in the blood. $t_{1/2}$ is defined as the time at which the amount of NPs in blood reaches 50% of the injected dose. The ideal $t_{1/2}$ varies in between NP applications and generally longer $t_{1/2}$ are needed for therapeutic than for diagnostic NPs [13].

1.3.2 Macrophage interactions

$t_{1/2}$ of NPs in blood is highly dependent on the interactions between the particles and the mononuclear phagocyte system (MPS) [10]. The MPS is a part of the immune system and consists of phagocytic cells. Phagocytic cells are cells that have the possibility of utilizing phagocytosis, i.e. cell "eating", as a route of internalization of extracellular components. Circulating macrophages (a type of white blood cells) and monocytes (undifferentiated macrophages, i.e. a white blood cell) constitute the major part of the cells in the MPS. Other cells such as Kupffer cells (macrophages residing in the liver) and histiocytes (tissue macrophages), as well as lymphatic vessels are also components of the MPS. The primary purpose of the cells in the MPS is to recognize and remove foreign material, such as bacteria and viruses, from the blood. Macrophages are the cells mainly involved in this removal. The interaction between macrophages and a foreign material arises due to the presence of opsonins on the surface of the material. The opsonins function as "flags" and interact with receptors on the surface of macrophages. In this way the foreign material is presented to the macrophages, which then internalize the material. Large components are normally internalized by phagocytosis, whereas other internalization routes are available for smaller components [10]. Following internalization, the foreign material is digested or accumulated. Digestion takes place inside the lysosomes within the macrophages. Hydrolytic enzymes assist in this digestion. Material that can not be digested by the lysosomes is transported to liver and spleen, where it is accumulated [14].

The removal of foreign material is vital in order to protect the human body from potential pathogens. For therapeutic and diagnostic NPs this removal, however, constitutes a major problem. Since non-bioinert NPs will be opsonized (see Figure 1.4), these particles will be regarded as foreign material, meaning that they will be internalized by the macrophages [10]. Thereafter the NPs will be digested in the lysosomes or accumulated in liver and spleen. In this way the NPs will be removed from the blood and as long as the NPs are not protected from being opsonized, this removal will start immediately upon administration of NPs to the blood [10]. This constitutes a major problem, due to the shortening of the NPs' $t_{1/2}$.

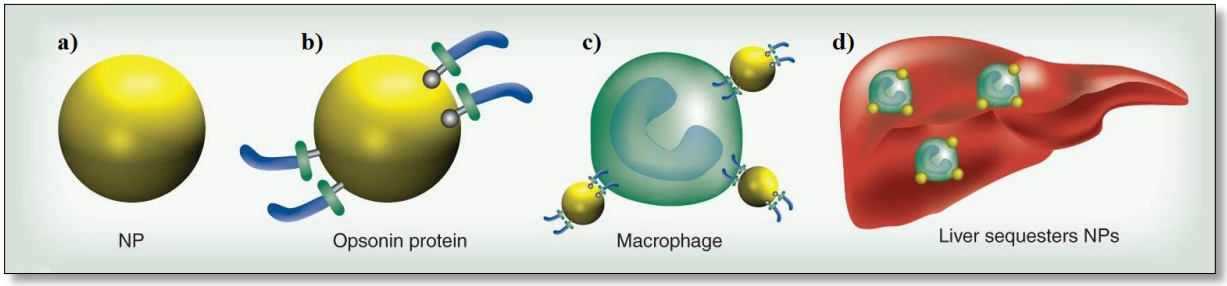

Figure 1.4. Process of removal of non-bioinert NPs from the blood. **a)** Non-bioinert NPs will become **b)** opsonized immediately upon administration to the blood. The opsonins will be recognized by **c)** macrophages, which will internalize the NPs. Following internalization, the NPs will be either digested within the macrophages or transported to the **d)** liver, where they will be accumulated. (Image modified from [13])

1.3.3 Liver interactions

NPs that can not be digested by the macrophages will be transported to the liver (and spleen). Here the NPs will be accumulated, still residing inside the macrophages (see Figure 1.4). Studies have suggested that once the macrophages die, the NPs are taken up by Kupffer cells, present in the liver [14]. Due to this, NP accumulation in the liver may last for a long time (months to years). This accumulation strongly reduces the amount of NPs delivered to tumor sites and in addition this accumulation may lead to toxic side-effects on liver cells.

Removal by MPS is one of three major routes for clearance of NPs from the blood. NPs that are not removed (or accumulated) by the MPS are removed by either renal or hepatobiliary clearance (see Figure 1.5). This is true for all NPs, i.e. even NPs that first reach the tumor site will subsequently be removed from the body by any of these three routes [14]. Particles smaller than ~6 nm can be removed from the blood via the renal clearance (kidneys), whereas bigger particles will be removed via the hepatobiliary clearance (liver). Hepatocytes are the cells mainly involved in the hepatobiliary clearance and this clearance is regarded as one of the basic functions of the liver. Hepatocytes are the most abundant cells in the liver and constitute approximately 70-80% of the liver cells [14].

Removal of NPs via the hepatobiliary clearance system starts when the NPs are internalized by the hepatocytes. Endocytic mechanisms are used for this internalization. Following uptake by hepatocytes, the NPs are degraded by enzymes. Degraded NPs are then excreted into the bile, which proceeds into the small intestine. The rate of this removal is highly dependent on the interactions between the NPs and the hepatocytes [14]. Uptake of NPs by hepatocytes has been shown to be affected by particle charge, core type, surface chemistry, size and shape [14]. Due to differences in these properties, NP clearance rate may vary considerably between different particles. While the renal clearance is relatively fast (hours-days), the hepatobiliary clearance has been shown [14] to be considerably slower (days-weeks). Due to this, concerns have been raised regarding toxic side effects to the hepatocytes and therefore studies of how liver cells are affected by long-term accumulation of NPs are of great importance.

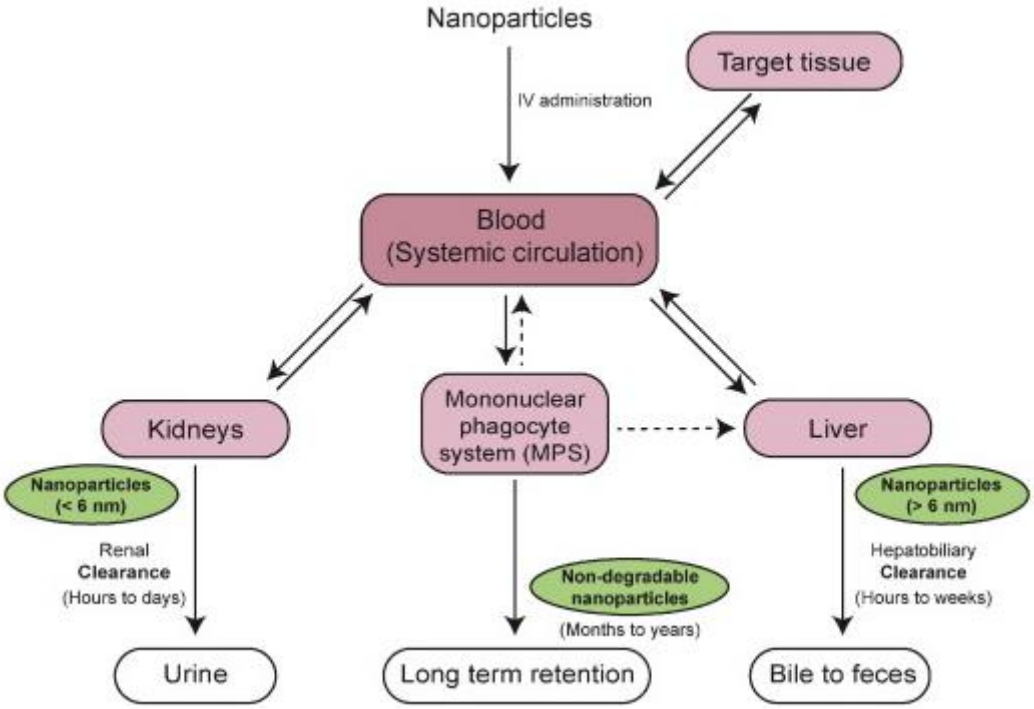

Figure 1.5. NP clearance pathways. NPs are cleared through any of the renal, hepatobiliary and mononuclear phagocyte systems. NPs smaller than 6 nm can be cleared by the renal clearance (kidney). NPs larger than 6 nm will be cleared by the hepatobiliary clearance or by the MPS. NPs not degradable by the MPS will be accumulated, whereas degradable NPs will be digested. Digestion products will then be removed by either renal or hepatobiliary clearance. (Image reproduced from [14])

1.3.4 Cellular internalization of nanoparticles

1.3.4.1 Endocytic uptake mechanisms

Accumulation of NPs in the MPS/liver and elimination of NPs via the hepatobiliary system occur due to uptake of NPs, mainly by macrophages and hepatocytes. Different endocytic mechanisms are responsible for this uptake. Endocytosis could be described as a group of passive uptake mechanisms by which material is taken up by a cell by invaginations in the plasma membrane. All cells throughout the body utilize endocytosis for internalization of nutrients, signaling molecules and other components important to their survival. Studies [15] have demonstrated that NPs are also internalized by endocytic mechanisms.

Generally, endocytosis is classified into two different types; phagocytosis and pinocytosis. Phagocytosis is referred to as cell "eating" and is the means by which the cell internalizes big solid particles. Pinocytosis is referred to as cell "drinking" and is the way by which cells internalize fluids containing smaller particles. Pinocytosis is sub-classified into macropinocytosis, clathrin-mediated endocytosis, caveolin-mediated endocytosis and clathrin- and caveolin-independent endocytosis (see Figure 1.6). All cells utilize pinocytic uptake mechanisms for internalization of extracellular components, whereas phagocytosis predominantly occurs in phagocytic cells, such as macrophages and monocytes. The endocytic mechanisms relevant for endocytosis of NPs depend on the size of the particles as well as on the presence of opsonins on the surface of the particles [15].

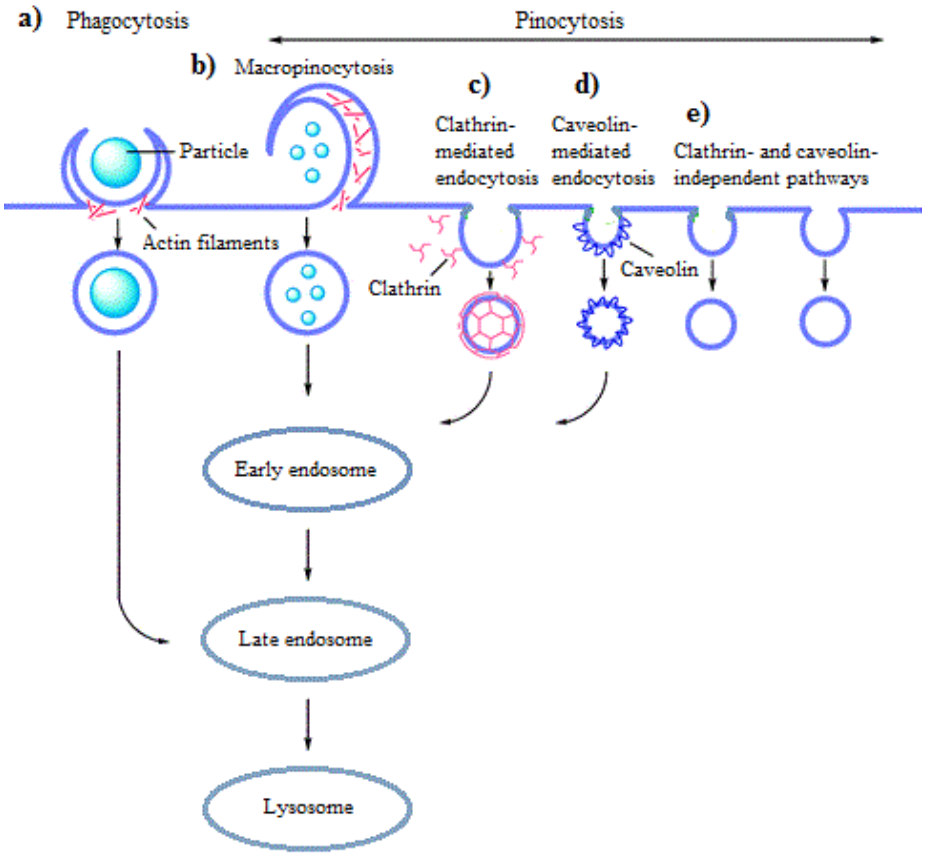

Figure 1.6. Endocytic internalization routes. Endocytosis is classified into phagocytosis (**a**) and pinocytosis (**b-e**). Pinocytosis is, in turn, sub-classified into **b)** macropinocytosis, **c)** clathrin-mediated endocytosis, **d)** caveolin-mediated endocytosis and **e)** clathrin- and caveolin-independent endocytosis. Materials internalized by any of these routes enter the endocytic pathway, which consists of early endosomes (EEs), late endosomes (LEs) and lysosomes. (Image modified from [16])

Large (micrometer sized) particles have the possibility to enter cells (phagocytes) via phagocytosis [15]. Phagocytosis relies on the presence of opsonins on the surface of the particles. By these opsonins, the particles will be recognized by the phagocytes and the particles will subsequently bind to receptors present on the cell surface. The cell membrane will start extending outwards from the cell surface, in a cup-shaped formation that encloses the particle. Subsequently, the particle will be internalized, enclosed in a vesicle called a phagosome (see Figure 1.6a). Smaller NPs, like the ones that have been used in this project (6-9 nm), are most likely not taken up via phagocytosis, unless they have aggregated.

Micrometer sized particles can also enter cells via the macropinocytic route [4], which can be found in almost all cells with a few exceptions. This route of entry is non-specific, meaning that no specific opsonins are needed. Through this endocytic process particles are internalized together with large quantities of extracellular fluid. Internalization starts upon activation of certain receptors on the surface of the cells. Membrane ruffles are formed and these ruffles enclose particles and extracellular fluid. Any enclosed material is then internalized by the cell, through the formation of a vesicle called a macropinosome (see Figure 1.6b). As with phagocytosis, micropinocytosis less likely occurs for small NPs.

Clathrin-mediated endocytosis is present in all cells [15] and this is believed to be one of the major routes by which NPs smaller than 10 nm are internalized by cells [15]. This is a likely internalization route for the NPs used in this project. This type of endocytosis has got its name from one of the cytosolic proteins, clathrin-1, mainly involved in the internalization process. Internalization of NPs by clathrin-mediated endocytosis is initiated when opsonized particles start interacting with receptors present on the cell membrane. These interactions lead to polymerization of clahtrin-1 on the cytosolic

side of the membrane. A clathrin-coated vesicle is formed (see Figure 1.6c) and after being wrapped inside, the NPs are enclosed in this vesicle, which is pinched off from the membrane. Studies [17] have suggested clathrin-mediated endocytosis as being one of the routes mainly involved in the internalization of certain NPs by HepG2 cells (hepatocyte cell line).

Caveolin-mediated endocytosis is also believed to be one of the major routes for internalization of NPs smaller than 10 nm [15] and should be regarded as a likely internalization route for NPs in this project. Caveolin, a protein that is present in any of three isoforms in most cells, is highly involved in the internalization of particles via this endocytic route. Caveolin-coated vesicles are formed (see Figure 1.6d) upon cellular interactions with opsonized particles, by a process similar to the one by which clathrin-coated vesicles are formed.

NPs can also be internalized by clathrin- and caveolin-independent endocytosis [4]. This endocytic route involves none of the proteins involved in clathrin- and caveolin-mediated endocytosis. Instead, internalization by this route is believed to rely on cholesterol and specific lipid compositions. The mechanisms of internalization (see Figure 1.6e), as well as the subsequent fate of internalized particles are however yet far from well understood.

1.3.4.2 The endocytic pathway

Upon internalization by a cell, most of the vesicles formed by macropinocytosis, clathrin-mediated pinocytosis and caveolin-mediated pinocytosis will fuse with vesicles present in the cytoplasm. These vesicles are called early endosomes (EEs) and constitute the first line in the endocytic pathway (see Figure 1.6), which is the pathway by which endocytosed material is either recycled to the cell membrane or passed on towards degradation in lysosomes. EEs often have a peripheral location, meaning that internalized vesicles will encounter these endosomes relatively early upon internalization. The internalized vesicles will fuse with the EEs, whereafter the vesicle membrane as well as the vesicle fluid are recycled to the cell membrane. This process lasts for about 10 minutes [18]. NPs that are not recycled to the membrane will pass on into late endosomes (LEs) in which the environment is mildly acidic. Here the NPs will encounter hydrolytic enzymes and digestion of the particles may be initiated. Vesicles formed by phagocytosis (phagosomes) will enter the endocytic pathway at this step (see Figure 1.6). About 10-40 minutes following the maturation of EEs into LEs, the LEs will fuse with lysosomes [18]. The lysosomes constitute the last part in the endocytic pathway. In the lysosomes, the pH is lower than in the LEs and the content of hydrolytic enzymes is higher. The final digestion of biodegradable NPs will be performed in the lysosomes [18].

Tracking NPs on their way through the endocytic pathway is important in order to fully understand how different NPs interact with cells. By staining NPs, as well as EEs, LEs and lysosomes, tracking can be performed with fluorescence microscopy. Rab5, specific for EEs, Rab7, specific for LEs and LAMP-1 in mature lysosomes are all proteins that can be stained for this purpose. Antibodies specific for these proteins are available on the market. In addition, fluorophores that stains acidic compartments in general (e.g. LysoTracker Deep red) are available on the market.

1.4 Nanoparticle – nanoparticle interactions

Interactions between NPs and cells from the MPS and liver may affect $t_{1/2}$ of the NPs. In addition interactions can occur between the particles themselves [13]. If the attraction between several NPs is larger than the attraction between NPs and the surrounding solvent, the particles will start interacting with each other. This, in turn, will lead to aggregation of NPs. Aggregation of NPs may be affected by pH and ionic strength (higher ionic strength will result in more aggregation) of the solution [19], as well as by the concentration of NPs (higher concentration of NPs will result in more aggregation) [13]. Upon aggregation of NPs, the size of the particles increases considerably. Due to this increase in size, the particles may become entrapped in capillaries in e.g. liver and lungs. This entrapment will lead to reduced $t_{1/2}$ of the NPs [13]. In addition, aggregated NPs have been suggested to behave differently within biological systems, compared to NPs in their single form [4]. For example, cellular uptake mechanisms may vary between uptake of aggregated and single NPs, due to considerable differences in particle size.

1.5 Coating of nanoparticles

Uptake of NPs by the MPS and the subsequent accumulation in the liver constitute major problems, both due to reduced $t_{1/2}$ of the NPs in the blood (which in turn reduces the therapeutic efficacy), but also due to the toxic side effects that may arise as a consequence of long-term accumulation of non-biodegradable NPs. Restricting uptake by macrophages is, however, troublesome, since this process will be initiated by any of the endocytic mechanisms as soon as the macrophages encounter opsonized NPs. Opsonization of NPs will, in turn, occur as long as the particles are non-bioinert. In order for NPs to avoid being removed by the MPS, the particles therefore have to be bioinert. The bioinertness of NPs can be increased by attaching a bioinert "coating" to the particle surface.

Polyethylene glycol (PEG) is one of the most common precursors, used for coating of NPs. This coating precursor is inexpensive and has been approved by the Food and Drug Administration (FDA). The process by which PEG precursors are attached to the surface of NPs is referred to as PEGylation [13]. PEGylation increases the bioinertness of NPs and studies [13] have demonstrated that PEGylated NPs have a lower uptake by the MPS, compared to their bare (no PEG) counterparts. In addition, longer $t_{1/2}$ and reduced accumulation in the liver (see Figure 1.7) have been noticed for PEGylated NPs [13].

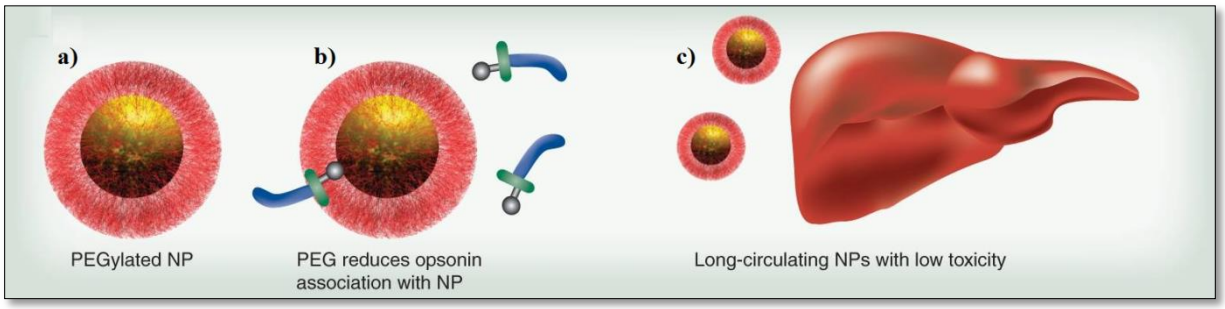

Figure 1.7. a) PEGylation increases bioinertness of NPs and subsequently reduces **b)** opsonization of the NPs (compared to Figure 1.4). This in turn leads to longer $t_{1/2}$ and **c)** lower accumulation in the liver. (Image modified from [13])

Generally, PEG precursors consist of three different parts (see Figure 1.8). The first end group (R_1) is used for attachment of the precursor to the NP surface. Attachment can be either covalent or non-covalent [13]. The second end group (R_2) will interact with the surrounding solvent and should ideally reduce protein adsorption (opsonization), increase hydrophilicity and prevent NP aggregation. Methoxy terminated ($R_2 = CH_3$) PEG precursors (mPEG) are commonly used due to their ability of reducing nonspecific protein binding, compared to PEG precursors with alternative terminus groups [13]. Any number (n) of ethylene glycol repeats connect R_1 and R_2. The ethylene glycol repeats are hydrophilic and this makes the PEG coated NPs more soluble in the blood.

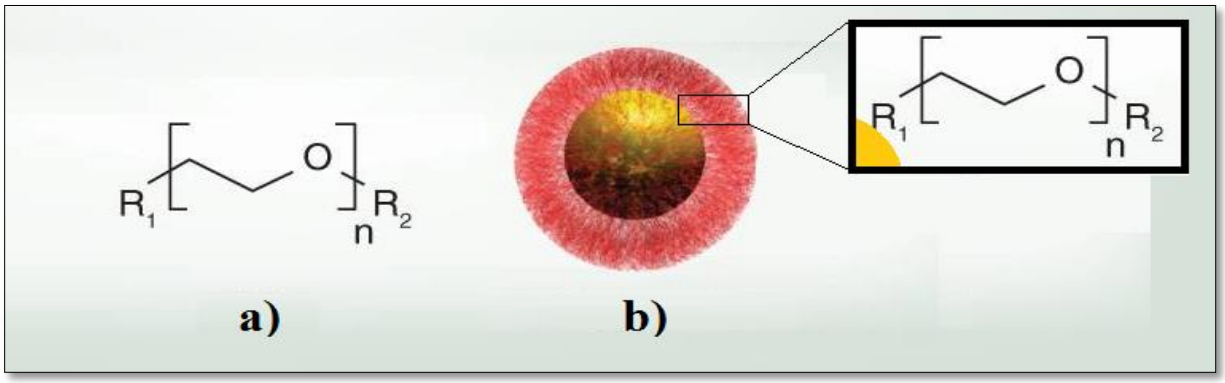

Figure 1.8. a) Structure of PEG, where any number (n) of ethylene glycol repeats connect R_1 and R_2. R_1 is used for attachment of the PEG precursor to the NP surface, whereas R_2 interacts with the surrounding solvent. **b)** PEGylated NP. (Image modified from [13])

PEG parameters such as length, conformation and coating density (density of PEG precursors on the surface of the NPs) have been shown [12] to affect opsonization and subsequent clearance of the NPs from the blood. For example, in several studies [12] increasing the length of the PEG precursors has been shown to reduce protein binding (opsonization) and uptake by macrophages. Increased flexibility and steric repulsion caused by longer PEG precursors could possibly explain this result [10]. Several studies have also shown a reduction in opsonization and macrophage uptake upon increase in coating density [19].

In this project, a method for quantification of cellular uptake of PEGylated NPs has been developed. This method constitutes a tool for studying the impact of PEG length and coating degree (density) on cellular uptake of NPs. A macrophage (Raw264.7) and a hepatocyte (HepG2) cell line have been used for uptake experiments. Due to what has been described in this chapter these cell lines are relevant with respect to the NP-cell interactions that would be expected *in vivo*. The NPs that have been used in the experiments are 6-9 nm and based on what has been described in this chapter, clathrin- and caveolin-mediated endocytosis are probable uptake routes for these particles.

2. OBJECTIVES OF THE PROJECT

The main goal of this project was to study whether coating degree and PEG precursor length of NPs had an impact on the uptake of these particles by Raw264.7 (macrophage cell line) and HepG2 (hepatocyte cell line) cells. Due to the impact of MPS and liver for clearance of NPs from the blood, addressing the interaction of these cells with NPs coated with different coatings is an important step in the attempt of developing bioinert NPs.

My first aim was to coat organosilicophosphonate core NPs with PEG precursors of three different lengths, each at two different coating degrees and to isolate coated NPs from side products, such as excess coating, by tangential flow filtration. Furthermore, I had to characterize the coating and filtration products, including determination of size, charge and real coating degree of the particles. For characterization of particles (bare as well as coated) techniques such as GPC (size), DLS (size), zeta potential measurements (charge) and ICP-OES (elemental analysis, coating degree determination) were used.

My second aim was to analyze the cellular uptake of the prepared NPs with a combined quantification method, constituting In-Cell ELISA, ELISA and flow cytometry. I also worked with developing this quantification method. By analyzing the NPs with a combination of quantification techniques the following issues were addressed:

- Impact of coating degree of NPs on NP uptake by Raw264.7 and HepG2 cells
- Impact of coating precursor length of NPs on NP uptake by Raw264.7 and HepG2 cells

My third aim was to study and visualize the localization of NPs taken up by cells with fluorescence microscopy.

3. MATERIALS AND METHODS

3.1 Coating of nanoparticles

3.1.1 Nanoparticles and coating precursors

The bare NPs that have been used for all of the coating experiments were synthesized by Spago Nanomedical AB. Four different glass flasks containing bare NPs from the same batch (labeled MS01024-3p.1r. B1-B4) were used during the coating experiments. The NPs were organic polymer particles, dispersed in water and contained equal molar amounts of silicon (Si) and phosphorus (P). Si and P concentrations were analyzed with inductively coupled plasma optical emission spectroscopy (ICP-OES) before project start. Preceding coating, the size of the bare NPs was analyzed with gel permeation chromatography (GPC) and dynamic light scattering (DLS). Four different coating precursors were used during the coating experiments; mPEG44-triethoxysilane (PEG44), mPEG21-triethoxysilane (PEG21), mPEG6-9-trimethoxysilane (PEG6-9) and 2-carbomethoxyethyltrimethoxy-silane (CC) (see Figure 3.1).

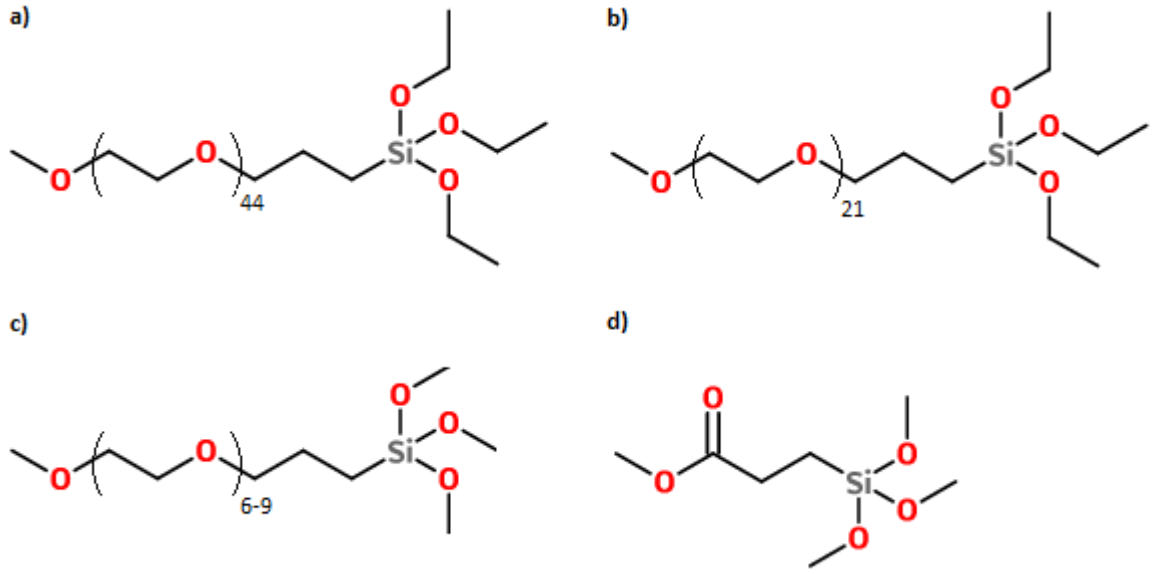

Figure 3.1. Coating precursors used for coating of bare NPs; **a)** mPEG44-triethoxysilane (AB386618 from abcr GmbH), M_W = 2174.67 g/mol, **b)** mPEG21-triethoxysilane (AB386629 from abcr GmbH), M_W = 1161.47 g/mol, **c)** mPEG6-9-trimethoxysilane (AB111226 from abcr GmbH), M_W = 524.694 g/mol and **d)** 2-carbomethoxyethyltrimethoxysilane (AB173883 from abcr GmbH), M_W = 208.290 g/mol

3.1.2 Preparation of the nanoparticles

The bare NPs were diluted in ethylene glycol (80 volume% ethylene glycol to 20 volume% NPs, dispersed in water) (see Table 3.1). pH of the NP solution was thereafter adjusted to 2.0 ± 0.5 by addition of 6 M HCl. Following this adjustment, the NP solution was transferred to a 500 ml three-necked round bottom flask, containing an egg-shaped stirring magnet. The leftmost neck was used for a thermometer (T_{in}), while a septum was put in the rightmost neck. This neck was then used for injection of coating precursor and for sampling. The third neck (middle) was connected to a condenser and to the vacuum/nitrogen gas line (see Figure 3.2).

3.1.3 Preparation of the coating precursors

Coating precursor (see Table 3.1) was dissolved in 50 ml ethylene glycol (for PEG6-9, PEG21 and CC) or in 50 ml ethylene glycol (50 volume%)/1,4-dioxane (50 volume%) (for PEG44). The dissolved coating precursors were transferred to a 50 ml syringe, with accompanying needle and the syringe was positioned in the syringe pump, with the needle penetrating the septum in the reaction flask. The needle was positioned so that the precursor solution would drop down in the middle, without touching the flask and without being immersed in the NP solution.

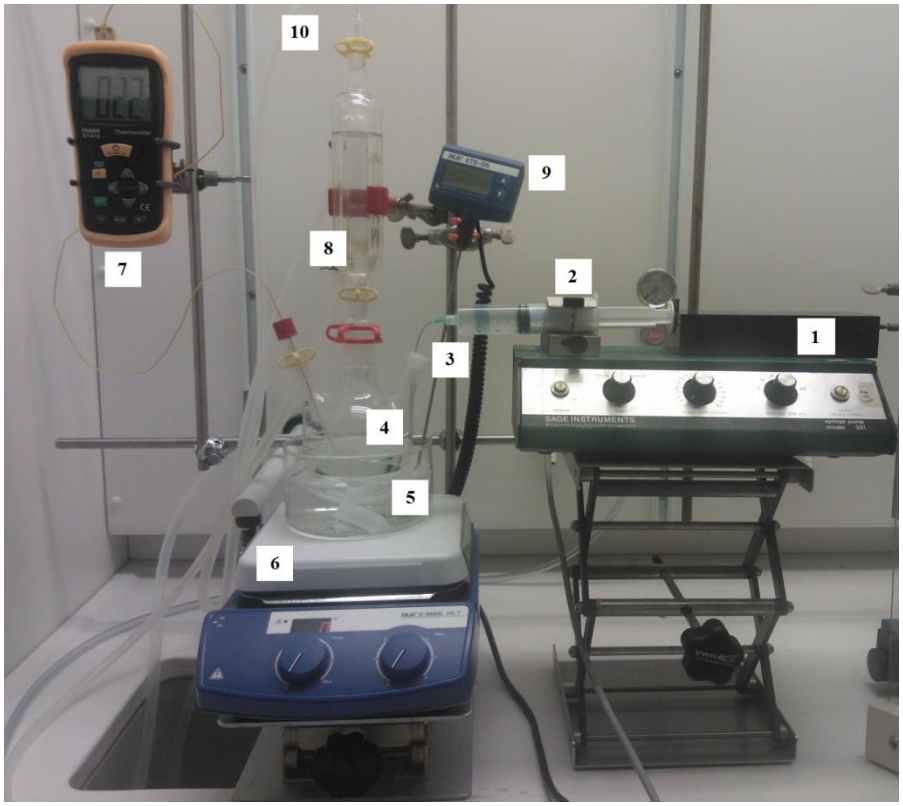

Figure 3.2. Coating equipment including **1)** syringe pump, **2)** 50 ml syringe, containing coating precursor, **3)** septum for sampling and coating injection, **4)** three-necked 500 ml reaction flask (round bottom), **5)** oil bath, **6)** hotplate stirrer, **7)** thermometer (T_{in}), **8)** condenser, **9)** temperature sensor (T_{set}) and **10)** line for N_2/vacuum.

Table 3.1. Amounts, masses and volumes of materials that have been used in the coating experiments, where EG1 = ethylene glycol, used for dilution of NPs; EG2 = ethylene glycol, used for dissolving of coating precursor; 1.4-d = 1,4-dioxane; NPM = NP monomer; CP = coating precursor. Bare NPs from the same batch (MS01024-3p.1r.), but from different flasks, labelled B1-B4 (see **NP flask** for details) were used during the coating experiments.

Coating precursor	Coating degree (mol%)	NP flask	V_{NP} (ml)	V_{EG1} (ml)	V_{EG2} (ml)	$V_{1.4\text{-}d}$ (ml)	n_{NPM} (µmoles)	n_{CP} (µmoles)	m_{CP} (g)
PEG6-9	20	B3	41	163	50	-	1532.8	306.56	0.161
PEG6-9	100	B3	41	163	50	-	1532.8	1532.8	0.804
PEG21	20	B2	41	163	50	-	1532.8	306.56	0.356
PEG21	100	B1	41	163	50	-	1532.8	1532.8	1.780
PEG44	20	B2	41	163	25	25	1532.8	306.56	0.667
PEG44	100	B1	41	163	25	25	1532.8	1532.8	3.333
CC	100	B4	41	163	50	-	1532.8	1532.8	0.319

3.1.4 Coating procedure

Stirring was turned on and the solution in the 500 ml round bottom reaction flask, containing ethylene glycol diluted NPs, was degassed by applying three vacuum/nitrogen gas cycles. Thereafter, the solution was heated at reflux under nitrogen. By having T_{set} = 106 °C in the silicon oil bath, the coating temperature T_{in} = 100 °C, was reached two hours after heating was turned on. Injection of coating precursor was initiated when heating was turned on (t = 0). The pump was run with the speed setting 0.15 ml/minute and was connected to a timer, which turned on the pump for 15 minutes out of every hour, meaning that the pump speed was 2.25 ml/h. The coating process was monitored by sampling every third hour (when possible) after heating and injection start. Approximately 1 ml was taken out with a syringe at sampling times (see Table 3.2). Samples were filtered with 0.2 µm syringe filters and NP size was analyzed with GPC and DLS. Heating and stirring was turned off 48 hours after injection start (t = 48h) and final NP size was analyzed.

Table 3.2. Sampling was performed at times marked with (x). No sampling was performed at times marked with (-).

Coating precursor	Coating degree (mol%)	3 h	6 h	18 h	21 h	24 h	27 h	30 h	42 h	45 h	48 h
PEG6-9	20	x	x	-	x	x	x	x	-	x	x
PEG6-9	100	x	-	x	x	x	x	-	-	-	x
PEG21	20	x	-	x	x	x	x	-	x	x	x
PEG21	100	x	x	-	x	x	x	x	-	x	x
PEG44	20	x	x	-	x	x	x	x	-	x	x
PEG44	100	x	x	-	x	x	x	x	-	-	x
CC	100	x	-	x	x	x	x	-	x	x	x

3.1.5 Treatment of coated nanoparticles

After finished coating the reaction flask was removed from the silicone oil bath and the coated NP solution was left cooling under nitrogen. Upon reaching room temperature, the coated NP solution was transferred to a 500 ml bottle. 205 ml MilliQ (MQ) water was added and pH was adjusted to 7-8 by addition of concentrated NaOH (see Table 3.3).

Table 3.3. Final pH of coated NPs after addition of concentrated NaOH.

Coating	Final pH
PEG6-9, 20 mol%	7.50
PEG6-9, 100 mol%	7.51
PEG21, 20 mol%	7.13
PEG21, 100 mol%	7.33
PEG44, 20 mol%	7.72
PEG44, 100 mol %	7.87
CC, 100 mol%	7.37

3.2 Size determination of nanoparticles

3.2.1 Size determination with GPC

3.2.1.1. Theoretical background

GPC is a chromatography technique that separates molecules by size. Here, a stagnant liquid in the pores of gel beads, packed into a column, works as the stationary phase, while a flowing liquid works as the mobile phase. When flowing through the column, the mobile phase flows between the beads and through them (through the pores of the beads). Particles that are present in the mobile phase will take different routes depending on their size. Big particles will not be able to pass through the pores of the beads, but will only flow in between them [20]. Small enough particles, on the other hand, will be able to enter the winding pores of the beads [20]. Due to this, the route through the column will be shorter for bigger particles than for smaller ones, meaning that big particles will be eluted earlier, i.e. have a shorter retention time. The elution of particles can be followed by using chromatograms, where particles of different sizes will give rise to different peaks (see Figure 3.3).

Except for the column that contains the stationary phase, a GPC equipment consists of a pump that pushes the mobile phase through the column, a port for sample injection, detector(s) for detection of eluted components and a software for control and display of results. The equipment that has been used during this project is shown in Figure 3.4. Two different detectors, an evaporating light scattering detector (ELSD) and a UV detector, have been used. After being pumped through the column, the sample was first detected by the UV detector and then by the ELSD. In order to keep track of particle sizes, particles can be run together with different protein standards, i.e. proteins of known sizes and retention times. In this project, bovine serum albumin (BSA) and myoglobin, with molecular weights of 66.5 kDa and 17.0 kDa, respectively, have been used as such standards.

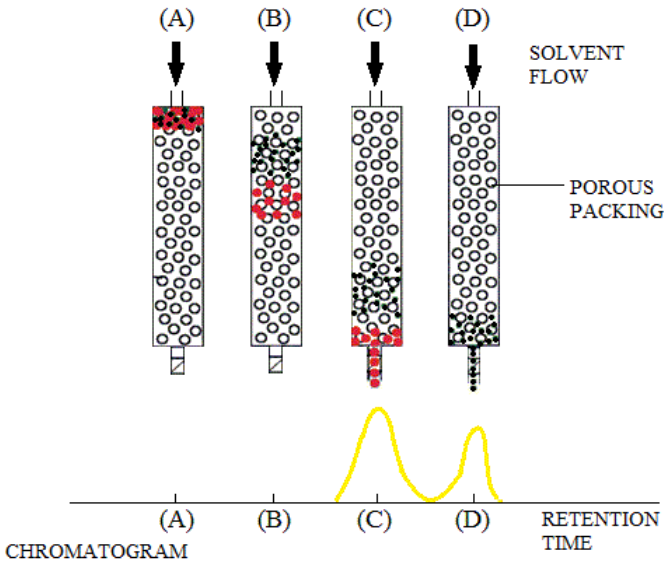

Figure 3.3. A) At the time of injection, particles of different sizes are mixed with each other. **B)** As the particles are pumped through the column, bigger particles (red) will be separated from smaller particles (black). **C)** The bigger particles will be eluted first, resulting in the first peak in the chromatogram. **D)** The smaller particles will be eluted later, resulting in the second peak in the chromatogram.

3.2.1.2 Methodology

For every NP batch that was synthesized, i.e. every combination of PEG length and coating degree, the size of the particles was determined by using GPC. For every synthesized particle batch this was done for the bare NPs, during the course of coating (every third hour when possible), after coating, after filtration and when the NPs had been stored for approximately two months (after coating). Every series of sample runs was preceded by purging of the system with 50 mM $(NH_4)_2CO_3$, pH 7.4 (pH adjusted with formic acid the same day and degassed by 10 minutes sonication). This was done in order to create straight baselines for the pressure, ELSD and UV signals. All samples were filtered with 0.2 µm filters (Acrodisc® 25 mm Syringe filter) preceding preparation.

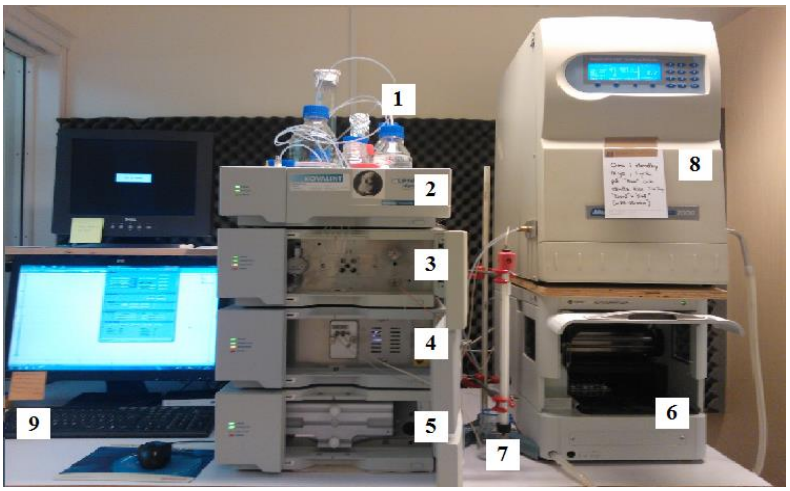

Figure 3.4. GPC equipment (YL9100 HPLC System). **1)** GPC running buffer, 50 mM $(NH_4)_2CO_3$ pH 7.4 **2)** Vacuum degasser **3)** Quaternary pump **4)** PDA detector UV lamp **5)** Column compartment **6)** Autosampler **7)** Column (Superose™ Increase 10/300 GL) **8)** Evaporative Light Scattering Detector (ELSD) **9)** Computer with software

3.2.1.2.1 Preparation of samples and adjustment of signals

Preceding GPC analysis of NP samples, the samples were prepared according to Table 3.4. The samples were prepared in screw-top vials, containing a 200 µl insert (see Figure 3.5). BSA and myoglobin, which were used as standard proteins, were diluted in GPC running buffer to a final concentration of 5 mg/ml. Note that every first (3h) sample, taken out during the coating procedure,

was run twice; once with ($NP_{DC,3h}$ in Table 3.4) and once without standard proteins (NP_{DC} in Table 3.4). The rest of the samples taken out during coating were only run once (NP_{DC} in Table 3.4). After running, all chromatograms were adjusted by offsetting the ELSD signal (with -0.4 or -0.1 minutes, depending on the delay time), compared to the UV signal.

Table 3.4. Summary of volumes used for GPC samples, where NP_b = bare NPs, NP_{DC} = NPs during coating, $NP_{DC, 3h}$ = first (3h) NP sample during coating, NP_{AC} = NPs after coating, NP_{AF} = NPs after 100 kDa diafiltration, and NP_{AS} = NPs after storing. Note that NP_{AF} comprises both permeates and retentates obtained during 100 kDa diafiltration.

Sample type	Volume of BSA (µl)	Volume of myoglobin (µl)	Volume of sample (µl)	Volume of GPC buffer (µl)	Injection volume (µl)	Delay time (min)
NP_b	40	10	60	90	20	0.4
NP_{DC}	-	-	60	140	20	0.4
$NP_{DC, 3h}$	40	10	60	90	20	0.4
NP_{AC}	-	-	60	140	20	0.4
NP_{AF}	-	-	60	140	50	0.4
NP_{AS}	-	-	60	140	50	0.1

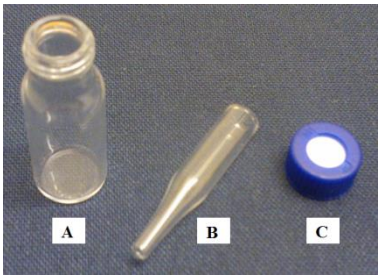

Figure 3.5. A) Vial, with accompanying **B)** 200 µL insert and **C)** lid

3.2.2 Size determination with DLS

3.2.2.1. Theoretical background

Dynamic light scattering (DLS) is another method used for determination of particle size. It can also be used for determination of size distribution of particles in a solution. By relying on the Stokes-Einstein equation (Eq. 1), the method of DLS relates the translational diffusion coefficient, *D*, to particle size.

$$D = \frac{k_B T}{3\pi\eta d_H} \quad \text{(Eq. 1)}$$

In the Stokes-Einstein equation k_B is the Boltzmann constant, while T and η are temperature and viscosity for the solvent. d_H is the hydrodynamic diameter of the particle, i.e. the diameter of an ideal hard spherical particle with the same translational diffusion coefficient as the one that is measured. The particle size that is obtained from the DLS measurement is thereby only an approximation based on the translational diffusion coefficient, which is the parameter that is actually (indirectly) measured [21]. The measurement of this parameter is based on light scattering from the particles. When hit by a light source, such as laser, particles scatter light in all directions. Light waves create an interference pattern at a detector located at 173° to the incident light beam. As the particles move through random Brownian motion, the interference pattern at the detector will fluctuate. The rate of these fluctuations is correlated to the size of the particle, where small particles will give rise to fast fluctuations, while big particles will give rise to slow fluctuations [22]. The rate of the fluctuations is then used for determination of the translational diffusion coefficient, which in turn is used for determination of the hydrodynamic diameter of the particle.

3.2.2.2 Methodology

Particle size was measured with DLS, using Zetasizer Nano-ZS (Malvern Instruments) and the accompanying Zetasizer Software v7.11 (see Figure 3.6). This was done for every NP batch before coating, during the course of coating (same time points as for GPC), after coating and after filtration. All samples were filtered with 0.2 µm filters (Acrodisc® 25 mm Syringe filter) preceding measurement.

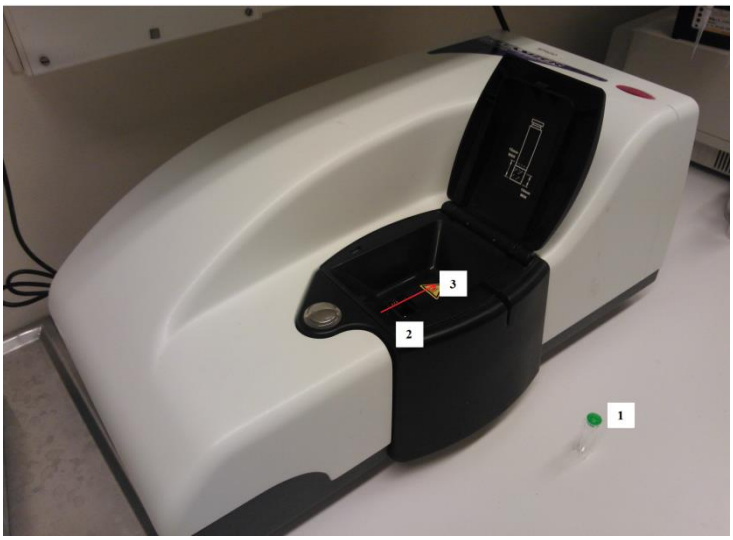

Figure 3.6. DLS equipment (Malvern Instruments, Zetasizer Nano-ZS). **1)** UV-cuvette micro **2)** Cuvette position **3)** Laser beam direction

Samples were prepared in cell disposable cuvettes (ZEN0040) (see Table 3.5). The final volume was 250 µl for all of the samples. Any bubbles were removed before measurements were performed. Particle size was measured and reported using the settings given in the *SOP for DLS size measurements of nanoparticles* (see Appendix I).

Table 3.5. Summary of volumes used for DLS samples, where NP_b = bare NPs, NP_{DC} = NPs during coating, NP_{AC} = NPs after coating and NP_{AF} = NPs after 100 kDa diafiltration. NP_{AF} only comprises retentates obtained during 100 kDa diafiltration.

Sample type	Volume of sample (µL)	Volume of GPC buffer (µL)
NP_b	25	225
NP_{DC}	250	-
NP_{AC}	250	-
NP_{AF}	100	150

3.3 Filtration and concentration of coated nanoparticles

3.3.1 Theoretical background

Tangential Flow Filtration (TFF) was used for filtration of the batches of coated NPs. The purpose of this filtration process was to remove components bigger (e.g. bacteria) and smaller (e.g. coating precursors and coating oligomers) than the coated NPs.

Filtration is a process driven by pressure and is used for separation of components in a solution. By using porous membranes, components of a solution can be separated by either size or charge. In this case, components have been separated by size. Normal Flow Filtration (NFF) and Tangential Flow Filtration are two of the most common operational modes of filtration (see Figure 3.7). These two modes differ in how the fluid is convected towards the membrane. In NFF, the fluid flow is directed normal to the surface of the membrane, while in TFF, the flow is directed tangentially along the

surface of the membrane. Both of the modes work under an applied pressure. In both of the modes, components that are too large to pass through the pores of the membrane are retained on the retentate side of the membrane. When using NFF, components that do not pass through the membrane will accumulate close to the membrane (due to the direction of the flow), while in TFF, retained components will be swept away [23].

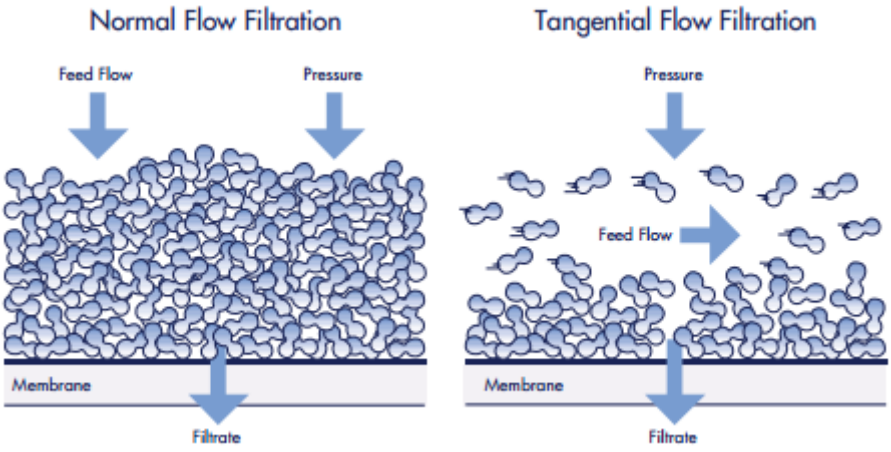

Figure 3.7. Two operational modes that can be used for filtration; NFF (left) and TFF (right). (Image reproduced from [23])

Two different TFF methods were used for filtration of the batches of coated NPs. Ultrafiltration, a filtration method in which molecules in a solution are separated based on size, was used for removal of components bigger than 300 kDa, i.e. a 300 kDa filter membrane was used. A second filtration, called diafiltration, was then performed for all of the batches. Generally, diafiltration is used for changing of chemical properties of the retentate under constant volume [24]. In this case, diafiltration with a 100 kDa filter was performed for all of the batches in order to change ethylene glycol and 1,4-dioxane, i.e. solvents used during the coating procedure, into MQ water. This was accomplished through introduction of MQ water into the system, at the same time as the permeate was removed. The permeate contained coating precursors, coating oligomers and solvents. Finally, the purified product was concentrated by removal of permeate.

3.3.2 Methodology

3.3.2.1 Selection of filter size and treatment of equipment and nanoparticles

Filter sizes (300 kDa for ultrafiltration and 100 kDa for diafiltration) were selected based on the coated NP size from GPC, to retain a high yield of NPs. All of the equipment used during the filtration process, including bottles with accompanying lids for collection of permeates and retentates, was autoclaved for three hours at 120 °C before usage. All NP solutions were pre-filtered using 0.2 µm sterile *Rapid-flow bottle top* filters in order to minimize fouling of the 300 kDa filter. The filtrate was then ultrafiltered with a 300 kDa tangential flow filter to remove any large aggregates. The permeates were diafiltered with a 100 kDa tangential flow filter to remove coating precursor, solvent (ethylene glycol or 1,4-dioxane) and partially coating oligomers. The permeates and retentates of 100 kDa filtrations were collected.

3.3.2.2 Filtration equipment

The equipment that has been used for ultrafiltration is presented in Figure 3.8. A similar equipment was used for diafiltration and concentration. Two different pumps have been used: a small membrane pump and a peristaltic pump. When using the peristaltic pump, a 100 rpm speed setting was used.

3.3.2.3 Starting up filtrations

In between filtration runs, the filter membranes were cleaned according to *3.3.2.6 Cleaning of filter membranes*. Filtrations were started up and run using a procedure described in an internal SOP developed by Spago Nanomedical AB. The same start-up procedure was used for both of the filters (300 kDa and 100 kDa).

3.3.2.4 Ultrafiltration using a 300 kDa TFF membrane

Ultrafiltration was performed using a 300 kDa filter (see Figure 3.9). During this filtration, aggregates and particles bigger than 300 kDa were removed. Retentate bottles were labeled EF020XX-3r., while permeate bottles were labeled EF020XX-3p (see Table 3.6). The permeates were proceeding to diafiltration and concentration.

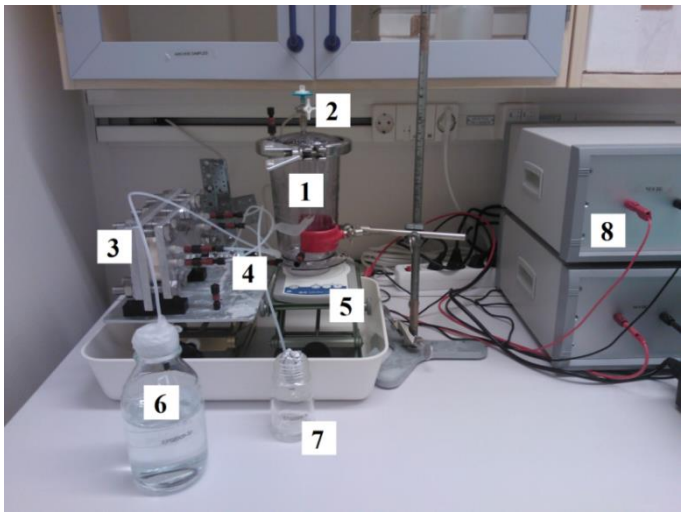

Figure 3.8. Ultrafiltration setup with **1)** reservoir with stirring magnet, **2)** air valve, **3)** Tangential Flow Filter (TFF) cassette with Omega TM Membrane, **4)** sterile Tygon tubing "PharMed-BPT", **5)** stirring plate, **6)** permeate bottle, **7)** retentate bottle and **8)** power supply connected to a small membrane pump (membrane pump positioned behind the equipment)

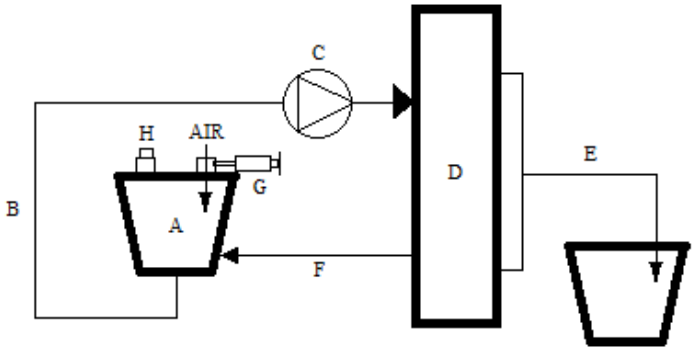

Figure 3.9. Ultrafiltration mode. **A)** Reservoir, **B)** Inlet line, **C)** Pump, **D)** Filter (300 kDa), **E)** Permeate line, directed to a permeate bottle, **F)** Outlet/Retentate line, connected to bottom inlet port, **G)** Lid inlet port connected to a syringe and **H)** Plugged lid inlet port

Table 3.6. Summary of batch codes. Coating degree refers to the amount of coating precursor added during synthesis, not to the amount of coating present on the NPs.

Code	Coating precursor	Coating degree (mol%)
EF02013	PEG6-9	20
EF02012	PEG6-9	100
EF02009	PEG21	20
EF02004	PEG21	100
EF02010	PEG44	20
EF02007	PEG44	100
EF02016	CC	100

3.3.2.5 Diafiltration and retentate concentration using a 100 kDa TFF membrane

Diafiltration was performed using a 100 kDa filter (see Figure 3.10). During this filtration, free coating precursor, coating oligomers and fragments of particles, smaller than 100 kDa were removed. Permeates were labeled EF020XX-3p.1p., while retentates were labeled EF020XX-3p.1r. Permeates and retentates from all of the filtrations were stored at room temperature.

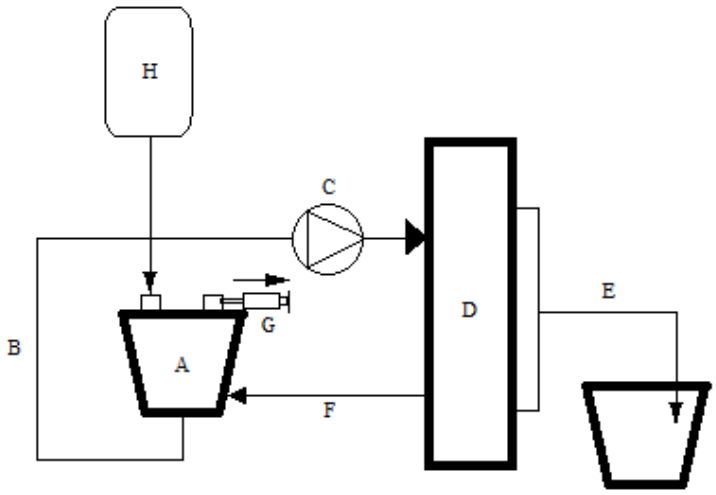

Figure 3.10. Diafiltration mode. **A)** Reservoir, **B)** Inlet line, **C)** Pump, **D)** Filter (100 kDa), **E)** Permeate line, directed to a permeate bottle, **F)** Outlet/Retentate line, connected to bottom inlet port, **G)** Lid inlet port connected to a syringe, used to create vacuum and **H)** MQ water tank connected to lid inlet port

3.3.2.6 Cleaning of filter membranes

After every filtration, the filter membranes were cleaned. The same procedure was used for both of the filters. The system was cleaned once with 1 L of MQ water (40 °C, collected in a sterile bottle), whereafter it was cleaned once with 1 L of 0.3 M NaOH (40 °C, prepared in a sterile bottle). Following this, 1 L of MQ water (room temperature) was recirculated in the system for 10 minutes. Then the filter was flushed with MQ water until pH of permeate and retentate lines reached 7-8. Finally, the reservoir was filled up with 70% ethanol, which was recirculated for 10 minutes. Thereafter, all lines were plugged. A more detailed description of the cleaning procedure can be found in the filtration SOP developed by Spago Nanomedical AB.

3.4 Elemental analysis of nanoparticle components

3.4.1 Theoretical background

Elemental analysis with inductively coupled plasma optical emission spectroscopy (ICP-OES) has been used for determination of P and Si concentrations for all batches of coated NPs. These concentrations have then, in turn, been used when calculating the real degree of coating for all NP batches. Every NP batch was analyzed twice; once before and once after filtration. Analysis was performed by Nooshin Yousefpour and Olof Björnberg.

Following this analysis, coating degree of the particles was calculated (see Eq. 2 and Appendix VIII).

$$\%\, coating = \left(\frac{[Si]_{coated}}{[P]_{coated}} - \frac{[Si]_{bare}}{[P]_{bare}}\right) \cdot 200\ \% \qquad \text{(Eq. 2)}$$

where

$[Si]_{coated}$ = Silicon from coating + core in coated NPs, measured after filtration
$[Si]_{bare}$ = Silicon in bare NPs, measured before coating
$[P]_{coated}$ = Phosphorus from core in coated NPs, measured after filtration
$[P]_{bare}$ = Phosphorus in bare NPs, measured before coating

Elemental analysis with ICP-OES is an analytical method used for quantification of trace metals in a sample. The technique relies on the emission of light that arises as elements become thermally excited. This thermal excitation starts when the sample, which is normally in liquid form, is introduced into the core of inductively coupled argon plasma [25]. Preceding this, the sample is converted into aerosol drops in a nebulizer and the aerosol is then carried into the plasma by an argon gas flow. In the plasma, the sample becomes vaporized and the gas that is formed is then further atomized and ionized [26]. The high temperature in the plasma will result in excitation of the ions and as the electrons then return to their ground states light is emitted. The wavelength of this light is characteristic for each element. Light that is emitted is collected by a spectrometer detector and is then further converted into a spectrum containing all wavelengths of the emitted light. By amplifying the intensity of the measurements, the emitted light can be converted into concentrations of the elements. Calibration standards are needed for this conversion to be correct [25].

3.5 Zeta potential measurements

3.5.1 Theoretical background

Particles in a solution will always exhibit a surface charge, or zeta potential, and knowing this zeta potential is crucial in the prediction of formulation stability and interaction between particles. A particle with a certain net surface charge will attract counter-ions, i.e. oppositely charged ions. This means that the concentration of counter-ions will increase in the proximity of the particle. The region, over which this attraction sustains, is called the electrical double layer (see Figure 3.11). This double layer consists of two separate layers; the Stern layer, which is the layer of strongly bound ions, and an outer layer, consisting of ions that are loosely associated to the particle. This layer is called the diffuse layer. All counter-ions present within a certain distance from the particle will move with the particle as it moves through the solution. Beyond this distance, counter-ions will, however, not move with the particle anymore. This boundary, present in the diffuse layer, is called the slipping plane, and the zeta potential is defined as the potential at this plane. If this potential is very negative or very positive, particles will repel each other, while if the potential is low (i.e. close to 0), particles tend to flocculate. Flocculation leads to instability of the solution. Flocculation might, however, be prevented by entropic repulsion if PEG precursors are attached to the surface of the particles [27].

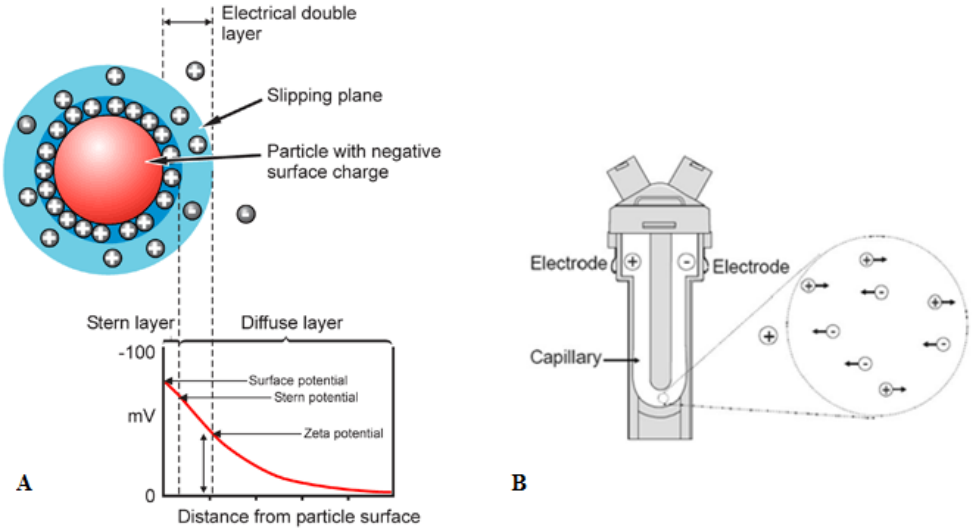

Figure 3.11. A) A particle with a negative surface charge will attract positive counter-ions. The zeta potential is the potential at the slipping plane. (Image reproduced from [28]) **B)** Reusable folded capillary cell used for zeta potential measurements. Arrows show the direction of the moving particles. (Image reproduced from [29])

When measuring zeta potential, pH of the solution always has to be taken into account, since this highly affects the charge of a particle. Zeta potential is commonly measured by applying an electric field across the sample. When this is done, charged particles start to move in a direction and with a velocity that depends on the applied field. The velocity by which the particles move is dependent on the zeta potential of the particles. This means that the zeta potential can be indirectly determined by measuring the particles' velocity *(U_E)* in the field. For calculation of the zeta potential, the strength of the electric field has to be known, as well as the dielectric constant *(ε)* and viscosity *(η)* of the solvent. These parameters are combined in the Henry Equation (Eq. 3), from which the zeta potential *(z)* can then be determined. In the equation *f(Ka)* is Henry's function, which generally adopts a value of 1.5 (the Smoluchowski approximation, used for aqueous solutions) or 1.0 (the Huckel approximation, used for non-polar solvents) [27].

$$U_E = \frac{2\varepsilon z f(Ka)}{3\eta} \qquad \text{(Eq. 3)}$$

3.5.2 Methodology

The zeta potential of the particles was measured using Zetasizer Nano-ZS (Malvern Instruments) and the accompanying Zetasizer Software v7.11. This was done for every NP batch after filtration. The zeta potential of NPs in 9 mM sodium phosphate buffer, pH 7.1 (0.0621 g $NaH_2PO_4 \cdot H_2O$ in 50 ml MQ water, pH adjusted by addition of 1 M NaOH) was determined (see Table 3.7).

Table 3.7. Volumes of NPs and buffer mixed for zeta potential measurements.

Coating precursor	Coating degree (mol%)	$V_{NP\ solution}$ (µl)	V_{buffer}(µl)	Final pH
PEG6-9	20	200	1800	7.11
PEG6-9	100	200	1800	7.11
PEG21	20	200	1800	7.12
PEG21	100	200	1800	7.10
PEG44	20	200	1800	7.11
PEG44	100	200	1800	7.12
CC	100	50	1950	7.10
Bare NP (B4)	0	200	1800	7.12

The sample was filtered through a 0.2 µm filter and was added to a reusable folded capillary cell (DTS1070), using a 20 ml syringe and. The solution should cover the electrodes. Before addition of a new sample to the cell, the cell was washed twice; once with ethanol and once with MQ water. Zeta potential of the particles was measured using the settings given in the *SOP for zeta potential measurements of nanoparticles* (see Appendix II).

3.6 Nanoparticle – medium compatibility

3.6.1 Calcium induced nanoparticle aggregation

3.6.1.1 Methodology

NP aggregation was provoked by addition of increasing amounts of calcium (Ca). Concentrated samples from all coated NP batches, as well as a sample of bare NPs (MS01024-3p.1r. B4), were diluted to 0.5 mM P in 0 mM, 0.13 mM, 0.25 mM, 0.50 mM, 1.00 mM and 2.00 mM buffered Ca solutions (buffer = 5 mM Tris-HCl + 75 mM NaCl pH 7.4), vortexted for a few seconds and left to stand for 1 hour at room temperature. Then, all samples were centrifuged for 10 minutes at 13.4 krpm and supernatants were collected. Concentrations of P and Si in the supernatants were analyzed with ICP-OES. P and Si concentrations in the supernatants were normalized to P and Si concentrations of the 0 mM Ca sample (corresponds to 100% retention of NPs) and were plotted versus Ca concentration. By doing this, the percentage of NPs still not precipitated, could be determined for each NP at each Ca concentration. The experiment was performed by Emil Aaltonen. Elemental analysis with ICP-OES was performed by Nooshin Yousefpour and Olof Björnberg.

3.6.2 Incubation of nanoparticles with culture media

3.6.2.1 Methodology

Compatibility of NPs at four different NP concentrations with both culture media that were used during cell culturing was examined by incubating NPs with each medium. Media that were used were RPMI – 1640 Medium – Liquid Media from HyClone (catalog number: SH30327) and Dulbecco's Modified Eagle's Medium (DMEM) – High Glucose – Liquid Media from HyClone (catalog number: SH30022). Both media were supplied with 10% fetal bovine serum (FBS) and 0.5% penicillin/streptomycin solution. For each NP batch, NPs were diluted in MQ water to an appropriate concentration. 750 µl of NP solution was then mixed with 750 µl medium in Eppendorf tubes, by vortexing. Final NP concentrations are given in Table 3.8.

Table 3.8. Final concentrations of P and Ca in incubation of NPs with culture media. RPMI has 0.4 mM Ca. DMEM has 2.6 mM Ca. Calcium concentration is halved because media are diluted by a factor 2.

Medium	NP concentration (mM [P])	Calcium concentration (mM)	[P]/[Ca]	V_{medium} (µl)	$V_{NP\ solution}$ (µl)
RPMI	3.0	0.2	5	750	750
RPMI	1.0	0.2	5	750	750
RPMI	0.1	0.2	5	750	750
RPMI	0.01	0.2	5	750	750
DMEM	3.0	1.3	0.77	750	750
DMEM	1.0	1.3	0.77	750	750
DMEM	0.1	1.3	0.77	750	750
DMEM	0.01	1.3	0.77	750	750

The procedure for analysis of NP precipitation is illustrated in Figure 3.12. Following analysis the percentage of NPs still not precipitated was plotted versus time.

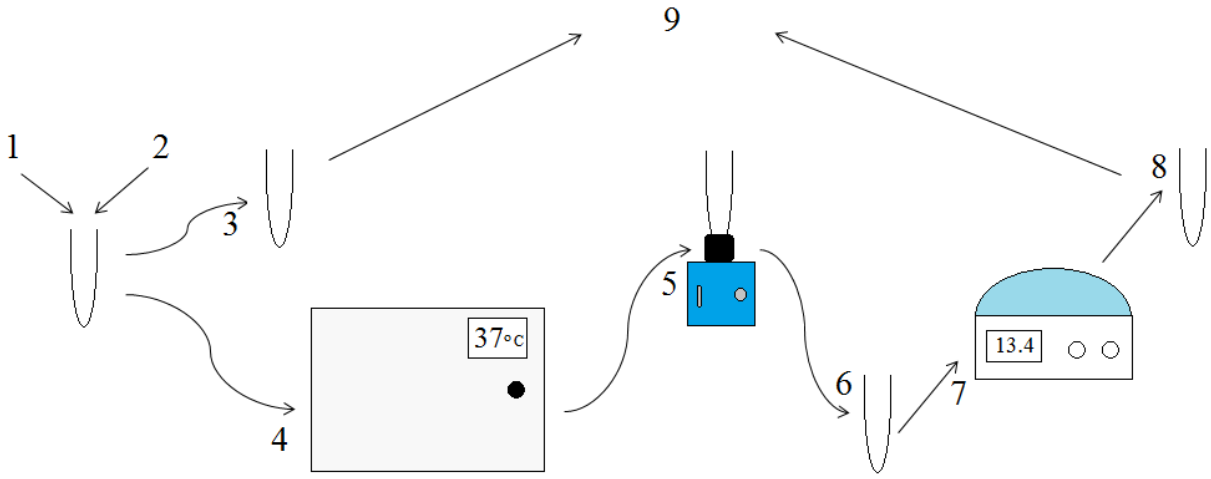

Figure 3.12. Procedure for incubation of NPs with culture medium, where mixing of **1)** 750 µl diluted NPs (6 mM, 2 mM, 0.2 mM or 0.02 mM P) with **2)** 750 µl medium (RPMI or DMEM) was followed by **3)** transfer of 100 µl of the mixture to a new tube, the "before" sample. The rest of the mixture was **4)** incubated at 37 °C for 1 hour, followed by **5)** vortexing of the tube. **6)** 300 µl was transferred to a new tube, which was **7)** centrifuged for 20 minutes at 13.4 krpm. **8)** Supernatant was transferred to a new tube, the "after" samples. Si and P concentration in "before" and "after" samples were then **9)** analyzed with ICP-OES by Nooshin Yousefpour and Olof Björnberg. The Si concentration of the "after" sample was normalized to the Si concentration of the corresponding "before" sample. By doing this, the percentage of NPs that did not precipitate could be determined.

3.7 Culturing of cells

3.7.1 Theoretical background

3.7.1.1 Counting of cells

Bürker chambers are commonly used for counting of cells. The device is a chamber consisting of a thick glass microscope slide covered with a cover slip. The chamber encloses a well-defined volume and is marked with a grid. Cells on the grid can be counted using a light microscope. The number of cells divided by the volume gives the overall concentration of cells in the sample. A Bürker chamber normally consists of two chambers that, in turn, consist of nine squares (called A squares, see Figure 3.13) each. The dimensions of each square are 1x1 mm. By applying a cover slip on top of the chamber, the enclosed volume of a "square" becomes 0.1 mm^3, i.e. 10^{-4} ml. This means that the concentration of cells per ml will be the average number of cells per square multiplied by 10^4. Dilutions also have to be taken into account. Normally, the cells are pre-diluted in a cell stain dye, before they are added to the chamber. This dye should be impermeable for viable cells, while dead cells will take up the dye, due to their permeability. This means that viable cells can be distinguished from dead cells in the counting. Erythrosin B and Trypan blue are commonly used staining dyes [30].

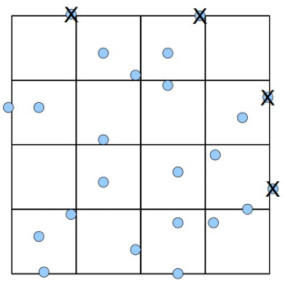

Figure 3.13. An A square with cells. Cells marked with an X are not counted in this square, since they are regarded as belonging to neighboring squares [31].

3.7.1.2 Growth curves

Growth curves are created in order to analyze the growth characteristics of cells or cell lines. The curves can be created in different ways, e.g. by measuring the optical density of cells or by counting the number of cells, using a Bürker chamber. A growth curve is specific for a certain cell and can be used for determination of e.g. population doubling time, lag time and saturation density for this cell. Lag time corresponds to the duration of what is later on referred to as the lag phase, while saturation density corresponds to the cell density in the stationary phase. Growth curves can also be used for analysis of biological response to certain factors, such as hormones and nutrients. The curve has four different phases; lag phase, log phase, stationary phase and death phase (see Figure 3.14). The lag phase occurs after subculturing and corresponds to the time required for the cells to recover, attach and spread. In the log phase, the number of cells increases exponentially, while in the stationary phase, growth rate slows until the number of new cells formed is the same as the number of dying cells. When the nutrients in the medium decrease the cells finally reach the death phase. In this phase, the number of dying cells exceeds the number of cells being born. This means that the population of cells decreases [32].

A term commonly used in cell culturing is confluence. Confluence of cells growing in a culture flask refers to the surface area occupied by cells. Confluence is reported as a percentage, e.g. cells that are 70% confluent cover 70% of the available growth area in the culture flask. As cells reach full confluence, contact inhibition occurs and cells start to proliferate at a lower rate. This corresponds to the stationary phase in Figure 3.14. If reseeded after reaching the stationary phase, longer time is needed for the cells to recover, compared to if the cells are reseeded while they are still in the log phase [33]. Therefore, cells should be passaged before they reach full confluence.

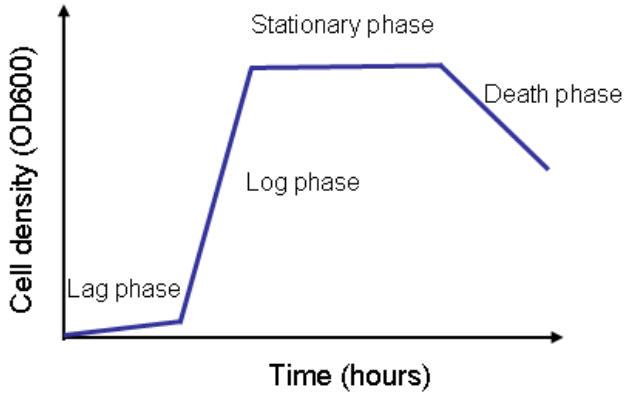

Figure 3.14. Growth curve with lag phase, log phase, stationary phase and death phase [34].

3.7.2 Methodology

3.7.2.1 Seeding and splitting of cell cultures

Two different cell lines were cultured for further biological experiments; Raw264.7 (ATCC® TIB-71™), a semi-adherent macrophage cell line derived from mouse, and HepG2 (ATCC® HB 8065™), an adherent hepatocyte cell line derived from human. Raw264.7 cells were cultured in RPMI medium, while HepG2 cells were cultured in DMEM. Both media were supplied with 10% FBS and 0.5% penicillin/streptomycin solution.

Preceding seeding of cells, 5 ml preheated (37 °C) medium was added to a T25 culture flask. Cells stored in freezing medium (culture medium with 10% dimethyl sulfoxide, 1 ml/vial) in liquid nitrogen at -196 °C were thawed by immersing the vial into preheated MQ water (37 °C). The content of the vial was then transferred to the T25 culture flask with a sterile pipette. The flask was tilted carefully, in order to spread out the cells. The cells were then incubated overnight at 37 °C in 5% CO_2 and 100% humidity in an incubator (Heraeus Instruments BBD 6220), after which the medium was aspirated and 5 ml fresh, preheated (37 °C) medium was added. Thereafter the flask was put back in the incubator.

When the cells had reached 70-80% confluency, they were transferred to a T75 flask. Medium was aspirated and 5 ml preheated (37 °C) 1x phosphate buffered saline (PBS) was added to the flask for washing of the cells. After washing, PBS was aspirated and 0.5 ml preheated (37 °C) trypsin (0.25% (1X) solution) was added to the flask by flushing it over the cells. The cells were then incubated at 37 °C, until all of them had detached. Flasks were firmly slapped to detach cells. 4.5 ml preheated (37 °C) medium was flushed over the bottom of the flask in order to detach the last cells and to inactivate the trypsin. Thereafter, all of the solution was transferred to a T75 culture flask using a sterile pipette. 10 ml of fresh medium (37 °C) was also added to the flask and the flask was labeled with the name of the cell line, passage number and date of splitting. The cells were incubated at 37 °C.

By watching the cells through an inverted light microscope, the degree of confluency of the cells was followed. Confluent cells were split using the procedure described above. However, since the cells were now growing in a bigger flask, 1 ml trypsin (0.25% (1X) solution) was added for detaching of cells. Detached cells were diluted in 9 ml medium (37 °C), whereafter some of this cell suspension was transferred to a new labeled flask (T75). For example, for a 1:2 splitting, 5 ml cell suspension was transferred to a new flask, containing 10 ml preheated (37 °C) medium. The final volume should always be 15 ml. The new flask was incubated at 37 °C, while the old flask was discarded. Cells were split every two to three days.

3.7.2.2 Freezing of cells

Before freezing of cells, medium was aspirated and the cells were washed once with 5 ml PBS. PBS was aspirated and the cells were trypsinated at 37 °C (1 ml trypsin, 0.25% (1X) solution, 37 °C), until all cells had detached from the bottom of the flask. 9 ml medium (37 °C) was added to the flask, whereafter 20 µl cell suspension was mixed with 20 µl Erythrosin B Dye in an Eppendorf tube. The mixture was loaded onto a Bürker chamber and the cells were counted. The rest of the cell suspension was transferred to a 15 ml sterile Sarstedt tube, which was then centrifuged for 5 minutes at 180 g. The supernatant was aspirated and the cell pellet was resuspended in freezing medium. The volume of freezing medium added to the cells, was based on the final cell concentration that was wanted in the freezing vials. 1 ml cell suspension was then transferred to each freezing vial. The vials were stored in liquid nitrogen a -196 °C.

3.7.2.3 Creation of growth curves

Medium was aspirated from Raw264.7 and HepG2 culture flasks and the cells were washed once with PBS, followed by trypsination. After detachment of all cells, the cells were diluted in 9 ml medium (37 °C). 20 µl cell solution was then mixed 1:1 with Erythrosin B and the cells were counted using a Bürker chamber. The cells were then diluted in medium to a final concentration of 20000 cells/ml. For each cell line 2.5 ml cell solution was added to two different wells on a 6-well plate. This was then repeated for another four 6-well plates (see Figure 3.15). The plates were incubated at 37 °C for 24h, 48h, 72h, 96h and 168h, respectively. At each time point, one of the plates was removed from the incubator. Medium was aspirated from the wells and the cells were washed once with 2 ml PBS. PBS was then aspirated and the cells were incubated with 300 µl trypsin (0.25% (1X) solution, 37 °C) at 37 °C, until all of the cells had detached from the bottom of the wells. 2.5 ml medium was then added to each well. For each well, 20 µl cell solution was mixed 1:1 with Erythrosin B. The number of viable cells present in each well was then counted using a Bürker chamber. Results were presented with growth curves, one for each cell line. Cell doubling time was also calculated for both cell lines. In the equation for cell doubling time (see Eq. 4) t is the incubation time (in any units), whereas Xb and Xe are the number of cells at the beginning and end of the incubation time, respectively [35].

$$t_{doubling} = t\ln(2)/\ln(Xe/Xb) \qquad \text{(Eq. 4)}$$

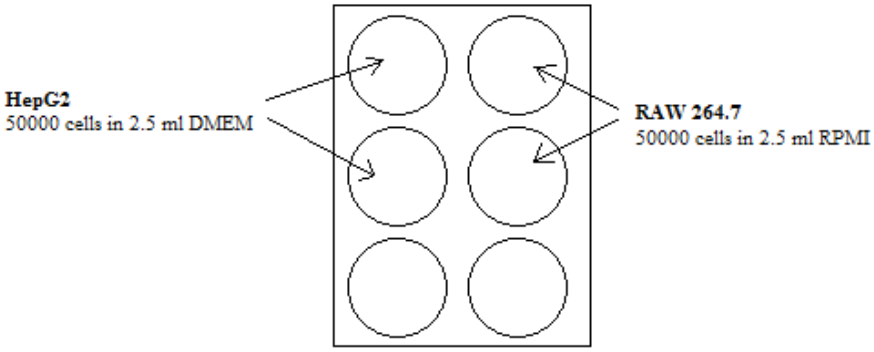

Figure 3.15. Plate layout for 6-well plates used for the cell growth experiment.

3.8 ELISA

3.8.1 Theoretical background

3.8.1.1 ELISA

The enzyme-linked immunosorbent assay (ELISA) is a plate-based sensitive technology used for detection and quantification of different substances. The technology relies on the interaction between immobilized antigens and enzyme-linked antibodies and is dependent on a highly specific antibody-antigen interaction. This interaction is detected by the addition of a substrate, compatible with the conjugated enzyme. Upon addition, the substrate is converted into a measurable product, which can then be used for quantification of the antigen. To enable quantification of unknown sample concentrations, standard curves have to be established [36].

ELISAs are normally divided into several subtypes (see Figure 3.16), which differ in the procedure by which antigens and antibodies are applied to the wells. In *direct ELISA* the antigen is adsorbed to the wells of a multi-well plate. This antigen is then detected by an antibody directly conjugated to an enzyme. In *indirect ELISA* the antigen is, as well, adsorbed to the plate wells, but here detection of the antigen includes two different antibodies: an unconjugated primary antibody, which complexes with the antigen, and an enzyme-conjugated secondary antibody, which complexes with the primary antibody. A third ELISA subtype is the *sandwich ELISA* in which coating or capture antibodies are used for the adsorption of the antigen to the well. The coating antibody is first adsorbed to the well, whereafter the antigen complexes with the coating antibody in a second step. Detection of the antigen is then performed directly or indirectly (indirectly in Figure 3.16). In all subtypes of ELISA, blocking steps are important in order to avoid unspecific binding [36].

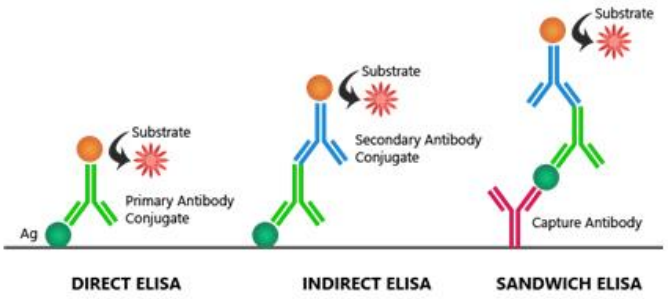

Figure 3.16. ELISA subtypes. Sandwich ELISA has been used during this project. (Image modified from [37])

3.8.1.2 Production of antibodies

Antibodies are one of the constituents of the immune system. They are responsible for binding of specific antigens (usually foreign material). Antibodies are produced by B cells, which belong to the lymphocytes, a subtype of white blood cells, found in the bone marrow, thymus, spleen and lymph nodes [38].

Antibodies used in ELISA are often referred to as monoclonal or polyclonal. While polyclonal antibodies are derived from different B cells and bind to different epitopes within one antigen, monoclonal antibodies are all derived from the same B cell clone and bind to a single epitope within an antigen. A common way of producing monoclonal antibodies is by using the hybridoma technique. By first immunizing a certain species against an antigen epitope, hybridomas can be generated by fusing B cell clones from the spleen of the immunized animal with an immortal myeloma cell line. By then screening for certain epitope specificity, a monoclonal antibody can be isolated. Hybridomas producing this antibody can then be stored in liquid nitrogen for further use. Polyclonal antibodies can be generated in a similar way, but instead of immunizing with a single epitope, the whole antigen is used for immunization of the animal [39]. The coating and primary antibodies that have been used during the ELISA described in 3.8.2 are both monoclonal antibodies. They interact with two different epitopes on the methoxy group of the PEG.

3.8.2 Methodology

3.8.2.1 Coating and blocking of wells

Coating ("capture" in Figure 3.16) antibody (anti-mPEG 7C6, Mouse IgG2a from CAPRA SCIENCE) with an initial concentration of 2.49 mg/ml was diluted in incubation buffer (0.1 M carbonate/bicarbonate buffer, pH 9.6) to a final concentration of 1 µg/ml. 100 µl coating antibody solution was then added to each well of a 96-well plate. The plate was covered with an adhesive plastic film and was then incubated overnight at 4 °C, whereafter the coating antibody solution was removed from all of the wells by flicking the plate over a sink, followed by patting the plate on a paper towel. This procedure was used in all steps where solutions were removed from the wells. Following this, the wells were washed once with 1X PBS, 200 µl/well. 1X PBS was then removed from the wells and 200 µl blocking solution (0.5% BSA in 1X PBS) was added to each well. The plate was incubated on a shaker for 2 hours at room temperature, whereafter the wells were washed three times with 1X PBS (200 µl/well). 1X PBS was removed from the wells after every wash.

3.8.2.2 Incubation with NPs

Filtered NPs were diluted in MQ water, RPMI and DMEM (three separate experiments). Both media were supplied with 10% FBS and 0.5% penicillin/streptomycin solution. NPs were then added to the 96-well plate according to the layout in Figure A.1 (Appendix III), 100 µl/well. In addition, bare NPs (MS01024-3p.1r. B4) and free PEG (polyethylene glycol methyl ether 550', Prod# 202487-500G from Sigma Aldrich) were diluted and added according to the layout. NPs were left out from four of the wells, i.e. only MQ water/RPMI/DMEM was added to these wells. The plate was then incubated on a shaker for 2 hours at room temperature, whereafter solutions were removed from all of the wells. This was followed by three 1X PBS washes, 200 µl/well. 1X PBS was removed from the wells after every wash.

3.8.2.3 Incubation with antibodies

Primary antibody (Anti-Polyethylene glycol antibody [PEG-B-47], ab51257 from Abcam), with an initial concentration of 0.906 mg/ml, was diluted in blocking solution to a final concentration of 5 µg/ml. 100 µl primary antibody solution was added to all wells not marked with *. To wells marked with * only blocking solution was added, 100 µl/well. These were the background controls. The plate was covered with an adhesive plastic film and was then incubated overnight at 4 °C, whereafter primary antibody solution was removed from all of the wells. This was followed by four washes with PBS-tween (0.25% Tween20 in 1X PBS). Secondary antibody (Goat Anti-Rabbit IgG (H+L) HRP, Prod# 31469 from Thermo Fisher Scientific) was diluted 1:15000 in blocking solution. 100 µl secondary antibody solution was then added to each well, whereafter the plate was incubated on a

shaker for 2 hours at room temperature. Secondary antibody solution was then removed from all wells and the wells were washed six times with PBS-tween, followed by two PBS washes.

3.8.2.4 TMB addition and plate reading

100 µl substrate (1-Step™ Ultra TMB-ELISA, Prod# 34028 from Thermo Fisher Scientific) was added to each well, whereafter the plate was incubated for 20 minutes at room temperature. 100 µl stop solution (2 M sulfuric acid) was then added to each well and absorbance was measured at 450 nm, using a Spectra MAX 340 Microplate reader. For all sample duplicates, the average absorbance was calculated, followed by subtraction of the corresponding background absorbance. For each NP in each medium (and MQ water), absorbance was then plotted against P concentration in order to create standard curves.

3.9 In-Cell ELISA

3.9.1 Theoretical background

In-Cell ELISA (ICE) is an immunocytochemistry method used for quantification of e.g. protein levels, posttranslational modifications and cellular uptake of extracellular material. The method is most commonly used for adherent cells that are cultured and fixed at the bottom of the wells of 96-well or 384-well plates (see Figure 3.17). By adding primary antibodies, cell targets are detected. Primary antibodies are, in turn, detected by labeled secondary antibodies [40]. A commonly used labeling is horse radish peroxidase (HRP), an enzyme that upon reaction with a substrate catalyzes oxidation of the substrate. This oxidation leads to a characteristic color that can be detected spectrophotometrically (colorimetric ICE) [41]. The intensity of the color that is developed upon addition of substrate, in turn, becomes a measure of the quantity of the target of interest. A common substrate used in ICE is 3,3',5,5'-Tetramethylbenzidine (TMB). ICE can also be performed using fluorophore labeled secondary antibodies.

Figure 3.17. Principle of colorimetric ICE. Cells are **1)** seeded and fixed in wells, whereafter targets of interest are **2)** detected using primary antibodies. These antibodies are, in turn, **3)** detected by labeled secondary antibodies. Upon **4)** addition of a substrate, color development can be measured spectrophotometrically (Image modified from Thermo Fisher Scientific [42]).

3.9.2 Methodology

3.9.2.1 Seeding of cells

Cells were pre-diluted in medium to a concentration of 300 000 cells/ml for Raw264.7 or 200 000 cells/ml for HepG2. Both media were supplied with 10% FBS and 0.5% penicillin/streptomycin solution. 100 µl cell suspension was added to each well of a 96-well plate, i.e. 30 000 cells or 20 000 cells were added to each well, respectively. The cells were incubated overnight at 37 °C with 5% CO_2 and 100% humidity.

3.9.2.2 Treatment of cells

Following overnight incubation, medium was aspirated from all of the wells. Each coated NP batch was diluted in culture medium, supplied with 10% FBS and 0.5% penicillin/streptomycin solution, to final P concentrations of 10 µM and 100 µM, whereas the bare NPs (MS01024-3p.1r. B4) were diluted to a final P concentration of 100 µM. 100 µl NP solution was added to the wells according to the layout in Figure A.2 (Appendix III). NPs were also left out from two of the wells. After addition of NPs, the cells were incubated at 37 °C with 5% CO_2 and 100% humidity for 1 hour. Except for being added to the wells, 300 µl of each NP solution at each P concentration was transferred into Eppendorf tubes, which were then stored at -22 °C. After incubation, NPs were aspirated from the wells and transferred into Eppendorf tubes, one tube per well. These tubes were also stored at -22 °C. These

samples were later on run with ELISA using the same produce as for the creation of the ELISA standard curves (section 3.8.2).

Following collection of NP solution, the wells were washed once with 200 µl 1X PBS. All washes were performed by addition, followed by removal of the solution used for washing. A multipipette was used for this. Cells were fixed by incubation with 4% paraformaldehyde solution (100 µl/well) for 15 minutes at room temperature. This was followed by three PBS washes (200 µl/well/wash). Cells were then incubated on a shaker with 200 µl freshly prepared permeabilization buffer (0.5 mg/ml saponine in 1X PBS) for 30 minutes at room temperature. After incubation, permeabilization buffer was removed and 200 µl of blocking solution (1X PBS + 1% BSA + 0.05% saponine) was added to each well. Cells were incubated on a shaker with blocking solution for 2 hours at room temperature.

3.9.2.3 Incubation with antibodies

Blocking solution was aspirated and 100 µl primary antibody solution (anti-mPEG 7C6, mouse IgG2a from CAPRA SCIENCE, diluted 1:1000 in 1X PBS) was added to all of the wells except to background controls (marked with * in Figure A.2). To the latter, 100 µl blocking solution was added. Cells were incubated with primary antibody overnight at 4 °C. Then, cells were washed four times with wash buffer (0.25% Tween20 in 1X PBS), 200 µl/well/wash. Wash buffer was aspirated and 100 µl secondary antibody solution (Anti-Mouse IgG (Fc) HRP, SAB3701023 from Sigma Aldrich, diluted 1:2000 in 1X PBS) was added to all wells. Cells were incubated on a shaker with secondary antibody solution for 2 hours at room temperature, whereafter all wells were washed four times with wash buffer, 200 µl/well/wash. Finally, all wells were washed once with 1X PBS. Wash buffer/1X PBS was aspirated properly after every wash.

3.9.2.4 TMB addition and plate reading

100 µl HRP development solution (TMB ELISA Substrate (High Sensitivity), ab171523 from Abcam) was added to all of the wells. Bubbles were removed and the color development was recorded immediately, using a Spectra MAX 340 Microplate reader. Measurements were run with kinetic mode. Absorbance was measured at 650 nm every 20 seconds for 30 minutes. The plate was shaken in between every measurement. For each well, color development data was obtained as area under curve. Mean area under curve was calculated for all duplicates, whereafter the mean background signal (signal for wells not containing primary antibody) for the corresponding NP was subtracted.

3.10 Flow cytometry

3.10.1 Theoretical background

Flow cytometry is a technology that can be employed in cell counting, cell sorting and biomarker detection. The use of flow cytometry allows for measurement of properties of individual cells or particles. As a sample enters the flow cytometer, it is ordered into a stream of single cells, something that is called hydrodynamic focusing (see Figure 3.18).

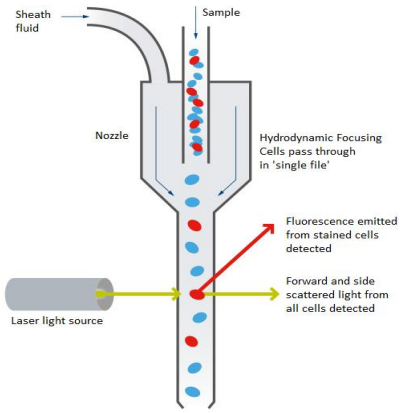

Figure 3.18. Principle of flow cytometry. The arrow marking detection of fluorescence points into the plane of the paper, orthogonal to the laser beam [43].

After being ordered in this way, the cells pass through one or more beams of light and are detected, one by one. Information about a cell's properties is provided both through light scattering and through emission of fluorescence. For the latter (fluorescence) to be provided, cells have to be labeled with a fluorophore. Normally, lasers are used as light sources [43]. When a cell is hit by a laser beam, it scatters light in all directions. Forward scatter (FSC), i.e. the light that is scattered in the forward direction, becomes a measure of the size of the cell, where more scattered light corresponds to a bigger cell. The light is collected by a photomultiplier tube (PMT). Light is however not only scattered in the forward direction, but also sideways. This scatter is called side scatter (SSC) and is measured at an angle approximately 90° to the laser beam. SSC provides information about the internal structures of the cell (e.g. granularity) where a high number corresponds to high internal complexity. Since all cells will be detected individually, all of them will be addressed with unique numbers of FSC and SSC. FSC and SSC results are normally presented in two dimensional scatter plots. Extra information regarding the properties of the cells can be provided from fluorophores, attached to the cells. Such fluorophores are often attached to cell surface receptors or intracellular molecules and through their emission of light at characteristic wavelengths, the existence of certain receptors and molecules can be proven [43]. Depending on which fluorophores that have been used, different detectors are used for detection. For example, FL1 detectors are used for detection of emitted light around 533 nm. This detector is equipped with a 533/30 filter, meaning that the filter is centered at 533 nm, with a width of 30 nm, i.e. emitted light at wavelengths between 503 nm and 563 nm is detected. In the same way, FL2 detectors equipped with 585/40 filters, allows detection of emitted light with wavelengths between 545 nm and 625 nm. FL3 and FL4 detectors detect emitted light with even longer wavelengths [44]. Information regarding emission of light is normally presented in two dimensional fluorescence plots (FL-plots) or in histograms. Commonly used fluorophores are single dyes such as fluorescein isothiocyanate (FITC), phycoerythrin (PE) and allophycocyanin (APC), but tandem dyes and fluorescent proteins are used frequently, as well. FITC is detected with FL1, while PE and APC are detected with FL2 and FL4, respectively [45].

3.10.2 Methodology

3.10.2.1 Seeding of cells

In all of the experiments, cells were seeded into the wells of 12-well plates. The cells were diluted in medium, supplied with 10% FBS and 0.5% penicillin/streptomycin solution, to a final concentration of $2 \cdot 10^6$ cells/ml. 500 µl cell solution was added to each well, i.e. 10^6 cells were seeded into each well. The cells were incubated overnight at 37 °C.

3.10.2.2 Treatment of cells

Following overnight incubation, medium in the 12-well plates was aspirated from all of the wells and NPs were diluted in the appropriate medium to a final P concentration of 100 µM. For PEG coated NPs, 100 mol% coated particles have been used. For each NP batch, 500 µl NP solution was added to two different wells and for each NP batch, one of the duplicate wells was later on treated as the "test" sample, while the other one was treated as the "background" sample. In addition, NPs were left out from two of the wells, i.e. these wells did only contain cells with medium (cell controls) (see Table 3.9). Following this, the cells were incubated at 37 °C for 1 hour. NP solution/medium was then aspirated and all of the wells were washed once with 2 ml PBS wash solution (1X PBS + 0.5% BSA). The wells were then filled up with PBS wash solution once more (1 ml/well), whereafter the cells were removed from the bottom of the wells using a cell scraper. The scraped cells were transferred into separate FACS vials. The vials were centrifuged for 5 minutes at 300 g. Supernatants were discarded and the cells were resuspended in 4% paraformaldehyde (1 ml/vial) for 15 minutes at room temperature, for fixation of the cells. After fixation, the vials were centrifuged for 5 minutes at 300 g. Supernatants were discarded and all vials were washed three times with PBS wash solution. In each washing round, cells were resuspended in 2 ml PBS wash solution, whereafter the FACS vials were centrifuged for 5 minutes at 300 g. Supernatants were discarded after every centrifugation step. Following washing, cells were permeabilized by incubation with saponine solution (1X PBS + 0.5% BSA + 0.05% saponine, 2 ml/vial) for 30 minutes. After permeabilization, the FACS vials were centrifuged for 5 minutes at 300 g. Supernatants were then discarded.

3.10.2.3 Staining with antibodies

Primary antibody (anti-mPEG 7C6, mouse IgG2a from CAPRA SCIENCE) with an initial concentration of 2.49 mg/ml, was diluted (1:500) in saponine solution. 500 µl diluted primary antibody solution was then added to the test sample vials, while saponine solution without antibody was added to the background sample vials (see * in Table 3.9). Primary antibody solution and saponine solution, respectively, were added to the two cell controls in the same way. Cells were incubated for 1 hour at room temperature. After incubation, all FACS vials were centrifuged for 5 minutes at 300 g. Supernatants were discarded and the cells were washed twice with saponine solution, using the same procedure as described earlier. FITC conjugated secondary antibody (Polyclonal Goat Anti-Mouse Immunoglobulins/FITC, F0479 from DAKO) with an initial concentration of 0.40 g/L was diluted (1:200) in saponine solution. 500 µl diluted secondary antibody solution was then added to all vials, except for to one of the cell controls (the one that did not receive primary antibody). The cells were then incubated with secondary antibody for 30 minutes at room temperature. All vials were protected from light during the incubation. Following incubation, the vials were centrifuged for 5 minutes at 300 g, whereafter the supernatants were discarded. The cells were washed twice with saponine solution and thereafter once with PBS wash solution. Finally, the cells were resuspended in 300 µl PBS wash solution.

Table 3.9. Plate layout for flow cytometry experiments.

	1	**2**	**3**	**4**
A	PEG6-9, 100 % 100 µM P	PEG6-9, 100 % 100 µM P *	Bare NP (B4) 100 µM P	Bare NP (B4) 100 µM P *
B	PEG21, 100 % 100 µM P	PEG21, 100 % 100 µM P *	No NP	No NP *
C	PEG44, 100 % 100 µM P	PEG44, 100 % 100 µM P *		

3.10.2.4 Running of samples

For each sample, results were reported with a scatter plot (SSC vs. FSC), an FL-plot (FL2-A vs. FL1-A) and a histogram (FL1-A). The scatter plot was gated so that the fraction containing the smallest cells was excluded, since these cells corresponded to dead cells. Only gated cells were reported in the histogram and in the FL-plot. The FL-plot obtained for the cell control (=no NPs) not treated with primary antibody, was used when setting the background. To compensate for interference between FL1 and FL2, FL1 was corrected by subtracting a percentage of 3.5% from FL2, while FL2 was corrected by subtracting a percentage of 7.0% from FL1. This was done for all of the samples, since all samples should be FL2 negative.

3.11 Fluorescence microscopy

3.11.1 Theoretical background

Fluorescence microscopy relies on the emission of light from certain molecules, and by using this technique it is possible to identify cells and components of cells, present in a sample. This identification can be done with a high degree of specificity. Samples can be fluorescing by themselves or when treated with certain staining fluorophores. A common way to stain samples is by using antibodies, conjugated to fluorophores [46]. Some commonly used fluorophores have already been mentioned in section 3.10.1. Except for these fluorophores, 4',6-diamidino-2-phenylindole (DAPI) is a commonly used fluorescent stain, used for staining of nuclear DNA. The DAPI molecule is heterocyclic and it is thought to bind to the minor groove of the DNA double helix [47].

As light collides with the atoms of a fluorophore sample, excitation of the electrons in the atoms occur. Following this excitation, the excited electrons relax to a lower energy state and the lost energy is emitted as light. This light will be of lower energy, i.e. have a longer wavelength, than the light used for excitation, and the emitted light will be visible in a fluorescence microscope. In the microscope, fluorescing parts will be clearly visible against a dark background [46].

3.11.2 Methodology

3.11.2.1 Seeding of cells

Circular cover glasses with a diameter of 12 mm were cleaned with ethanol, whereafter they were put in the wells of a 12-well plate, one cover glass in each well. Raw264.7 cells were diluted in RPMI medium, supplied with 10% FBS and 0.5% penicillin/streptomycin solution to a final concentration of 10^5 cells/ml. 100 µl cell solution was added onto each cover glass, i.e. 10^4 cells were seeded on each cover glass. The cells were then left to adhere for 2-3 hours at 37 °C, whereafter 1 ml RPMI medium was added to each well. The cells were then incubated overnight at 37 °C in 5% CO_2 and 100% humidity.

3.11.2.2 Treatment of cells

Following overnight incubation, NPs (same as for flow cytometry) were diluted in RPMI medium to a final P concentration of 100 µM. Medium was aspirated from all of the wells, and diluted NPs were added using the same plate layout as for flow cytometry (see Table 3.9). 500 µl NP solution/culture medium was added to each well. Cells were then incubated for one hour at 37 °C. Following this, NP solution/medium was aspirated and all of the wells were washed once with 2 ml PBS wash solution (1X PBS + 0.5% BSA). PBS wash solution was then aspirated. LysoTracker Deep Red (Thermo Fisher Scientific, catalog number: L12492), with an initial concentration of 1 mM was diluted in RPMI medium to a final concentration of 200 nM. This dye was used for labeling and tracking of acidic organelles, such as lysosomes, in the cells. 300 µl diluted LysoTracker solution was added to each well. In all steps where solutions were added to the wells, the cover glasses had to be completely covered by the solution. The cells were incubated for one hour at 37 °C, whereafter the LysoTracker solution was aspirated. All of the wells were then washed twice with 2 ml PBS wash solution. PBS wash solution was aspirated after every wash. The cells were fixed and permeabilized, using the same reagents and procedures as for flow cytometry. In between fixation and permeabilization, the cells were washed three times with PBS wash solution.

3.11.2.3 Staining with antibodies

The cells were stained using the same antibodies, concentration, volumes and procedure as for flow cytometry. Incubation with primary antibody lasted for 1 hour.

3.11.2.4 DAPI staining and mounting

Following antibody staining, DAPI stock solution (Thermo Fisher Scientific, catalog number: D1306) with an initial concentration of 150 mM was diluted to 300 nM in PBS wash solution. 500 µl DAPI staining solution was then added to each well and the cells were incubated for 5 minutes at room temperature, protected from light. DAPI staining solution was then aspirated from all of the wells and the wells were washed five times with PBS wash solution. PBS wash solution was aspirated after every wash. Glass slides (one for each cover glass) were cleaned with disinfection solution and one drop of ProLong® Gold Antifade Mountant (Thermo Fisher Scientific, catalog number: P36934) was added onto each slide. The cover glasses were then lifted up from the wells using a pincette and were placed upside down on the glass slides (with the cells facing the mounting solution). The slides were protected from light until microscopy was performed. Fluorescence microscopy was performed with an Olympus upright microscope (Olympus AX70) operated by Dr. Nishtman Dizeyi, Translational Research, Lund University, CRC, Malmö.

4. RESULTS AND DISCUSSION

4.1 Characterization of coated nanoparticles

The main aim of my Master's project was to investigate the impact of varying coating lengths and coating degrees on cellular uptake of PEG coated NPs. The first milestone was to characterize the NPs that were used for these uptake experiments. According to the literature, particle size, particle charge, as well as coating degree, are some of the important parameters affecting opsonization and cellular uptake of NPs [12]. Having information about these parameters is therefore important in order to make correct conclusions regarding the uptake of NPs *in vivo*. Measuring particle size is also a valuable tool for monitoring of the coating process, which is why it was measured frequently in the project during the course of coating.

4.1.1 Nanoparticle structure

In this project, NPs consisting of a core and a coating shell were used (see Figure 4.1). The core NPs consisted of crosslinked organosilicophosphonate monomers (from now on referred to as **NP monomers**). Each NP monomer contained two atoms of Si and two atoms of P. Throughout this thesis NP concentration has been reported as the concentration of any of these two elements. I coated the core NPs with four different coating precursors; PEG44, PEG21, PEG6-9 and a control coating (CC) (see Figure 4.2). These coating precursors were selected to vary the chain length. The control coating was negatively charged (end methyl group was lost) and was expected to have a high cellular uptake. I varied the amount of coating precursor added during coating between a high amount of coating (100 molecules coating per 100 molecules NP monomer = 100 mol%) and a low amount of coating (20 mol%). Coating precursors were expected to attach to the surface of the core NPs by binding to silane groups present in the NP monomer.

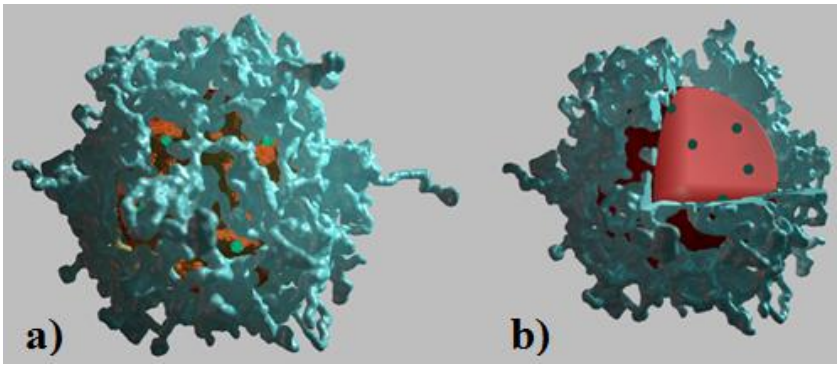

Figure 4.1. a) NP structure with core and coating shell (PEG44). **b)** Cross section of the NP structure in a). (Image from Spago Nanomedical AB)

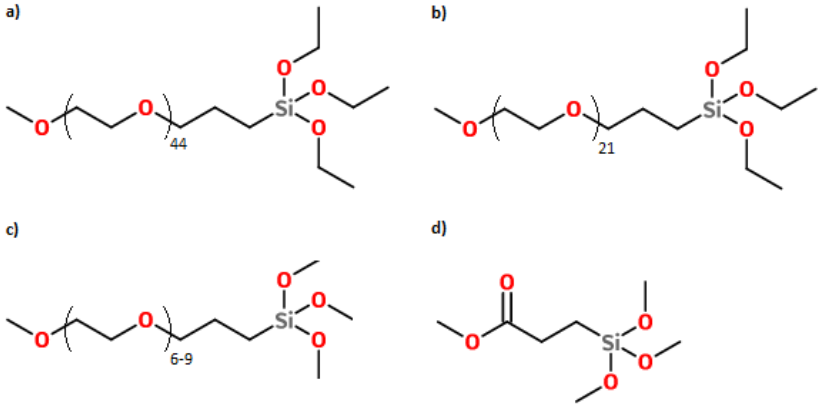

Figure 4.2. Coating precursors. **a)** PEG44 (mPEG44-triethoxysilane), **b)** PEG21 (mPEG21-triethoxysilane), **c)** PEG6-9 (mPEG6-9-trimethoxysilane), and **d)** CC (2-carbomethoxyethyltrimethoxysilane).

4.1.2 Size analysis

Since size of particles is crucial for cellular uptake [12], I analyzed NP size with GPC and DLS following coating. GPC and DLS analysis were also performed during the course of coating in order to keep track of size changes as well as amounts of reactants and products, as the amounts of free coating precursors and coating oligomers (coating precursors bound to each other) should vary over time, due to the injection and consumption of coating. By keeping track of the amount of free coating I was able to determine whether particles were coated or not, since this amount should decrease upon coating of particles. The amount of NPs was expected to be constant over time. However, an increase or decrease in size of these particles could occur, due to the binding of coating. All NP batches were also analyzed with GPC and DLS following filtration, in order to determine the final particle size and for evaluation of the quality of the filtrations.

4.1.2.1 Identification of chromatogram peaks

A typical GPC chromatogram obtained during coating showed several peaks (see Figure 4.3), which I had to identify.

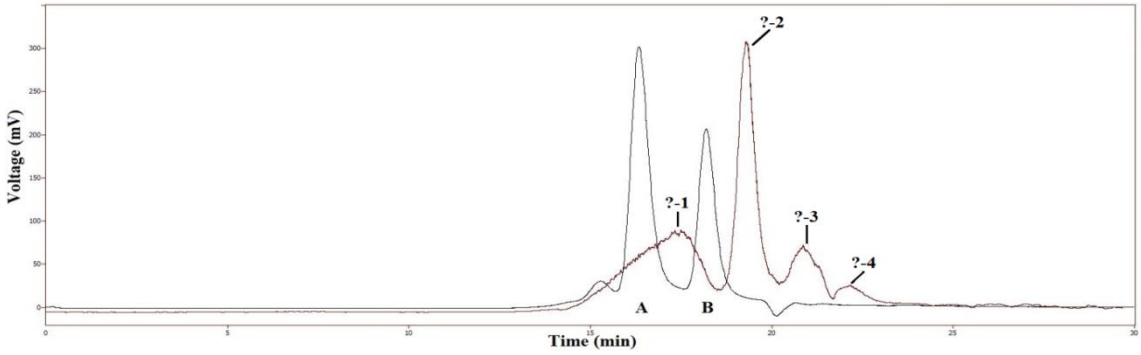

Figure 4.3. Chromatogram for 100 mol% PEG6-9 coated NPs at 48h after injection start. Unidentified ELSD peaks (red) have been labeled with question marks. UV peaks (black) labeled **A** and **B** correspond to BSA and myoglobin (standard proteins), respectively.

Some of these peaks were identified by comparing the 48h coating chromatogram for 100 mol% PEG6-9 coated NPs (see Figure 4.3) with the chromatogram for bare NPs (see Figure 4.4). The peaks in the latter chromatogram were identified preceding the start of this project and were found to correspond to NPs (**1**), side product from NP monomer synthesis (**2**) and salts (**3**), respectively. DLS measurements of bare NPs (6.5 nm) confirmed that the GPC peak for these particles was expected to be between the two proteins in size (in DLS, BSA and myoglobin were 7 nm and 4 nm, respectively). Upon comparison of these chromatograms, I found that NPs (**1**) and salts (**3**) in the chromatogram for bare NPs (see Figure 4.4) corresponded to the leftmost (**?-1**) and rightmost (**?-4**) peaks in the coating chromatogram (see Figure 4.3), whereas the peak corresponding to the NP monomer side product most likely was not visible in the chromatogram for 100 mol% PEG6-9 coated NPs.

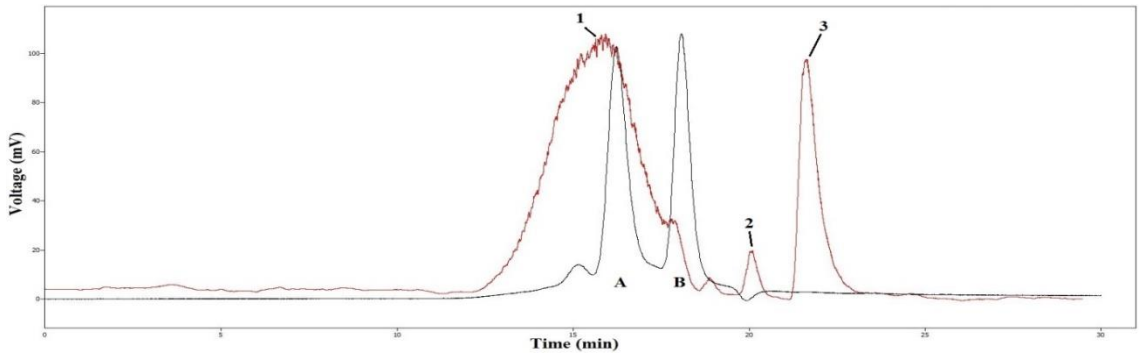

Figure 4.4. Chromatogram for bare NPs (MS01024-3p.1r. B1). UV peaks (black) labeled **A** and **B** correspond to BSA and myoglobin (standard proteins), respectively. ELSD peaks correspond to **1)** NPs, **2)** side product from NP monomer synthesis and **3)** salts.

Peaks corresponding to NPs and salts were found in all chromatograms, regardless of which coating precursor that was used (see Appendix IV). In the 48h coating chromatogram for 100 mol% PEG6-9 coated NPs (see Figure 4.3) I, however, found two more peaks, which were not present in the chromatogram for bare NPs. In order to identify these peaks I compared the 48h coating chromatogram for 100 mol% PEG6-9 coated NPs, with the rest of the chromatograms generated for these particles (100 mol% PEG6-9) during the course of coating (see Figure 4.5). I found that the height of one of the peaks (peak **3** in Figure 4.5, corresponding to **?-2** in Figure 4.3) varied with time, suggesting that this peak should correspond to coating precursor, i.e. coating molecules not bound to NPs. The height of this peak most likely varied due to the injection and consumption of coating precursors.

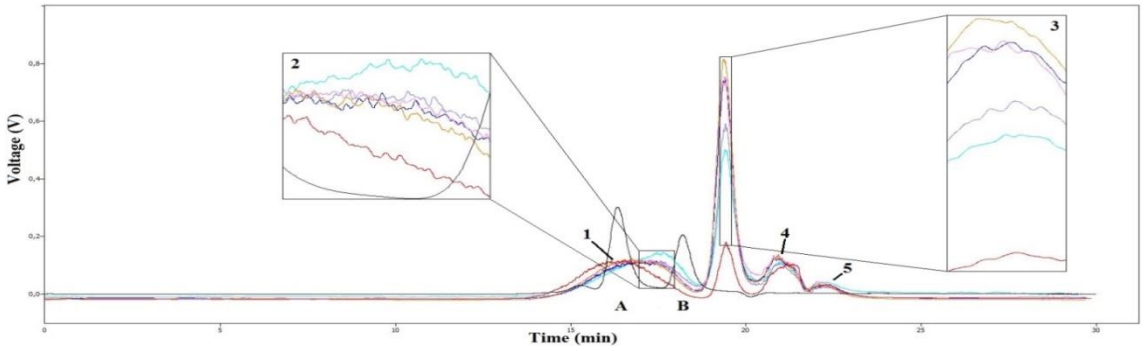

Figure 4.5. Chromatogram for coating of NPs with 100 mol% PEG6-9. UV peaks (black) labeled **A** and **B** correspond to BSA and myoglobin (standard proteins), respectively. ELSD color codes: red = 3h, orange = 18h, pink = 21h, blue = 24h, purple = 27h and, turquoise = 48h.

The height of the other peak (peak **4** in Figure 4.5, corresponding to **?-3** in Figure 4.3) remained rather constant during the course of coating. This peak was present in all chromatograms for coated NPs, but not in the chromatogram for bare NPs, suggesting that this peak corresponded to ethylene glycol, the solvent in which all coating experiments were conducted. This was verified by generating a chromatogram for this solvent solely (see Figure 4.6).

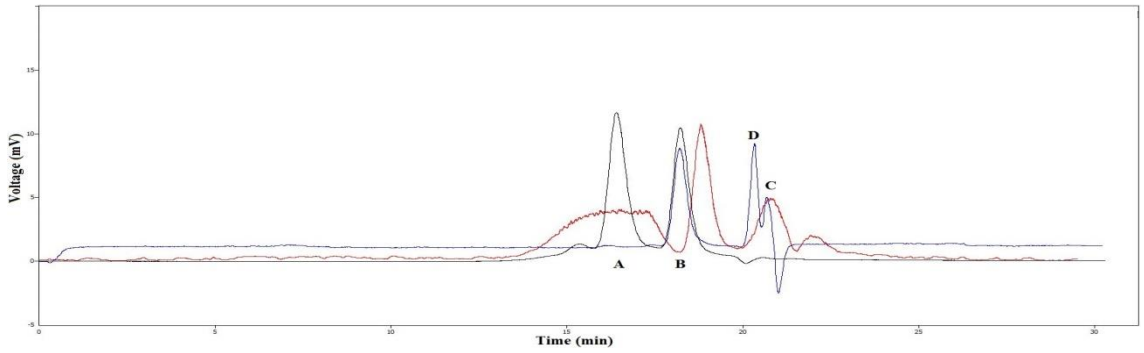

Figure 4.6. Chromatograms for ethylene glycol (blue) and 20 mol% PEG21 coated NPs at 48h (red). UV peaks (black) labeled **A** and **B** correspond to BSA and myoglobin (standard proteins), respectively. **B** was present in the chromatogram for ethylene glycol as well. **C** corresponds to ethylene glycol, whereas **D** corresponds to an unknown impurity.

Except for the four main peaks, which I now have identified, a fifth peak (peak **2** in Figure 4.5) which partly coincided with the NP peak was seen in the chromatogram for 100 mol% PEG6-9 coated NPs. The height of this peak varied with time, but not as much as the coating precursor peak (peak **3** in Figure 4.5). Compared to the coating precursor peak, peak **2** was positioned more to the left, indicating that these molecules were bigger than the free coating precursors. Variations in height of peak **2**, however, indicated that this peak still should be attributed to the presence of coating precursors, but not free ones. Instead, this peak probably corresponded to coating oligomers, i.e. coating precursors bound to each other in particle-like structures. These oligomers were formed when silane groups on adjacent coating precursors reacted with each other to form siloxane bridges. This reaction was the same as the one by which coating precursors bound to NPs.

It is worth mentioning that depending on the coating precursor used, the position of the coating precursor peak varied (see Figure 4.7). This should be attributed to the different sizes of these precursors and was another indication on that the coating precursor peak had been correctly identified.

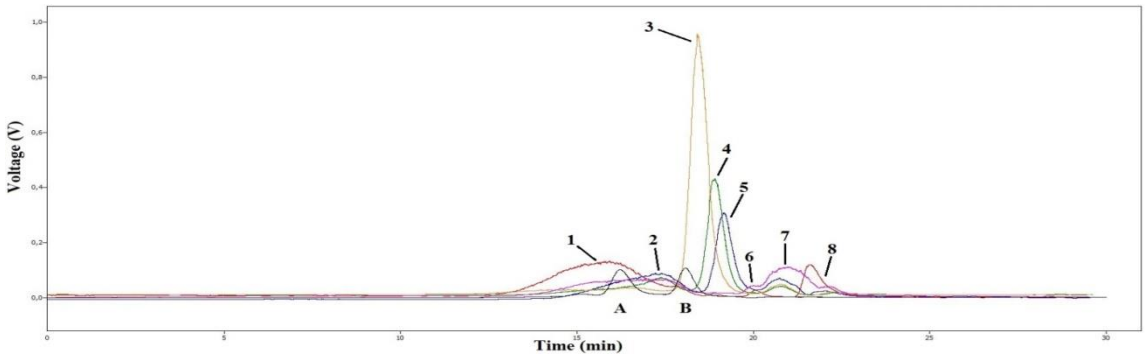

Figure 4.7. Identification of all chromatogram peaks where; **1)** NPs, **2)** coating oligomers, **3)** free PEG44 precursors, **4)** free PEG21 precursors, **5)** free PEG6-9 precursors, **6)** free CC precursors, **7)** ethylene glycol, and **8)** salts. UV peaks (black) labeled **A** and **B** correspond to BSA and myoglobin (standard proteins), respectively. ELSD color codes: red = bare NPs (MS01024-3p.1r. B1), blue = 100 mol% PEG6-9 coated NPs, green = 100 mol% PEG21 coated NPs, yellow = 100 mol% PEG44 coated NPs, and pink = 100 mol% CC coated NPs.

The peaks (NPs, coating oligomers, coating precursors, ethylene glycol and salts) that have been identified in this section, were seen for all NP batches during the course of coating, regardless of which coating precursor that was used. The position of the coating precursor peak, however, varied in between the experiments.

4.1.2.2 Behavior of the coating precursor peak during coating

In order to monitor the coating procedure, samples collected during coating were analyzed with GPC and DLS. During all coating experiments, regardless of which coating precursor that was used, I found that the height of the coating precursor peak varied with time (see Appendix IV). In all experiments, this peak was lowest for the first sample (3h), which could be explained by that only a small amount of coating precursor had been injected at this time point. The peak height then increased over time, as more coating precursor was injected, suggesting that coating precursor was injected faster than it was consumed (see Figure 4.8).

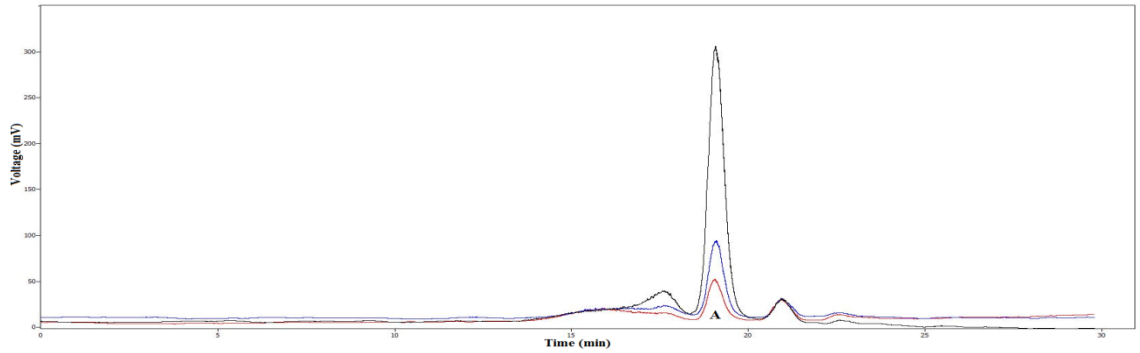

Figure 4.8. Chromatograms for 100 mol% PEG21 coated NPs at t = 3h (red), 6h (blue) and 21h (black). The height of the coating precursor peak (**A**) increased over time, indicating that coating precursor was injected faster than it was consumed.

In several of the experiments the coating precursor peak reached a maximum height within 48 hours and thereafter it decreased. This decrease in height (i.e. decrease in concentration of free coating precursors), was attributed to that coating precursors were used up by 1) attachment to NPs, and 2) the formation of coating oligomers. The time at which this decrease was seen varied in between the experiments. In most experiments in which the coating precursor peak reached a maximum within 48 hours, this maximum was not reached until several hours after injection of coating precursor was finished (22.5h), i.e. the peak increased for some hours, even after finished injection (see Figure 4.9). This behavior might be attributed to the loss of coating precursors from NPs and to decomposition of

coating oligomers, something that indicated that coating of NPs is a dynamic process that goes in both directions. As well as coating oligomers were formed when silane groups reacted with each other to form siloxane bridges, these siloxane bridges could break, regenerating free coating precursors. In all experiments free coating precursors were still present in the solution after the coating procedure was finished.

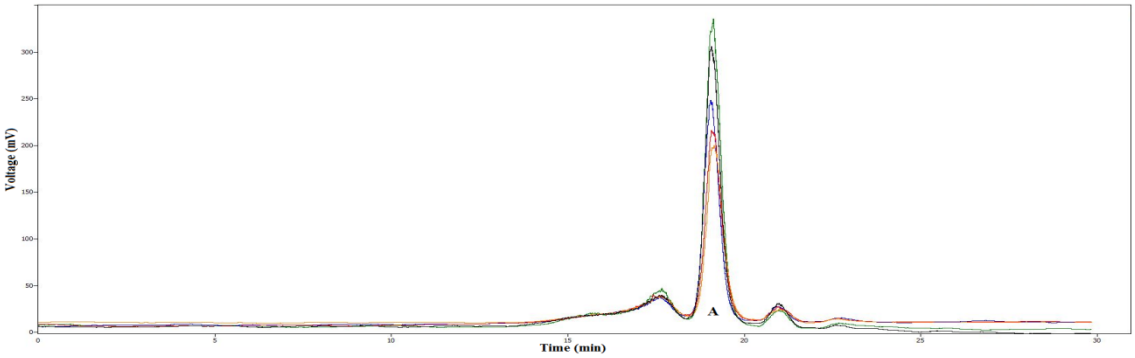

Figure 4.9. Chromatograms for 100 mol% PEG21 coated NPs at t = 21h (black), 24h (blue), 30h (green), 45h (red) and 48h (orange). Injection of coating precursor was stopped at 22.5 h, but yet the coating precursor peak (**A**) reached a maximum at t = 30 h. Thereafter the peak decreased.

4.1.2.3 Size analysis during coating

The size of the NPs was measured using GPC and DLS and according to the chromatograms (see Appendix IV) the size remained relatively constant during coating (the NP peak was not considerably shifted to the left, see Figure 4.10).

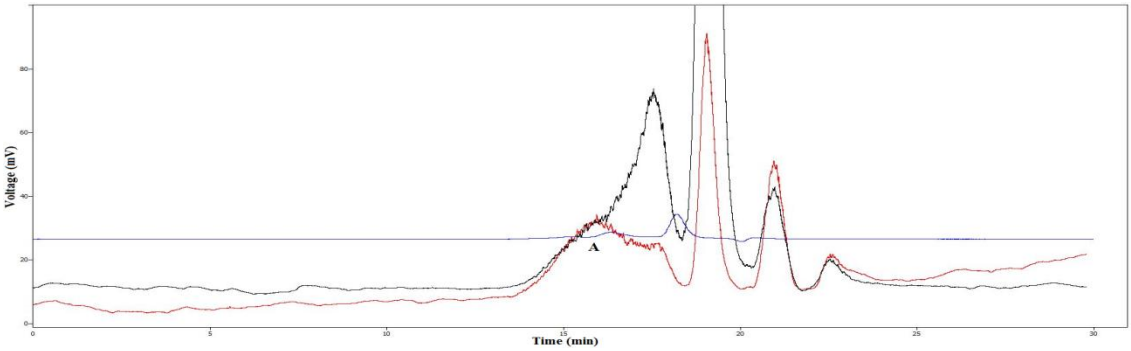

Figure 4.10. Chromatograms for 100 mol% PEG21 coated NPs at t = 3h (red) and 48h (black). The blue chromatogram corresponds to the UV signal for standard proteins (BSA and myoglobin). The size of the NPs (**A**) remained relatively constant during coating.

These GPC results were consistent with the DLS results (see Table 4.1 and Appendix VII), in which no considerable size change was noticed during the course of coating. For example, for 100 mol% PEG21 coated NPs, NP size was stable around 4.2 to 4.8 nm (see Table 4.1 and Figure 4.11). Possible explanations to why NPs did not increase in size during coating could be that coating precursors were not able to bind to the NPs (this is however rather unlikely, since there are indications of consumption of coating precursors) or that coating precursors have bound to NPs in between NP monomers, resulting in fragmentation of the NPs. The latter would probably be more prevalent for short coating precursors (PEG6-9 and CC). Another explanation is that samples taken out during coating also contained molecules smaller than the NPs (e.g. coating precursors and coating oligomers). Thereby, the population distribution in DLS possibly was affected, resulting in an overall smaller particle size. In addition, due to their flexibility it is possible that deformation of PEG precursors on NPs occurred during GPC analysis. This possibly allowed these NPs to pass through gel beads, leading to longer retention time (i.e. smaller particle size), than what would have been the case if the coating precursors were not deformed. Since measured particle size might have been affected by the DLS and GPC techniques themselves, DLS and GPC measurements performed during the course of coating should

only be used as a tool for monitoring the coating process, not for determination of absolute particle size. In none of the experiments, considerable changes in particle size occurred during coating, indicating that the coating process went in the right direction. Big changes towards bigger particle size would have indicated that aggregation and precipitation of NPs occurred, something that should be avoided.

Table 4.1. DLS results for 100 mol% PEG21 coated NPs. At each time point, NP size was reported as the size of the highest bar in the statistics graph (Figure 4.11), with a size range including all bars with a volume percent of ≥ 5.

	0h	**6h**	**21h**	**24h**	**27h**	**30h**	**45h**	**48h**	**After filtration**
$d_{H.\ max}$ (nm)	10.1	8.7	11.7	10.1	8.7	10.1	8.7	11.7	10.1
$d_{H.\ min}$ (nm)	4.8	4.2	4.8	4.8	4.2	4.2	3.6	4.8	4.2
$d_{H.\ mode}$ (nm)	6.5	5.6	7.0	6.5	5.6	5.6	5.6	6.5	6.5

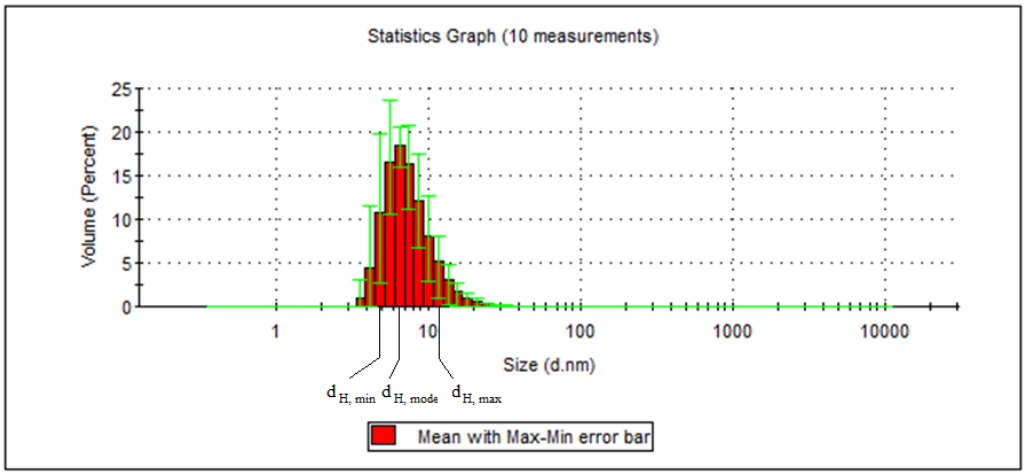

Figure 4.11. DLS volume distribution for 100 mol% PEG21 coated NPs at 48 hours after injection start, with labels on bars corresponding to $d_{H,\ min}$ = 4.8 nm, $d_{H,\ mode}$ = 6.5 nm and $d_{H,\ max}$ = 11.7 nm. 87.4% of the particles were comprised within this size range.

4.1.2.4 Size analysis following filtration

Following coating, I filtered all NP batches in order to remove free coating precursors and coating oligomers, since I wanted to study cellular uptake of NPs only. The final product only contained coated NPs (bare NPs could be present as well). The quality of the filtrations was analyzed by running all permeates and retentates from the 100 kDa filtration on GPC. Permeate and retentate chromatograms contained peaks corresponding to molecules smaller and bigger than 100 kDa, respectively. By comparing retentate and permeate chromatograms, with chromatograms for unfiltered NPs (see Figure 4.12 and Appendix V) I was able to identify which constituents that had been removed during filtration. I found that the peak corresponding to free coating precursors was present in the permeates for all NP batches, while the peak corresponding to NPs was present in the retentates, which means that I selected a good filter size for separation of NPs and coating precursors. The coating precursor peak was absent in the retentate chromatograms for all filtered NP batches, except for 100 mol% PEG44 coated NPs (see Figure 4.12). In the latter, a small coating precursor peak (**3**) was visible, suggesting that coating precursors had not been completely removed. For the rest of the batches, filtration was regarded as successful with respect to the removal of free coating precursors.

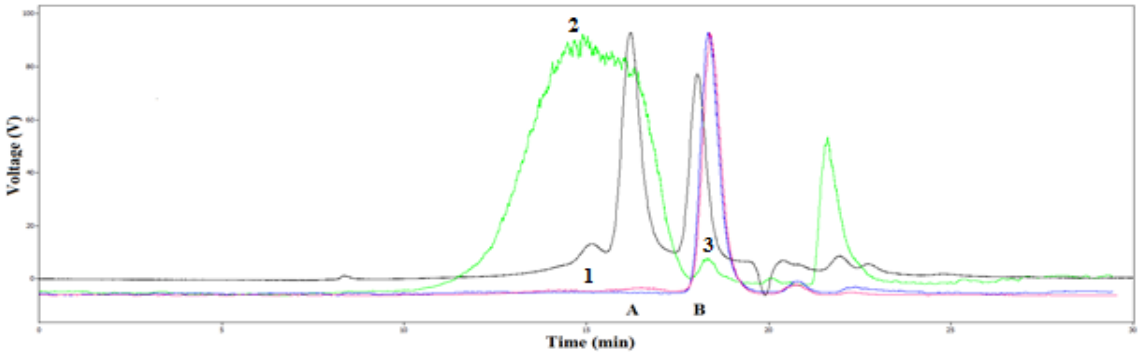

Figure 4.12. Chromatogram for 100 mol% PEG44 coated NPs. Blue, green and red ELSD curves correspond to permeate, retentate and unfiltered NPs, respectively. UV peaks (black) labeled **A** and **B** correspond to BSA and myoglobin (standard proteins), respectively, while **1** and **2** marks the position of the NP peaks. **3** marks the position of the coating precursor peak.

In order to fully outline the quality of the filtrations, removal of coating oligomers had to be taken into account as well. Since the coating oligomers did not constitute separate peaks, but partly coincided with the NP peak, removal of these oligomers was analyzed by examining the shape of the NP peak. For all NP batches, except for PEG44 coated NPs (both coating degrees, see Appendix V), the NP peak adopted a more symmetric profile after filtration, compared to before (see Figure 4.13). These profile alterations should be attributed to the removal of molecules smaller than the NPs, i.e. coating oligomers. Based on this reasoning, filtrations were regarded as successful for all NP batches, aside from PEG44 coated NPs. The unsuccessful removal of PEG44 coating oligomers could be attributed to these oligomers' bigger size, resulting in these oligomers' retention on the retentate side of the 100 kDa filter.

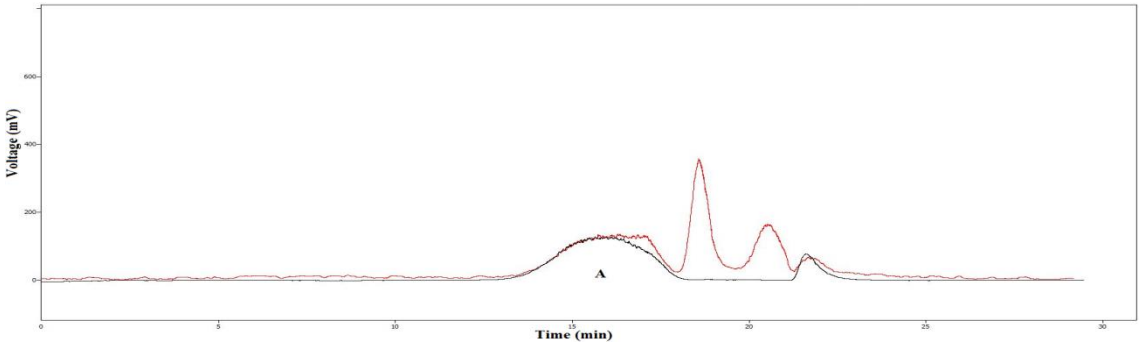

Figure 4.13. Chromatogram for 20 mol% PEG21 coated NPs at 48h (red) and after 100 kDa filtration (black). The NP peak (**A**) adopted a more symmetric profile after filtration, compared to before.

Even though particle size remained relatively constant during the coating procedure (see Appendix V and Appendix VII), GPC and DLS results generated after filtration showed that most of the coated NPs were bigger after filtration compared to before coating (see Figure 4.14 and Table 4.2). According to DLS results, 20 mol% PEG6-9 coated NPs were the only particles that were smaller after filtration, compared to before coating (see Table 4.2). These particles were also among the smallest according to GPC results (see Figure 4.14). The increase in particle size seen for the rest of the particles was attributed to the removal of smaller molecules during filtration. The removal of small molecules shifted the population distribution towards bigger particle size. Internal size relations between NPs coated with different coatings and coating degrees were generally, however, not consistent in between GPC and DLS results. According to DLS results, mode size of PEG coated NPs landed in between 5.6 nm and 8.7 nm for all filtered NP batches, whereas CC coated NPs tended to be slightly bigger, 11.7 nm (see Table 4.2). This result was not consistent with the GPC results in which PEG44 coated NPs seemingly were bigger than the other particles (see Figure 4.14).

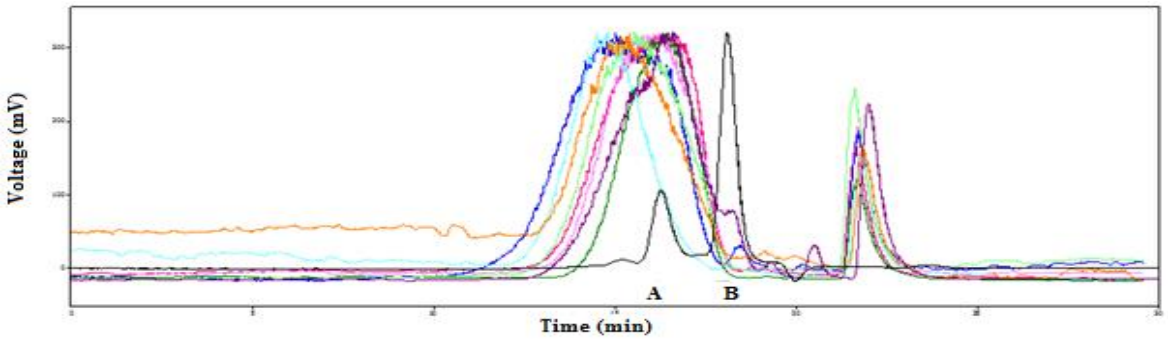

Figure 4.14. Chromatograms of 100 kDa retentates for all coated NP batches (the final product), as well as bare NPs (MS01024-3p.1r. B1). UV peaks (black) labeled **A** and **B** correspond to BSA and myoglobin (standard proteins). ELSD color codes: purple = bare NPs (MS01024-3p.1r. B1), light green = 20 mol% PEG6-9 coated NPs, green = 100 mol% PEG6-9 coated NPs, light pink = 20 mol% PEG21 coated NPs, pink = 100 mol% PEG21 coated NPs, light blue = 20 mol% PEG44 coated NPs, blue = 100 mol% PEG44 coated NPs, and orange = 100 mol% CC coated NPs.

Table 4.2. Size of coated NPs following filtration, measured with DLS. The size of bare NPs (MS01024-3p.1r. B1) has also been measured.

Nanoparticle	$d_{H,\ min}$ (nm)	$d_{H,\ mode}$ (nm)	$d_{H,\ max}$ (nm)
NP_{bare}	4.8	6.5	10.1
$NP_{PEG6\text{-}9,\ 20\ mol\%}$	4.2	5.6	10.1
$NP_{PEG6\text{-}9,\ 100\ mol\%}$	5.6	8.7	13.5
$NP_{PEG21,\ 20\ mol\%}$	5.6	7.5	11.7
$NP_{PEG21,\ 100\ mol\%}$	4.2	6.5	10.1
$NP_{PEG44,\ 20\ mol\%}$	5.6	7.5	11.7
$NP_{PEG44,\ 100\ mol\%}$	6.5	8.7	13.5
$NP_{CC,\ 100\ mol\%}$	8.7	11.7	21.0

4.1.2.5 Size analysis following storage

I also analyzed the size of the coated NPs with GPC after 30 days of storage (after finished filtration) at room temperature. The analysis was performed in order to investigate the impact of storage on NP size and coating. For all NP batches I noticed that the NP peak was shifted slightly to the right in the chromatograms generated after storage (see Figure 4.15 and Appendix VI), compared to in the corresponding chromatograms generated directly after filtration, showing that particle size decreased during storage. In addition, a new small peak at the position of free coating precursors appeared in all chromatograms generated after storage, suggesting loss of coating precursors from the NPs. The arising of this peak also explains the decrease in NP size, since loss of coating precursors should lead to a smaller particle. The results obtained from this size analysis, indicate that the coating degree of the particles is affected by storage, which should be kept in mind for the cell uptake experiments. A complementary proof would be to filter off the loose coating with 100 kDa filter and measure concentrations of P and Si by ICP-OES, to see a change in the degree of coating. Loss of coating precursors would be characterized by a decreased Si to P ratio.

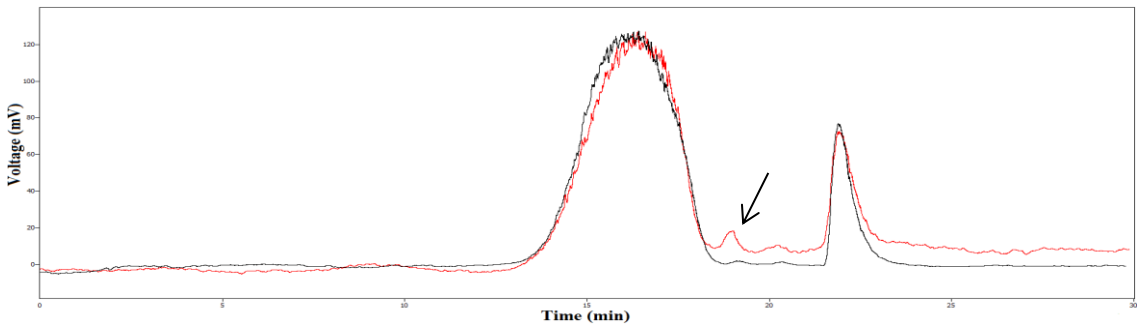

Figure 4.15. Chromatograms for 20 mol% PEG21 coated NPs. ELSD color codes: black = 100 kDa retentate directly after filtration, red = 100 kDa retentate after being stored for 30 days at room temperature. The arrow marks the position of the coating precursor peak.

4.1.3 Coating degree of nanoparticles

According to the chromatograms (see Appendix IV) free coating precursor was still present in the NP solutions after finished coating. The excess coating was removed by filtration. To determine the real degree of coating, concentrations of Si and P were determined with ICP-OES after filtration of the NP batches (see Table 4.3). Si was present in the coating, as well as in the NP core, whereas P was only present in the core. For each coated NP batch, coating degree was calculated using an equation found in Appendix VIII. I aimed to synthesize NPs with a low and a high degree of coating, in order to be able to compare the effect of coating degree on cellular uptake. From Table 4.3 it is apparent that I have succeeded since all 100 mol% coated NPs have a higher coating degree than the corresponding 20 mol% coated NPs. However, in all of the coating experiments (see Appendix IV) free coating precursor was still present in solution after 48 hours. It is possible that I would have been able to reach even higher coating degrees if the NPs had been heated for a longer time at another temperature. Most likely, the maximum coating degree (in mol%) would have been higher for NPs coated with shorter coating precursors, than for NPs coated with longer coating precursors. Compared to shorter precursors, longer coating precursors would probably occupy bigger surface areas, preventing other coating precursors from binding. However, if having the same real coating degree (in mol%), NPs coated with a longer coating precursor would probably be more covered than NPs coated with a shorter precursor, due to the longer precursor's ability of occupying more of the NPs' surface area (see Figure 4.16).

Table 4.3. [Si] and [P] in mM for coated and filtered NPs. These concentrations, as well as [Si] and [P] for bare NPs (these were 77.02 mM and 75.41 mM for Si and P, respectively), were used for calculation of coating degree of the particles (see Eq. 2).

Nanoparticle	$[Si]_{after\ filtration}$ (mM)	$[P]_{after\ filtration}$ (mM)	Coating degree (mol%)
$NP_{PEG6\text{-}9,\ 20\ mol\%}$	18.13	16.48	15.75
$NP_{PEG6\text{-}9,\ 100\ mol\%}$	15.53	13.42	27.18
$NP_{PEG21,\ 20\ mol\%}$	15.22	13.79	16.47
$NP_{PEG21,\ 100\ mol\%}$	18.94	15.88	34.27
$NP_{PEG44,\ 20\ mol\%}$	10.95	9.53	25.53
$NP_{PEG44,\ 100\ mol\%}$	22.47	15.08	93.74
$NP_{CC,\ 100\ mol\%}$	8.07	6.49	44.42

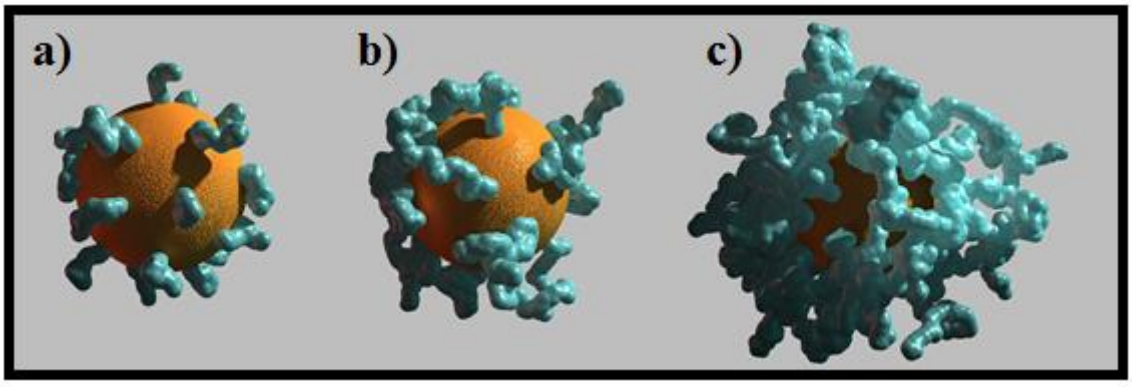

Figure 4.16. Coverage of 6.5 nm NPs, coated with **a)** PEG6-9, **b)** PEG21 and **c)** PEG44. The real coating degree is 16 mol% for all particles. (Image from Spago Nanomedical AB)

NPs coated with PEG44 seemed to have a considerably higher coating degree than the corresponding PEG6-9 and PEG21 coated NPs (see Table 4.3). GPC chromatograms (see Figure V.V and Figure V.VI in Appendix V) show that the higher coating degree was due to the unsuccessful removal of PEG44 oligomers and some free precursors during filtration of these batches. The PEG44 coated batches contained coating, which was not attached to the NPs. The real coating degree obtained for PEG44 coated NPs was therefore lower than given in Table 4.3. For the shorter coating precursors (CC, PEG6-9 and PEG21), oligomers seemingly were small enough to be successfully removed during

filtration (see Figure V.I-V.IV and Figure V.VII in Appendix V). Therefore, measured real coating degree for these batches was regarded as correct.

4.1.4 Zeta potential

NP charge strongly affects cellular uptake of NPs and previous studies have shown that charged particles are opsonized faster than neutral ones [12]. By measuring the zeta potential of bare (MS01024-3p.1r. B4) and coated NPs, I aimed to estimate the magnitude of the particle charge. I also aimed to use the magnitude of the zeta potential as a complementary proof of that particles had been coated.

Upon zeta potential measurements at pH 7.11 of all NP batches I found that bare NPs had a zeta potential peak around -50 mV. As the particles were coated with 100 mol% CC, the zeta potential increased to about -40 mV, while at 20 mol% of PEG coating, another increase to around -30 mV could be seen. The zeta potential increased even more, to around -20 mV, when particles were coated with 100 mol% PEG coating, indicating that zeta potential of NPs was affected by the degree and type of coating (see Table 4.4). Different PEG lengths did, however, not show a significant impact on zeta potential. As noticed, the most negative zeta potential was obtained for bare NPs, while less negative zeta potentials were then obtained for coated NPs. These results could possibly be explained by the dielectric constants of the solvents surrounding the NPs. Bare NPs were fully surrounded by water, while coated NPs were surrounded by water as well as coating. Since the dielectric constant of water (80.1) was higher than the dielectric constant of the coating (here referred to as the dielectric constant of 1,2-dimethoxyethane, 7.2), water was able to isolate the negative NP charge and prevent positive counter-ions from approaching, while these counter-ions probably were more prevalent in the proximity of the coated NPs, giving the latter particles less negative zeta potentials. The differences seen in zeta potential for 20 mol% and 100 mol% PEG coated NPs could be explained in a similar way. Due to the lower degree of coating precursors surrounding 20 mol% coated particles, more water molecules were expected to reside close to these NPs, compared to the 100 mol% coated NPs, giving better charge shielding (i.e. more negative zeta potential) for particles with lower coating degree (see Figure 4.17). It is also worth mentioning that zeta potential decreases with increased distance of the slipping plane from the particle surface [28]. Another explanation for the less negative zeta potentials obtained for coated NPs, compared to bare ones could therefore be that upon coating of NPs, the slipping plane was moved outwards from the particle surface, resulting in less negative zeta potentials for these particles. The zeta potential of CC coated NPs, just slightly less negative than that of bare NPs, was attributed to the negative charge of this coating, in combination with a slipping plane, slightly moved outwards from the particle surface.

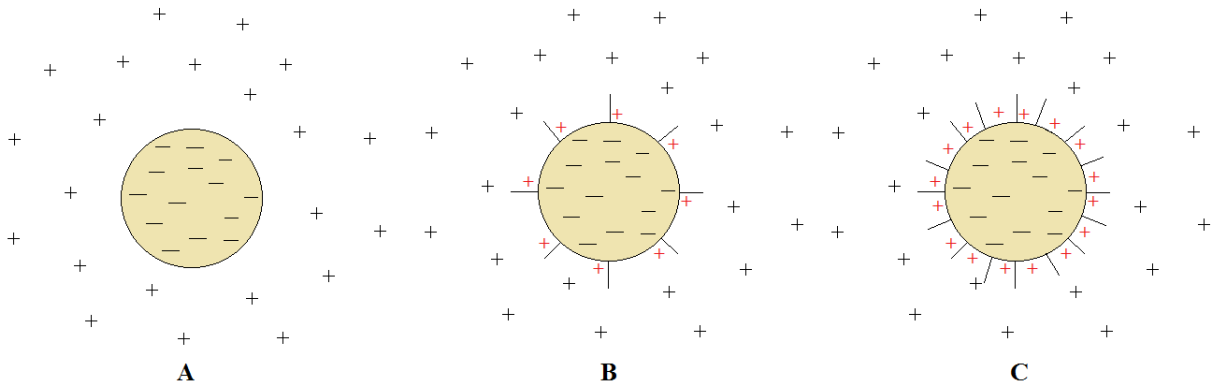

Figure 4.17. Impact of dielectric constants of solvents on zeta potential of NPs. **A)** Bare NPs were surrounded by water. Due to the high dielectric constant of water, isolation of NP charge occurred and a high (negative) zeta potential was obtained. **B)** NPs partly coated with PEG had a less negative zeta potential, compared to the bare NPs, due to the lower dielectric constant of PEG compared to water. Some water molecules were, however, still present in between coating precursors. **C)** As the coating degree was increased, more water molecules were pushed away and charge isolation of the NPs decreased even more, resulting in an even less negative zeta potential.

4.1.5. Nanoparticle characteristics summary

Characteristics of the particles that have been used in subsequent experiments throughout this Master's thesis project are summarized in Table 4.4. Particles had a similar size and pH and were diluted to the same concentration for cell uptake experiments. Except for one particle (100 mol% CC coated NPs), all particles that were used for further experiments ended up in the size range of 5.6 nm to 8.7 nm, indicating that NP size was only slightly affected by the coating process (see Table 4.4). pH was within the range 7-8 for all particles (see Table 4.4). Coating degree (mol%) varied in between the particles in such a way that all 20 mol% coated NPs had a lower coating degree (mol%), compared to the corresponding 100 mol% coated NPs (see Table 4.4). Due to filtration and to the attachment of coating, [P] (mM) and [Si] (mM) varied in between the particle batches (see Table 4.4). Preceding cellular uptake experiments, all NPs were diluted in order to have the same NP ([P] in mM) concentration. [Si] (mM) still varied in between the diluted particle batches, allowing me to examine the impact of coating degree on cellular uptake of the particles. I also aimed to study the impact of coating length on cellular uptake.

Table 4.4. Summarized characteristics of NPs used in subsequent experiments.

Coating	$d_{h,\ mode}$ (nm)	pH	Zeta potential, ζ (mV)	[P] (mM)	[Si] (mM)	Coating degree (mol%)
PEG6-9, 20 mol%	5.6	7.50	-28	18.13	16.48	15.75
PEG6-9, 100 mol%	8.7	7.51	-19	15.53	13.42	27.18
PEG21, 20 mol%	7.5	7.13	-30	15.22	13.79	16.47
PEG21, 100 mol%	6.5	7.33	-21	18.94	15.88	34.27
PEG44, 20 mol%	7.5	7.72	-33	10.95	9.53	25.53
PEG44, 100 mol%	8.7	7.87	-20	22.47	15.08	93.74
CC, 100 mol%	11.7	7.37	-40	8.07	6.49	44.42
Bare NPs (B4)	6.5	7.96	-50	75.41	77.02	0

4.2 Calcium stability and aggregation analysis

RPMI and DMEM were used as culture media in the biological experiments in this project. The composition of these media was supposed to simulate physiological conditions. Studies have shown that aggregation of NPs may occur as the particles encounter biological environments [4]. Since aggregates of NPs may affect the targeting efficiency of NPs, as well as the cellular uptake mechanisms [4], I wanted to analyze the aggregating behavior of the NPs in the culture media. Calcium (Ca) is believed to be one of the main factors contributing to aggregation of NPs in culture media (due to chelation) and therefore the aggregating behavior of NPs in pure Ca solutions was also examined. Ca concentrations in Ca solutions (0 - 2.0 mM), as well as in culture media (0.2 mM for RPMI and 1.3 mM for DMEM), were in the same range as the real physiological Ca concentration (~ 2.2 mM in human plasma, half of it free, half of it bound). I have used *aggregation* synonymously with *precipitation* throughout sections 4.2.1 and 4.2.2. It is however possible that smaller aggregates also have been formed without causing precipitation.

4.2.1 Calcium induced nanoparticle aggregation

The effect of Ca concentration on NP aggregation was analyzed by incubation of NPs with buffered Ca solutions with increasing Ca concentration. I found that high-amount PEG coated NPs were able to tolerate higher Ca concentrations without aggregating, compared to their low-amount PEG coated counterparts (see Figure 4.18). For all low-amount PEG coated NPs, increased aggregation was seen as the Ca concentration was increased from 0.25 to 0.50 mM. At the latter Ca concentration, considerable aggregation was noticed for 100 mol% CC coated and bare NPs, as well (see Figure 4.18). For high coating degree, Ca induced aggregation correlated inversely with coating length. The particles tolerating the highest Ca concentration without aggregating were the high-amount (100 mol%) PEG44 coated NPs, followed by high-amount (100 mol%) PEG21 coated and high-amount (100 mol%) PEG6-9 coated NPs (see Figure 4.18). For low coating degree, Ca induced aggregation behavior was the same as for bare NPs.

At low Ca concentration, no particle aggregation was seen, regardless of which coating precursor was used and even in the absence of coating. Most likely, Ca chelating sites were present both inside and on the surface of NPs, with preference for chelating sites inside the particles. My interpretation of the Ca aggregation results is that at low Ca concentration, chelating sites inside the particles were occupied first (see Figure 4.19a). This would explain why no considerable particle aggregation occurred at low Ca concentration. When Ca concentration increased, Ca ions could occupy chelating sites on the surface of NPs as well, leading to aggregation of these particles as they were approaching each other (see Figure 4.19b). Most likely, this was what happened to the bare NPs, as well as the particles with low coating degree and CC coated NPs, as Ca concentration was increased from 0.25 to 0.50 mM. Most of the particles with high coating degree, on the other hand, remained in solution at 0.50 mM Ca, which I attribute to the fact that these particles were prevented from approaching each other, due to their coating layer. Probably, the low coating degree was not high enough to keep these particles separated by such a distance that chelation and aggregation did not occur. The high coating degree, however, seemed to prevent considerable interaction between Ca chelating sites of adjacent NPs (see Figure 4.19c). Therefore, less aggregation was seen for these particles.

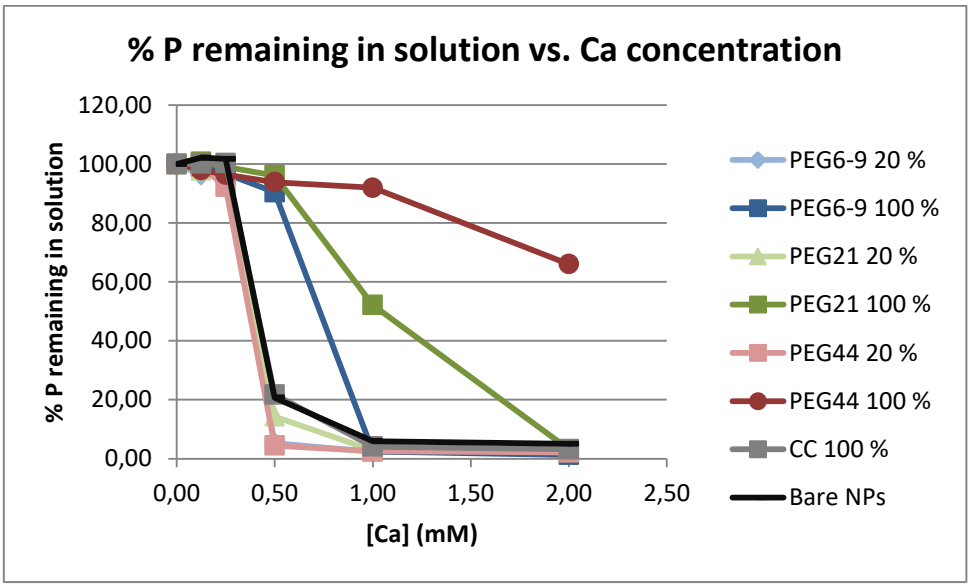

Figure 4.18. Percentage of NPs (P) remaining in solution (= % of NPs not aggregated) versus [Ca] (mM). The curve corresponding to 20 mol% PEG6-9 coated NPs (light blue) is hidden behind the curve corresponding to 20 mol% PEG44 coated NPs (pink). NPs were diluted to 0.5 mM P.

The fact that bare NPs and NPs with low coating degree, aggregated at 0.5 mM Ca may indicate that PEG length probably had no considerable impact on aggregation of poorly coated NPs. For high-amount coated NPs I, however, found indications of that PEG length had an impact on the Ca induced NP aggregation. This behavior could possibly be attributed to the longer PEG precursors' ability of covering more of the particle surface, compared to shorter PEG precursors, which was shown previously (see Figure 4.16). Another explanation could be that NPs coated with longer coating precursors repelled each other more efficiently, compared to NPs coated with shorter coating precursors, due to the higher flexibility of the longer precursors. Entropic repulsion is proportional to the flexibility of the molecule causing the repulsion and thereby repulsion should be larger for NPs coated with longer, more flexible coating precursors [10]. Both these were possibly factors contributing to increased steric hindrance between NPs, which in turn prevented Ca chelating sites on adjacent particles from getting close to each other. Thereby, NP aggregation probably was prevented or, at least, reduced. Even though the CC coated NPs were coated with a high amount of coating, aggregation to the same extent as for bare and low-amount PEG coated NPs could be seen for these particles (see Figure 4.18). This could possibly be attributed to the charge, as well as to the length of this coating precursor. In addition to being negatively charged, this coating precursor was much shorter than all PEG precursors, not contributing to steric hindrance between particles. Therefore, interaction between Ca ions and chelating sites on NPs was likely to occur among these particles.

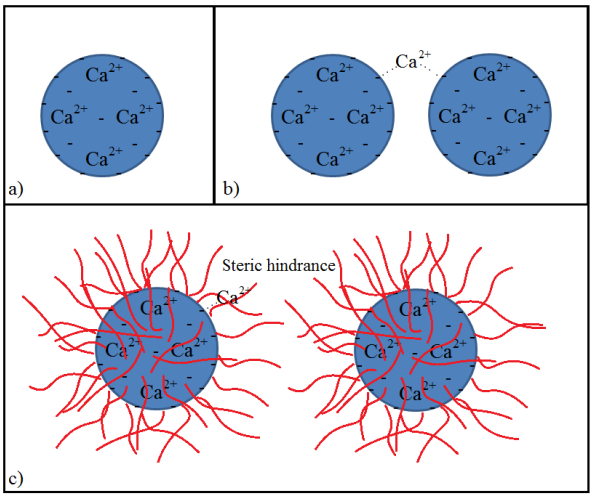

Figure 4.19. Aggregating behavior of NPs at **a)** low [Ca], **b)** high [Ca], and **c)** high [Ca], but with coated NPs (steric hindrance prevents aggregation).

4.2.2 Nanoparticle aggregation in culture media

Aggregation of NPs in culture media was analyzed by incubating NPs with RPMI and DMEM media. This analysis was performed in order to find a suitable NP concentration that could be used for studies of cellular uptake of the particles. Instead of varying [Ca] (this was kept constant at 0.2 mM and 1.3 mM in RPMI and DMEM incubations, respectively) NP concentration ([P] in mM) was varied (see Table 4.5).

Table 4.5. Percentage of Si remaining in solution (= % of NPs not aggregated) for NPs in RPMI and DMEM. %Si was used to quantify unprecipitated NPs instead of %P, due to high background P content in the cell media.

	RPMI				**DMEM**			
	% Si remaining in solution for [P] (mM):				**% Si remaining in solution for [P] (mM):**			
	0.01	**0.1**	**1.0**	**3.0**	**0.01**	**0.1**	**1.0**	**3.0**
$NP_{PEG6\text{-}9,\ 20\ mol\%}$	105	2.89	7.13	94.4	86.9	3.71	0.944	1.44
$NP_{PEG6\text{-}9,\ 100\ mol\%}$	208	7.14	10.3	95.4	117	0	1.16	20.8
$NP_{PEG21,\ 20\ mol\%}$	203	14.6	1.48	95.3	71.4	1.60	1.23	1.80
$NP_{PEG21,\ 100\ mol\%}$	197	31.3	75.8	101	64.7	106	2.15	90.0
$NP_{PEG44,\ 20\ mol\%}$	195	9.28	1.59	94.0	113	1.99	1.41	1.67
$NP_{PEG44,\ 100\ mol\%}$	196	91.1	101	99.6	104	35.2	6.47	94.3
$NP_{CC,\ 100\ mol\%}$	93.4	13.0	18.0	91.6	53.7	4.39	5.40	11.3
NP_{bare}	90.7	9.69	7.31	96.4	57.4	83.1	11.3	6.13

I found that particles generally aggregated more in DMEM medium (see Figure 4.21 and Table 4.5), compared to in RPMI medium (see Figure 4.20 and Table 4.5). I attribute this behavior to Ca-dependent aggregation, as [Ca] was higher in DMEM than in RPMI, which should cause more chelation of Ca and aggregation of NPs in DMEM. I varied NP concentration ([P] in mM), with the hypothesis that NP aggregation is related to NP concentration and that by reducing the NP concentration, I would reach a point where aggregation was very low. For both media, the least degree of aggregation was seen for [P] = 0.01 mM (lowest particle concentration) and [P] = 3.0 mM (highest particle concentration). In RPMI all particles remained in solution with more than 90% for [P] = 0.01 mM, whereas in DMEM all particles remained in solution with more than 50% at this [P]. This result was in agreement with my hypothesis that at this low [P], particles were too few to aggregate in the presence of Ca, i.e. chelation did not occur due to the large distance in between the particles. For [P] = 3.0 mM all particles remained in solution with more than 90% in RPMI, whereas in DMEM, two particle batches remained in solution with more than 90%. My hypothesis is that at this high [P] the abundance of NPs prevented full aggregation of the particles, due to complete uptake of Ca in the inner chelation sites of the NPs. For NP concentrations in between [P] = 0.01 mM and [P] = 3.0 mM ([P] = 0.1 mM and [P] = 1.0 mM) several particles aggregated considerably in both media.

More particles seemed to remain in solution at [P] = 0.1 mM, compared to at [P] = 1.0 mM, indicating that lower [P] probably would be more favorable in order to avoid aggregation of NPs, in agreement with my hypothesis at the start of the experiment. Similarly to what was found for NPs in section 4.2.1, indications of PEG length dependent aggregation were found for NPs in culture media. This experiment demonstrated that high-amount (100 mol%) PEG44 and high-amount (100 mol%) PEG21 coated NPs generally tolerated a broader range of [P], compared to the rest of the particles (see Figure 4.20, Figure 4.21 and Table 4.5). This could possibly be explained using the same reasoning as in section 4.2.1, i.e. due to steric hindrance caused by longer PEG precursors, aggregation was prevented. This trend was, however, less obvious here, compared to in section 4.2.1.

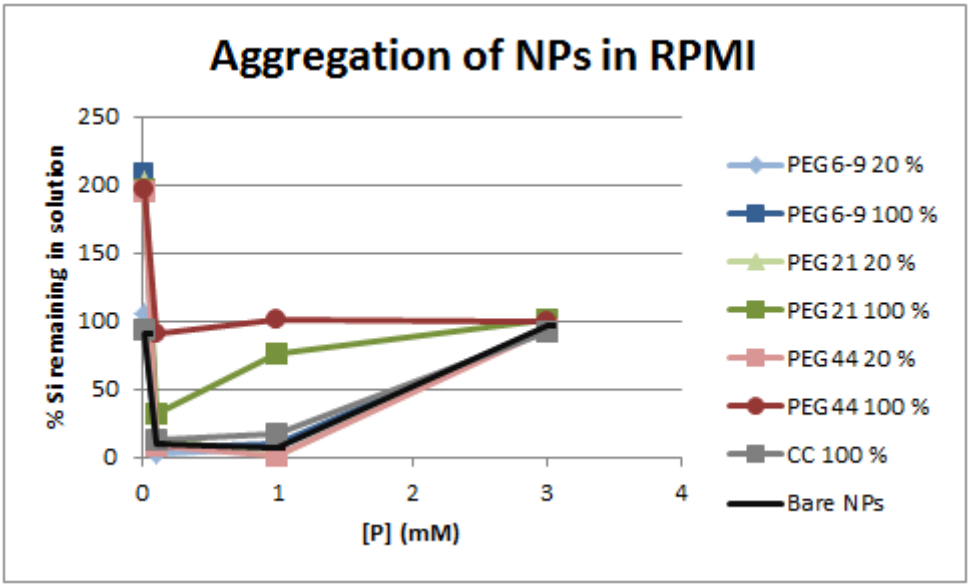

Figure 4.20. Percentage of Si (= % of NPs not aggregated) remaining in solution vs. [P] (mM) for NPs in RPMI.

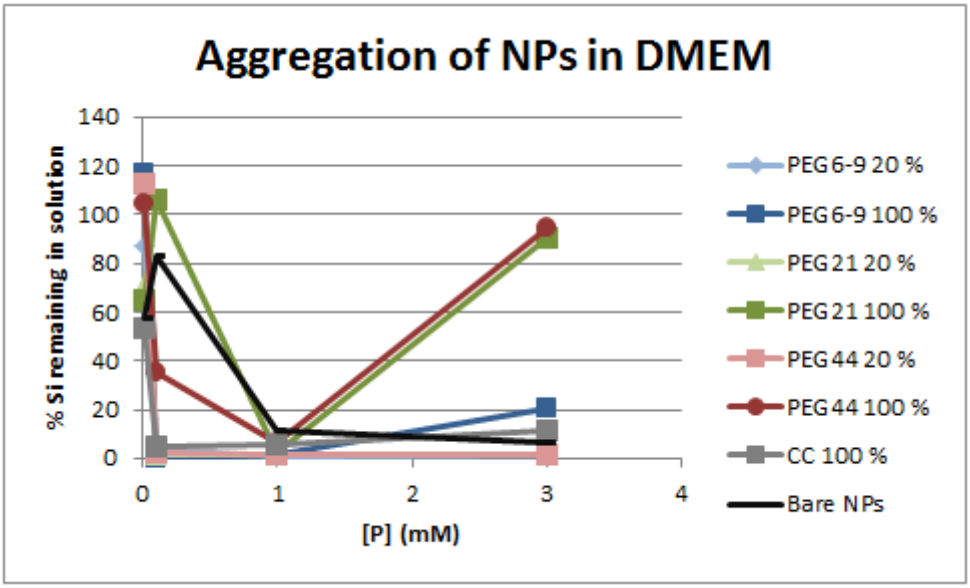

Figure 4.21. Percentage of Si (= % of NPs not aggregated) remaining in solution vs. [P] (mM) for NPs in DMEM.

Since I aimed to study the cellular uptake of single NPs and not aggregates of NPs, a particle concentration ([P] in mM) at which particles were not fully aggregated was preferred. Based on what was found regarding aggregation and precipitation behavior of the particles in RPMI and DMEM, [P] = 0.01 mM and [P] = 0.1 mM were chosen as NP concentrations to be tested in cellular uptake experiments. Although several particles fully remained in solution for [P] = 3.0 mM, this particle concentration was regarded as inappropriate to use in the cellular uptake experiments, due to possible toxicity. According to my hypothesis, complete uptake of Ca occurred at [P] = 3.0 mM, leading to

depletion of Ca. Since Ca is used in several signaling pathways throughout the cells, Ca depletion most likely would affect the health of the cells in a negative way. Toxicity of the NPs was evaluated (results not presented in this thesis) for [P] = 0.01 mM and [P] = 0.1 mM. At these concentrations, no indications on toxic effects on the cell lines (Raw264.7 and HepG2) were found. Since no toxicity evaluation was conducted for particles at [P] = 3.0 mM, this concentration was left out of further biological studies in this thesis, i.e. NP concentrations on [P] = 0.01 mM and [P] = 0.1 mM were the only ones that I aimed to use for cellular uptake experiments.

4.3 Cell culture

Raw264.7 and HepG2 cell lines were used for the biological experiments performed in this project. Before performing biological experiments, in which cells were treated with NPs, I created growth curves for both cell lines (see Figure 4.22).

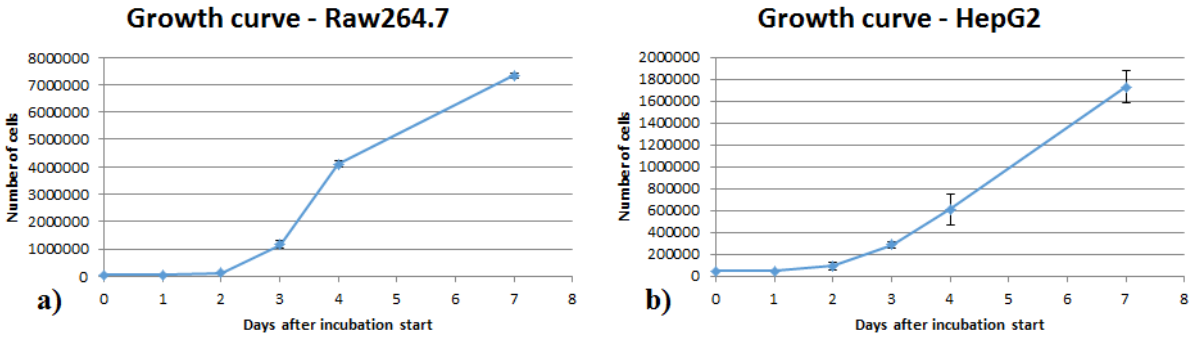

Figure 4.22. Growth curves for **a)** Raw264.7, and **b)** HepG2. Standard deviation is presented as error bars (n=2).

These growth curves were used for further determination of doubling time of the cells (see Table 4.6 and Eq. 4), which in turn was used for determination of when to perform NP uptake experiments.

Table 4.6. Cell number (average) at the beginning and end of the incubation. Both cell lines were incubated for 7 days.

Cell line	No. of cells at t = 0	No. of cells at t = 7	$t_{doubling}$ (days)
Raw264.7	50 000	7 340 000	0.97
HepG2	50 000	1 728 000	1.37

According to growth curves and cell doubling time calculations, doubling time was shorter for Raw264.7 cells than for HepG2 cells (see Table 4.6), i.e. Raw264.7 cells grew faster than HepG2 cells.

Neither of the cell lines manifested all four phases of cell growth. For the HepG2 cells, lag and log-phases were the only phases noted (see Figure 4.22b), indicating that these cells had not reached full confluency at the seventh day of incubation. Raw264.7 cells did however seem to be approaching full confluency at this time, since lag and log-phases, as well as the initial part of the stationary phase were noted for these cells (see Figure 4.22a). The death phase was not seen for any of the cell lines. By monitoring cells through an inverted light microscope I noted that HepG2 cells were considerably bigger than the Raw264.7 cells. Due to this, both cell lines were split with the same time interval, even though doubling time was shorter for Raw264.7 cells than for HepG2 cells. Based on what was found regarding doubling time of the cell lines, I chose to seed both Raw264.7 and HepG2 cells at such a density that both of them could be treated with NPs after one day (overnight) of incubation. This meant that Raw264.7 cells were treated with NPs slightly after reaching double seeding density, whereas HepG2 cells were treated with NPs some hours before reaching double seeding density.

4.4 Quantitative analysis of cellular uptake of nanoparticles

4.4.1 Overview of the quantification method

One aim of my Master's thesis project was to develop a biological method for quantitative analysis of cellular uptake of NPs. Based on the results obtained from this analysis, conclusions regarding the impact of different NP coatings (precursor lengths and coating degrees) on cellular uptake of these particles could be drawn. Due to the involvement of MPS and liver in the clearance of NPs from the bloodstream, Raw264.7 (macrophage cell line) and HepG2 (hepatocyte cell line) cells were used for studies of cellular uptake of NPs. The quantification method developed in this Master's thesis project was a combined method, constituting both In-Cell ELISA and ELISA (see Figure 4.23). Flow cytometry was used for additional analysis.

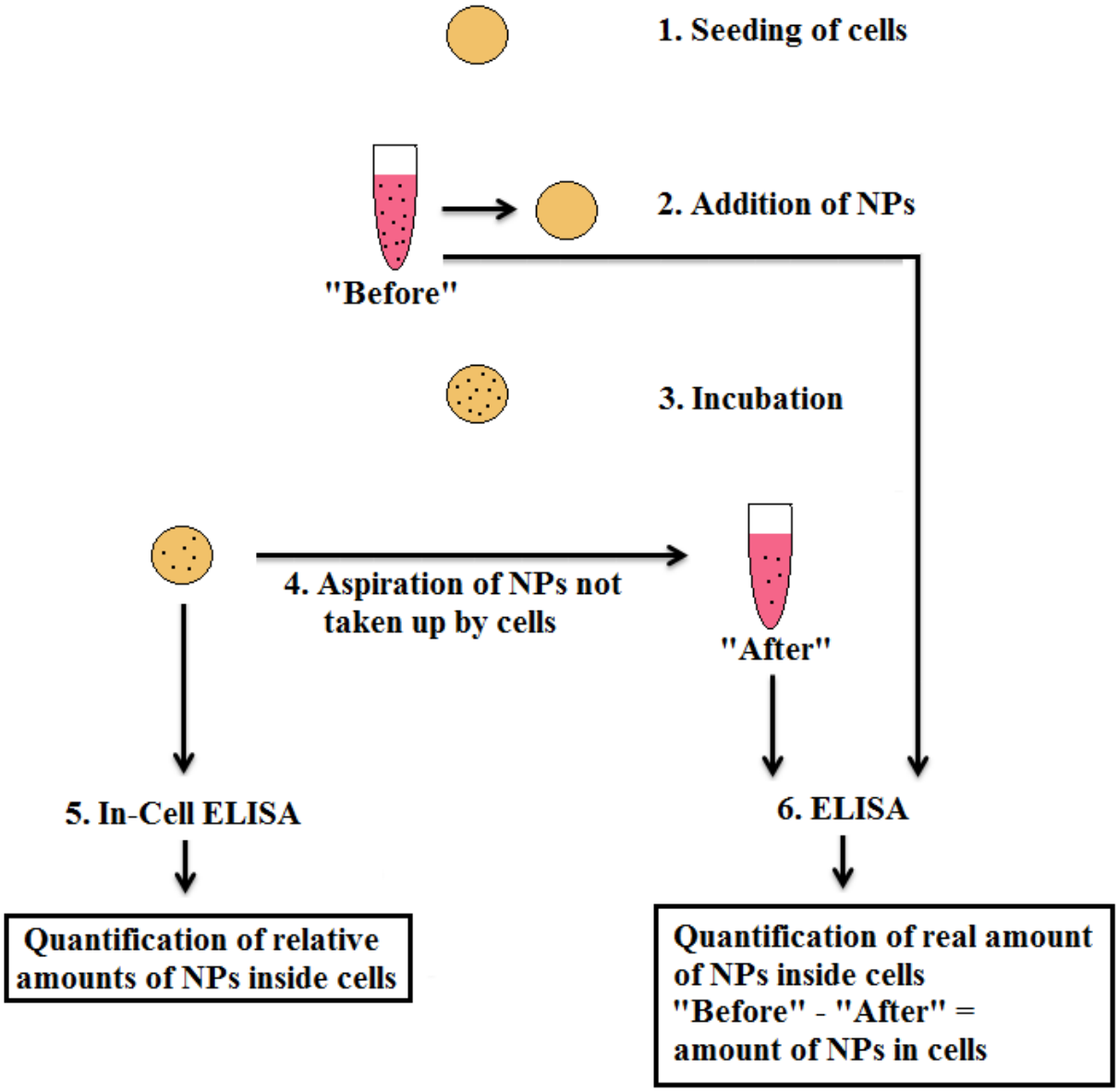

Figure 4.23. Method for quantitative analysis of cellular uptake of NPs. **1)** Cells were seeded in microplate wells. **2)** NPs diluted in culture medium (called **"Before"**) were added to the cells. The rest of these "Before" NPs were saved for further ELISA. **3)** Cells were incubated with NPs for 1h. **4)** NPs not taken up by the cells were aspirated and transferred to an Eppendorf tube labeled **"After"**. **5)** In-Cell ELISA was used for quantification of relative amounts of NPs present inside cells. **6)** ELISA was used for quantification of the amounts of NPs present in "Before" and "After" samples. These amounts were then used for calculation of the real amount of NPs present inside cells. For ELISA to be correct, standard curves were needed.

In order to study cellular uptake of NPs, cells were incubated with particles (see Figure 4.23). After incubation, particles could be present both inside and outside cells. I wanted to quantify the amount of NPs taken up by cells, both by quantifying the amount of NPs present inside cells and by quantifying the amount of NPs present outside cells after incubation. Following incubation, culture medium containing particles not taken up by the cells was aspirated and kept in Eppendorf tubes at -18 °C until analysis. I wanted to quantify the amount of NPs present inside the cells by using In-Cell ELISA. No standard curves were, however, used for this analysis, meaning that this analysis only allowed me to determine relative amounts of NPs taken up by the cells. Instead, I decided to indirectly quantify the real amounts of NPs taken up by cells, by quantifying the amounts of NPs present in the aspirated medium. For this quantification I had to prepare standard curves for ELISA.

4.4.2 Quantification of nanoparticles in cells

In order to quantify the amounts of NPs taken up by the two cell lines (Raw264.7 and HepG2) I used the In-Cell ELISA method described in sections 3.9 and 4.4.1. The main aim of the quantitative analysis was to investigate if length of the coating precursor, as well as the coating degree, had an impact on the amounts of NPs taken up by the cells. Based on what was found regarding aggregation of NPs in culture media, I chose to incubate the cells with particles of two different concentrations (of each NP batch); [P] = 0.01 mM and [P] = 0.1 mM. According to toxicity experiments, none of the particles showed indications of toxicity for either of the cell lines at these concentrations (results not shown in this thesis). Results from the 0.1 mM P incubations are the only ones presented in this thesis, since this was the only NP concentration that was tested in further flow cytometry and fluorescence microscopy experiments.

4.4.2.1 Method development: Absorbance background

For detection and quantification of PEG coated NPs taken up by cells I wanted to use an anti-PEG primary antibody. For the quantification method to be reliable, binding of the primary antibody had to be specific, i.e. the absorbance (background) for cells not incubated with PEG coated NPs had to be low. In order to evaluate the specificity of the anti-PEG primary antibody I included bare NPs, CC coated NPs and culture medium (= no NP) as negative controls in all experiments. Since the negative controls did not contain PEG, any absorbance obtained for these controls was attributed to unspecific binding of the primary antibody. I found that absorbance values obtained for the negative controls generally were lower compared to absorbance values obtained for PEG coated NPs, demonstrating a low degree of unspecific binding of the primary antibody (see Figure 4.24, Figure 4.25 and Figure 4.26).

4.4.2.2 Method development: Normalization of absorbance signal

The uptake of 0.1 mM P NPs by Raw264.7 and HepG2 cells was analyzed. For Raw264.7 cells, I performed two identical In-Cell ELISA experiments, whereas for HepG2 cells, only one such experiment was performed, due to time limitations. In all experiments duplicate samples were analyzed for each NP. When analyzing the raw data obtained in the experiments, I found that higher signals generally were obtained for cells incubated with high-amount (100 mol%) PEG coated NPs, than for cells incubated with the low-amount PEG coated counterparts (see Figure 4.24, Figure 4.25 and Figure 4.26). This was seen for both cell lines. This result was attributed to the fact that a PEG binding primary antibody was used for detection of NPs taken up by the cells. Due to this, NPs coated with high amount of PEG would give a higher signal than the same amount of NPs coated with low amount of PEG.

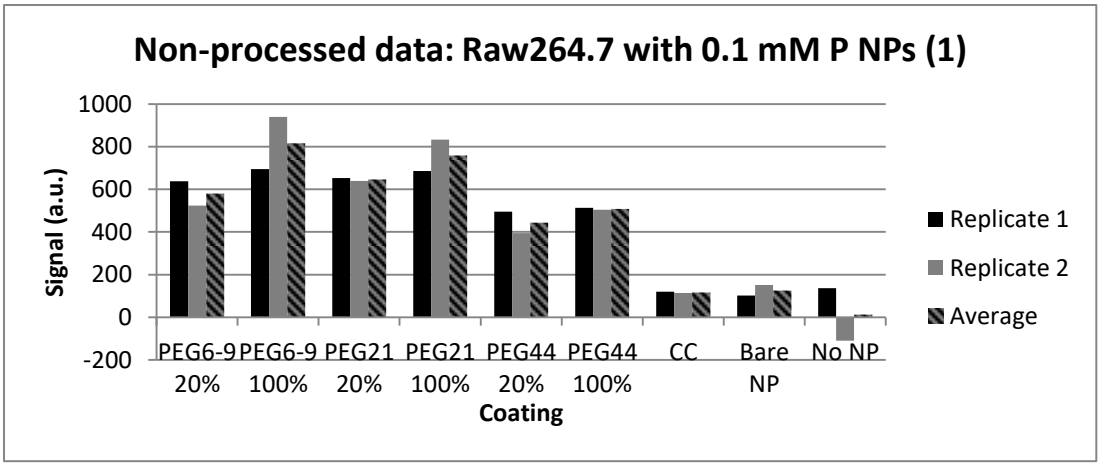

Figure 4.24. Non-processed data for incubation of Raw264.7 with 0.1 mM P NPs (Experiment 1).
No NP = RPMI culture medium.

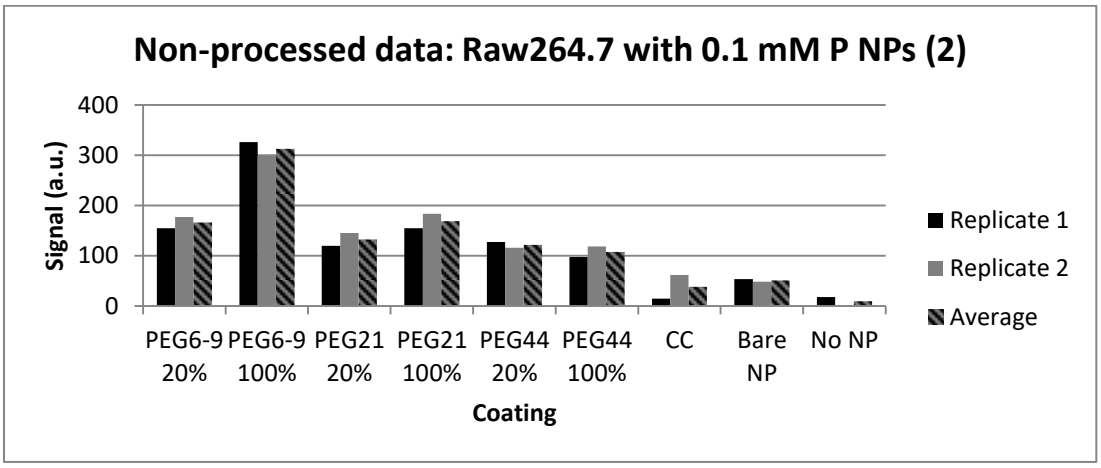

Figure 4.25. Non-processed data for incubation of Raw264.7 with 0.1 mM P NPs (Experiment 2).
No NP = RPMI culture medium.

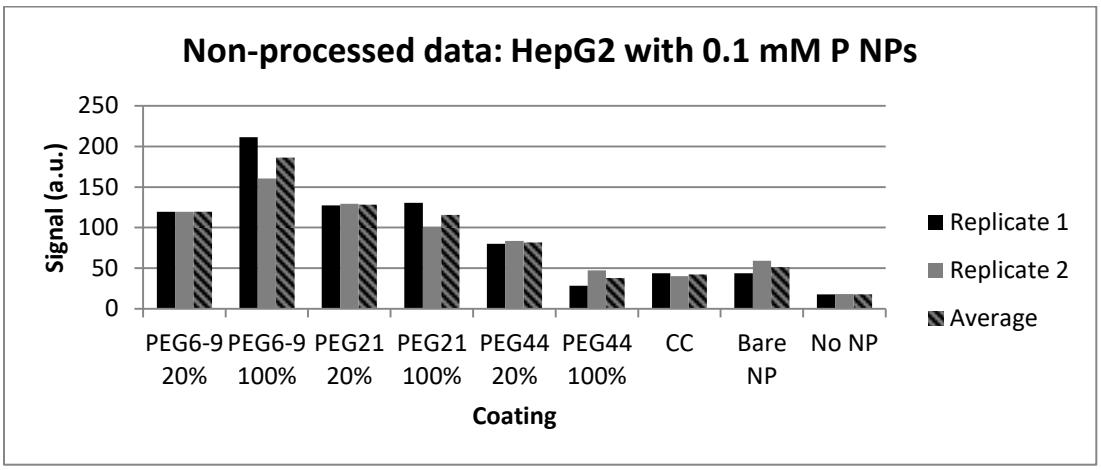

.

Figure 4.26. Non-processed data for incubation of HepG2 with 0.1 mM P NPs.
No NP = DMEM culture medium.

In order to compare the cellular uptake of NPs coated with different amounts of PEG, I chose to normalize the signals to the real amount of coating (see Table 4.3) present on the particles. In normalization calculations (see Table 4.7, Table 4.8 and Table 4.9) NP monomer concentration was calculated based on the assumption that every NP monomer contained two P atoms ([P] = 0.1 mM).

Concentration of coating precursor was calculated by multiplying NP monomer concentration with the real coating degree. By normalizing the signals, differences in coating degree were taken into account, enabling comparison of cellular uptake of NPs coated with different coating degrees (see Figure 4.27, Figure 4.28 and Figure 4.29). For high-amount (100 mol%) PEG44 coated NPs, coating oligomers were not successfully removed during filtration (see Figure 4.12). Therefore, the real coating degree of these particles probably was considerably lower than the one determined by ICP-OES (93.74%). By instead assuming that the real coating degree of these particles was in the same range (30%) as for the other high-amount PEG coated NPs (see Table 4.3), I calculated an adjusted normalized signal for cells incubated with these particles (see Table 4.7, Table 4.8 and Table 4.9). A coating degree of 30% was a more realistic assumption than 93.74% and was also higher than the low-amount PEG44 coated NPs (25.53%). Therefore, I regarded cellular uptake results obtained for high-amount PEG44 coated NPs as more reliable when assuming that the real coating degree was 30%. Even with adjustment of the coating degree to a lower number, high-amount PEG44 coated NPs still gave the lowest normalized signal in all experiments, increasing confidence in the observed uptake results (see Table 4.7, Table 4.8 and Table 4.9).

Table 4.7. Normalized average signals for Raw264.7 cells after incubation with PEG coated NPs (Experiment 1).

Coating	Signal (a.u.)	[NP monomer] (mM)	Real coating degree (mol%)	[PEG] (µM)	Normalized signal (a.u./µM of PEG^{-1})
PEG6-9 20 mol%	581.365	0.05	15.75	7.875	73.8
PEG6-9 100 mol%	817.460	0.05	27.18	13.59	60.2
PEG21 20 mol%	646.425	0.05	16.47	8.235	78.5
PEG21 100 mol%	759.495	0.05	34.27	17.14	44.3
PEG44 20 mol%	444.660	0.05	25.53	12.77	34.8
PEG44 100 mol%	508.930	0.05	93.74	46.87	10.9
PEG44 100 mol% (adj.)	508.930	0.05	30.00	15.00	33.9

Table 4.8. Normalized average signals for Raw264.7 cells after incubation with PEG coated NPs (Experiment 2).

Coating	Signal (a.u.)	[NP monomer] (mM)	Real coating degree (mol%)	[PEG] (µM)	Normalized signal (a.u./µM of PEG^{-1})
PEG6-9 20 mol%	165.995	0.05	15.75	7.875	21.1
PEG6-9 100 mol%	312.470	0.05	27.18	13.59	23.0
PEG21 20 mol%	132.320	0.05	16.47	8.235	16.1
PEG21 100 mol%	168.825	0.05	34.27	17.14	9.85
PEG44 20 mol%	121.590	0.05	25.53	12.77	9.53
PEG44 100 mol%	107.810	0.05	93.74	46.87	2.30
PEG44 100 mol% (adj.)	107.810	0.05	30.00	15.00	7.19

Table 4.9. Normalized average signals for HepG2 cells after incubation with PEG coated NPs.

Coating	Signal (a.u.)	[NP monomer] (mM)	Real coating degree (mol%)	[PEG] (µM)	Normalized signal (a.u./µM of PEG^{-1})
PEG6-9 20 mol%	119.500	0.05	15.75	7.875	15.7
PEG6-9 100 mol%	186.025	0.05	27.18	13.59	13.9
PEG21 20 mol%	128.240	0.05	16.47	8.235	15.6
PEG21 100 mol%	115.570	0.05	34.27	17.14	6.74
PEG44 20 mol%	81.8000	0.05	25.53	12.77	6.41
PEG44 100 mol%	38.0000	0.05	93.74	46.87	0.811
PEG44 100 mol% (adj.)	38.0000	0.05	30.00	15.00	2.53

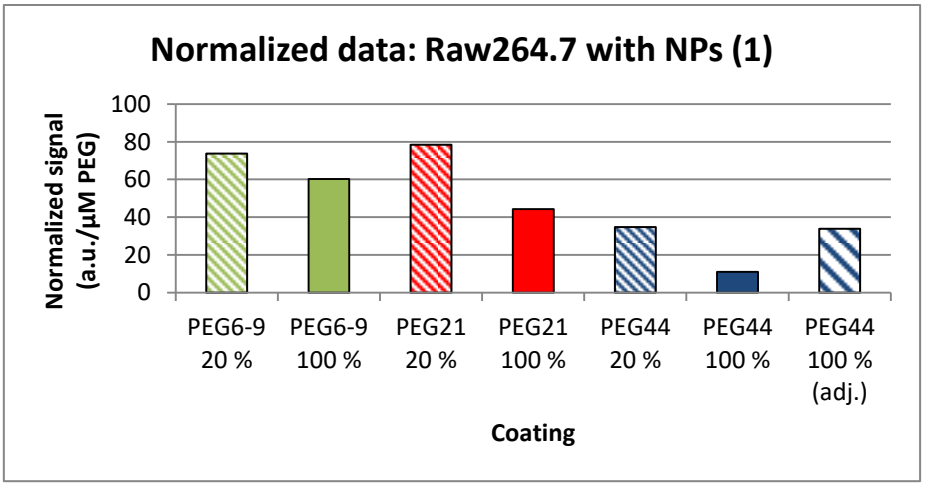

Figure 4.27. Normalized average signals (n=2) for Raw264.7 cells after incubation with PEG coated NPs (Experiment 1).

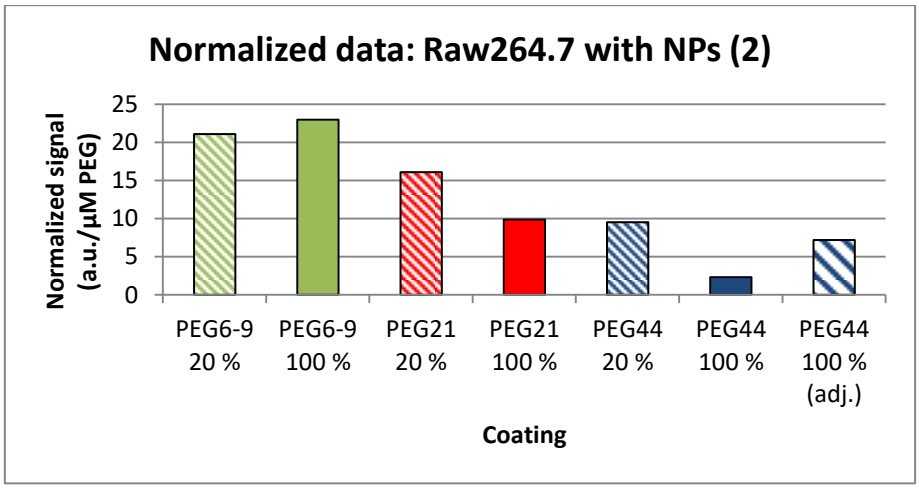

Figure 4.28. Normalized average signals (n=2) for Raw264.7 cells after incubation with PEG coated NPs (Experiment 2).

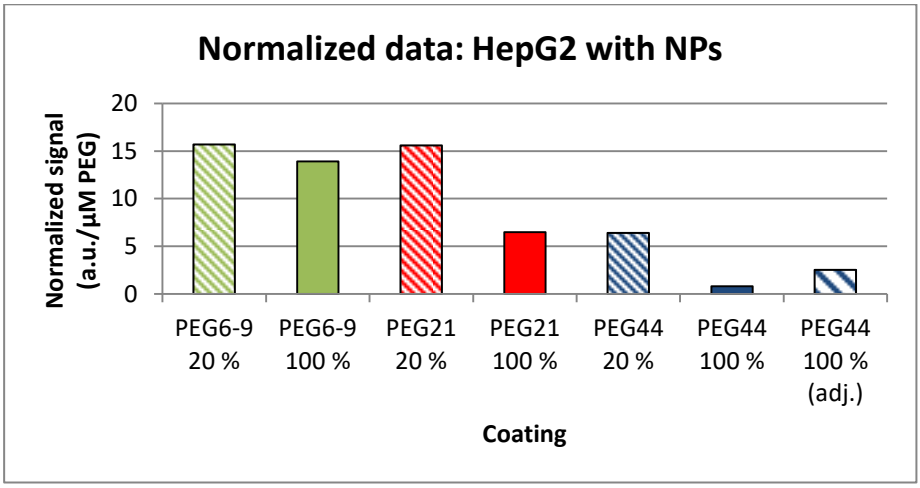

Figure 4.29. Normalized average signals (n=2) for HepG2 cells after incubation with PEG coated NPs.

4.4.2.3 Effect of degree of coating on uptake by Raw264.7 and HepG2 cells

Raw264.7 and HepG2 cells were incubated with low-amount (20 mol%) and high-amount (100 mol%) PEG coated NPs, with PEG precursors of three different lengths. A higher normalized absorbance signal should correspond to a higher cellular uptake. I found that the uptake of NPs coated with high

amount of PEG generally was lower than the uptake of NPs with low amount of PEG coating, by both Raw264.7 and HepG2 cells (see Figure 4.27, Figure 4.28 and Figure 4.29).

4.4.2.4 Effect of coating length on uptake by Raw264.7 and HepG2 cells

Normalized absorbance signals, where a higher signal should correspond to a higher cellular uptake, were also compared in order evaluate the effect of coating precursor length on uptake by Raw264.7 and HepG2 cells. I found that for all NPs coated with a high amount of PEG, higher PEG precursor length gave a lower uptake of NPs by both Raw264.7 and HepG2 cells (see Figure 4.27, Figure 4.28 and Figure 4.29). For low-amount PEG coated NPs, NPs coated with the longest PEG precursor were the ones that were taken up the least, while no clear difference between PEG6-9 and PEG21 was observed (see Figure 4.27, Figure 4.28 and Figure 4.29). When comparing impact of both amount of PEG and PEG length on uptake by Raw264.7 and HepG2 cells, I found that a medium PEG length (PEG21) was critical (see Table 4.10). Uptake of PEG21 coated NPs was relatively low as long as the amount of coating was high. Below this PEG length (PEG6-9), uptake of NPs was high, regardless of the amount of coating (see Table 4.10), whereas above this PEG length (PEG44), uptake was relatively low even at low amount of PEG (see Table 4.10). These results indicate that PEG length, rather than the amount of PEG was critical for cellular uptake of NPs.

Table 4.10. Normalized absorbance signals taken from tables 4.7, 4.8 and 4.9 for cells incubated with PEG coated NPs. Color codes: red = high uptake, yellow = medium uptake, green = low uptake. Color code setting was based on rough approximations.

	Coating length			
	Low (PEG6-9)	**Medium (PEG21)**	**High (PEG44)**	
High amount of PEG	60.2	44.3	33.9	Raw264.7 (1)
	23.0	9.85	7.19	Raw264.7 (2)
	13.9	6.74	2.53	HepG2
Low amount of PEG	73.8	78.5	34.8	Raw264.7 (1)
	21.1	16.1	9.53	Raw264.7 (2)
	15.7	15.6	6.41	HepG2

4.4.2.5 Cellular uptake experiments discussion

Lower uptake of high-amount high-length PEG coated NPs could be explained by the notion that these particles possibly were better protected from interacting with proteins present in the culture medium. Less NP-protein interaction possibly led to less uptake by Raw264.7 and HepG2 cells, compared to low-amount low-length PEG coated NPs. The better protection (larger repulsion of proteins) provided by longer PEG precursors was attributed to the increased flexibility of these precursors. According to literature, entropic repulsion of macromolecules such as proteins is proportional to the flexibility of the molecule causing the repulsion [10]. Due to their length, PEG44 precursors were more flexible than PEG21 and PEG6-9 precursors. Thereby, repulsion of proteins caused by PEG44 precursors was larger than the repulsion caused by the shorter PEG precursors, possibly leading to less protein interaction and further cellular uptake of NPs coated with PEG44. Better protection provided by higher coating degree was attributed to an increased number of flexible coating precursors.

It should be emphasized that the results obtained in these experiments are just indicative. For validation of the results, more experiments must be performed. Also, the absorbance signal strength varied considerably in between the experiments, possibly due to sensitivity variations in the Spectra MAX 340 Microplate reader. This means that it is reliable to compare absorbance signal within one experiment where the absorbance reading was simultaneous, but not between experiments. Signal variations could possibly also be explained by variations in cell seeding density. Such variations would be remedied by normalization of the signal to the amount of cells and also by increasing the number of replicates. Normalization of the signal to the amount of cells would also enable comparison of the signals between the two cell lines.

4.4.3 Quantification of nanoparticles outside cells

When NPs were incubated with cells, the particles could either be taken up by the cells, or stay outside, in the culture medium. Relative amounts of NPs taken up by the cells were quantified with In-Cell ELISA (see sections 3.9 and 4.4.2). In addition to quantify the amounts of NPs present inside cells, I wanted to use ELISA (see section 3.8 and Figure 4.23) and analyze the amount of NPs present in the original samples added to cells minus the amount of NPs not taken up by the cells (see Figure 4.23).

4.4.3.1 Method development: PEG specificity of the primary antibody

One of the fundamentals for having a successful quantification method was that the anti-PEG primary antibody was specific only for PEG conjugated to NPs. It was especially important that the primary antibody did not bind to PEG precursors and PEG oligomers, because these were present in solution (free coating precursors, see Figure 4.15 and Appendix VI; PEG44 coating oligomers, see Figure 4.12 and Table 4.3). In order to determine whether the anti-PEG primary antibody reacted to free PEG, I analyzed PEG12 methyl ether (PEG12) with ELISA (see Figure 4.30).

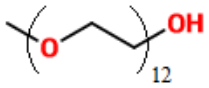

Figure 4.30. Structure of PEG12 methyl ether.

The mean absorbance signals for PEG12 had approximately the same intensity as the negative controls (bare NPs and RPMI culture medium) and considerably lower signals than the positive control (see Figure 4.31), indicating that the anti-PEG primary antibody did not detect free PEG precursors. I did not test whether the primary antibody could detect PEG oligomers.

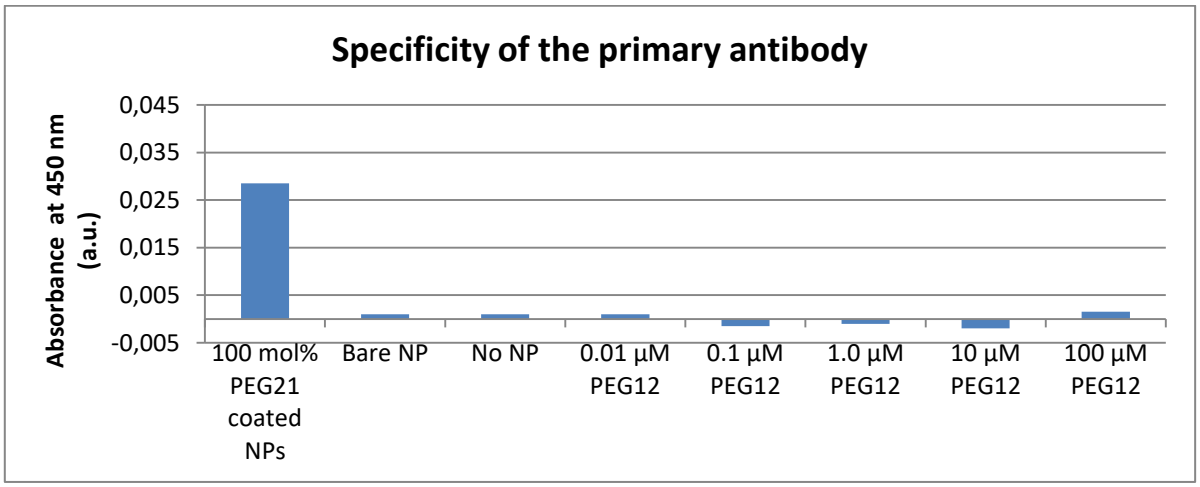

Figure 4.31. Mean absorbance signals (n=2) for 0.01 mM P 100 mol% PEG21 coated NPs (positive control), bare NPs and RPMI culture medium (= no NP) (negative controls) and free PEG12 precursors diluted in RPMI at five different concentrations.

4.4.3.2 Method development: ELISA standard curves

In order to quantify the amount of PEG coated NPs present in the culture medium after incubation with cells, I needed to create ELISA standard curves for each particle batch in each culture medium. I decided to use 100 µM P as the highest NP concentration in the dilution series for each NP when preparing the standard curves, because this was the concentration of NPs added to the cells in the incubation experiments (see section 4.4.2) and was the highest concentration that could be reached in the culture medium following incubation (if no particles were taken up by the cells).

4.4.3.2.1 ELISA reproducibility

For each PEG coated NP, the following NP concentrations were prepared in both culture media; 100 µM P, 10 µM P, 1.0 µM P, 0.1 µM P and 0.01 µM P. Absorbance for these concentrations was measured by using ELISA. Bare NPs were included as a negative control in all experiments. Four experiments for high-amount (100 mol%) PEG21 coated NPs in RPMI were performed.

The general intensity of the absorbance signals, as well as the absorbance ratios between NP concentrations within the same dilution series tended to vary in between the experiments (see Table 4.11). The variations in general intensity of the absorbance signals were investigated and were attributed to sensitivity variations (demonstrated in other experiments) in the Spectra MAX 340 Microplate reader. Due to these variations a "general" standard curve for quantification of high-amount (100 mol%) PEG21 coated NPs in RPMI could not be created. To overcome the issue with sensitivity variations of the plate reader one could create a new standard curve every time a certain particle was analyzed or buy a new plate reader.

Variations in the absorbance ratios between NP concentrations within the same dilution series were probably not due to malfunction of the plate reader. These variations were explained by that the NPs (diluted to 1 mM P in culture media) precipitated in the culture media (see Table 4.5). Since my aim was to analyze uptake of NPs and not uptake of NP aggregates, it would be better to dilute NPs in MQ water to 20 µM P (see Table 4.5) and use these to prepare a dilution series in culture medium (resulting in 10 µM P as the highest NP concentration in the dilutions series). Another reason to use 10 µM P as the highest concentration for the standard curve is an estimation showing that NP saturation of the microplate wells occurred for [P] slightly below 10 µM (see Appendix X).

Table 4.11. Mean (n=2) absorbance signals (a.u.) at 450 nm for dilution series of 100 mol% PEG21 coated NPs in RPMI. Bare NPs were included as a negative control.

	Mean absorbance (a.u.) at 450 nm for [P] (µM):					
Experiment	**0.01**	**0.1**	**1.0**	**10**	**100**	**Bare NPs**
1	0.035	0.068	0.106	0.102	0.099	0.012
2	0.028	0.161	0.390	0.371	0.318	0.027
3	0.621	1.591	1.486	1.527	1.501	0.282
4	0.001	0.007	0.019	0.029	0.032	0.001

4.4.3.2.2 Working range of standard curves

The highest concentration to be used in the standard curves should be 10 µM P. The lowest concentration should be determined by the level of quantification, LOQ (LOQ = Mean absorbance of negative control + 10 * standard deviation of negative control).

4.4.3.2.3 Evaluation of the ELISA procedure

I performed an experiment in which the PEG coated NPs were diluted in MQ water, instead of in culture medium. Since the NPs were not expected to precipitate in MQ water, I wanted to use this experiment to verify that the ELISA procedure worked properly. I found that the absorbance generally increased with increased NP concentration (see Figure 4.32), indicating that dilution series were now prepared correctly. In addition, higher absorbance signals were obtained for high-amount PEG coated NPs, compared to low-amount PEG coated NPs (see Figure 4.32). The reproducibility of the procedure could not be evaluated since only one experiment was performed.

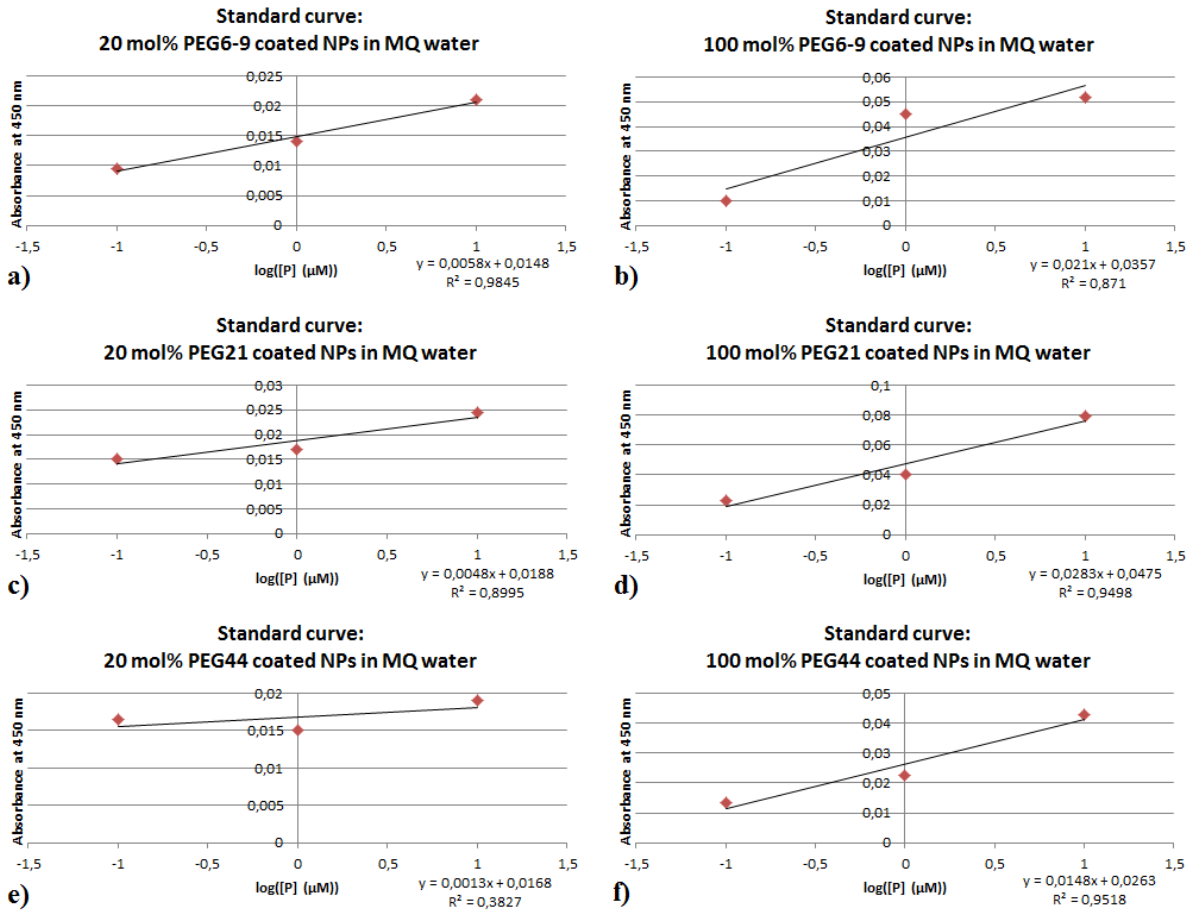

Figure 4.32. Mean absorbance signals (n=2) obtained for serial diluted **a)** 20 mol% PEG6-9 coated NPs, **b)** 100 mol% PEG6-9 coated NPs, **c)** 20 mol% PEG21 coated NPs, **d)** 100 mol% PEG21 coated NPs, **e)** 20 mol% PEG44 coated NPs and **f)** 100 mol% PEG44 coated NPs. All NPs were diluted in MQ water. Absorbance signal for bare NPs = 0.0095.

Since reproducibility of the ELISA was low and since the cause of this low reproducibility could not be overcome by simply creating a new standard curve for every analysis, I chose not to create standard curves for any of the other particles. Further optimization of the method is required and this was not within the time scope of this project.

4.4.4 Complementary quantification of nanoparticles in cells

In addition to quantify the relative cellular uptake of NPs by Raw264.7 and HepG2 cells by using In-Cell ELISA, I also studied this uptake with flow cytometry. The aim of this analysis was to use two complementary methods in order to build confidence in the observed influence of coating length and coating amount on cellular uptake of NPs. The two methods differed in their way of quantifying NPs taken up by cells. While In-Cell ELISA quantified the amount of NPs taken up by all cells, i.e. amount of NPs/cell, flow cytometry quantified the ratio of the viable cell population that had taken up NPs. Due to time limitations, only high-amount PEG coated NPs (100 mol% PEG6-9, 100 mol% PEG21 and 100 mol% PEG44 coated NPs) were included in the experiments in the flow cytometry study. These particles were selected based on the In-Cell ELISA results that indicated that PEG length, rather than coating degree was critical for cellular uptake of NPs (see Table 4.10). Bare NPs were included as a negative control, in order to evaluate the specificity of the primary antibody. In total, two cellular uptake experiments were performed for Raw264.7 cells, whereas one experiment was performed for HepG2 cells.

4.4.4.1 Method development

The uptake of high-amount PEG coated 0.1 mM P NPs by Raw264.7 and HepG2 cells was analyzed with flow cytometry. The same cell culture protocol was used for these experiments as for the In-Cell ELISA experiments. For each sample, raw data results were displayed with a scatter plot (SSC vs. FSC), an FL-plot (FL2-A vs. FL1-A) and a histogram (FL1-A) (see Figure 4.33 and Appendix IX). FSC is a measure of cell size (high FSC = large cell), while SSC is a measure of cell granularity (high SSC = high granularity). FL1-A provides quantification of FITC-labeled secondary antibody inside the cells. FL2-A corresponds to another fluorescence wavelength and should be low in these experiments. I gated the scatter plot in such a way that non-viable cells were excluded, thus only viable cells were shown in the subsequent FL-plot and histogram.

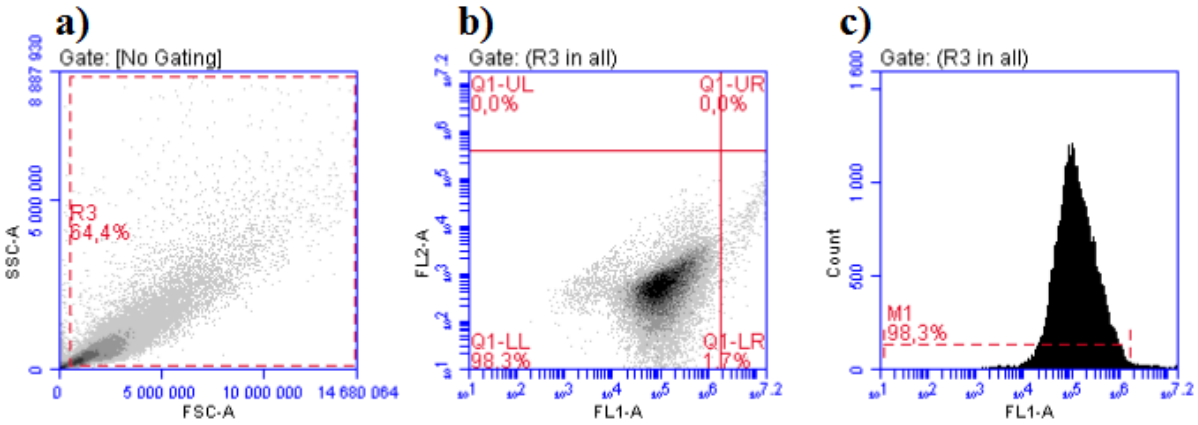

Figure 4.33. Flow cytometry results for Raw264.7 cells incubated with primary antibody (no NPs), reported as **a)** scatter plot, **b)** FL-plot and **c)** histogram. Only gated cells are reported in the FL-plot and histogram, respectively.

In order to eliminate background fluorescence, I aimed to gate the FL-plot for the background sample (cells incubated with primary antibody, but without NPs) in such a way that no cells were reported as FL1-A and FL2-A positive. This gate setting should be used for all other FL-plots within the same experiment in order to determine the percentage of FL1-A positive cells in the samples. Using this gate setting was, however, not possible since a considerable amount of cells were reported as FL1-A positive even in the absence of NPs. I attributed this to that a too high concentration of primary antibody was used throughout the experiments, something that possibly contributed to frequent unspecific binding of primary antibody to cells. Since optimization of primary antibody concentration was not within the time scope of my Master's thesis project, I chose instead to account for the background fluorescence due to unspecific binding by setting the FL gate so that no FL1-A and FL2-A positive cells were obtained for the cells incubated without both NPs and primary antibody (see Figure 4.34a). This gate setting was then adopted for all other FL-plots within the same experiment. Any

positive FL1-A signal obtained for cells incubated without NPs, but with primary antibody (see Figure 4.34b), was subtracted from the positive FL1-A signal, obtained for cells incubated with NPs and primary antibody (see Figure 4.34c and Table IX.I in Appendix IX). In this way the percentage of FL1-A positive cells, attributed to the presence of NPs inside cells, could be calculated (see Table 4.12).

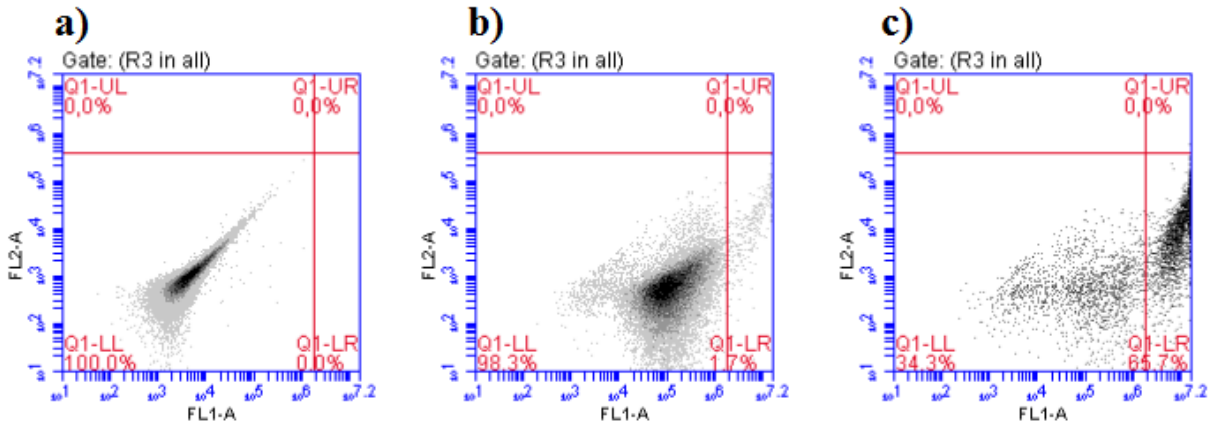

Figure 4.34. FL-plots for Raw264.7 cells incubated **a)** without NPs and without primary antibody, **b)** without NPs, but with primary antibody and **c)** with 100 mol% PEG6-9 coated NPs and primary antibody. The FL gate was set so that no FL1-A and FL2-A positive cells were obtained for the cells incubated without NPs and primary antibody (**a**). By adopting this gate setting for cells incubated without NPs, but with primary antibody (**b**), as well as for cells incubated with both NPs and primary antibody (**c**), the percentage of cells containing NPs could be calculated as % of FL1-A positive cells in c (lower right quadrant) - % of FL1-A positive cells in b (lower right quadrant) (in this case 65.7 – 1.7 % = 64.0 %).

Table 4.12. Percentage FL1-A positive cells after subtraction of background (see Appendix IX).

	% of FL1-A positive cells for:			
Cell line	**PEG6-9 coated NPs**	**PEG21 coated NPs**	**PEG44 coated NPs**	**Bare NPs**
Raw264.7 (1)	64.0	62.8	56.8	0.7
Raw264.7 (2)	16.6	12.9	6.6	0
HepG2	33.2	33.3	27.3	0.2

In contrast to when analyzing cellular uptake of NPs with In-Cell ELISA, I chose not to normalize the percentage of FL1-A positive cells to the amount of coating present on the particles. In In-Cell ELISA, such a normalization was necessary, since higher signals were obtained as a consequence of higher coating degree, but since flow cytometry results relied on counting of cells normalization was not needed.

The specificity of the primary antibody was evaluated by including bare NPs as a negative control in all experiments. Since these particles did not contain PEG, cells incubated with these NPs were not expected to be FL1-A positive. Some cells incubated with these particles were, however, still reported as FL1-A positive (see Figure IX.IVc, Figure IX.Vc and Figure IX.VIc in Appendix IX). This was attributed to the non-optimized concentration of primary antibody. When I compared the positive FL1-A signal for cells incubated with bare NPs and primary antibody, with the corresponding signal for cells incubated without NPs, but with primary antibody, I found that these signals were at approximately the same level (see Figure 4.35a,e). For cells incubated with PEG coated NPs, signals had a considerably higher intensity (see Figure 4.35b-d,f-h), indicating that the primary antibody was specific for PEG coated NPs. This was seen for both cell lines (see Figure 4.35).

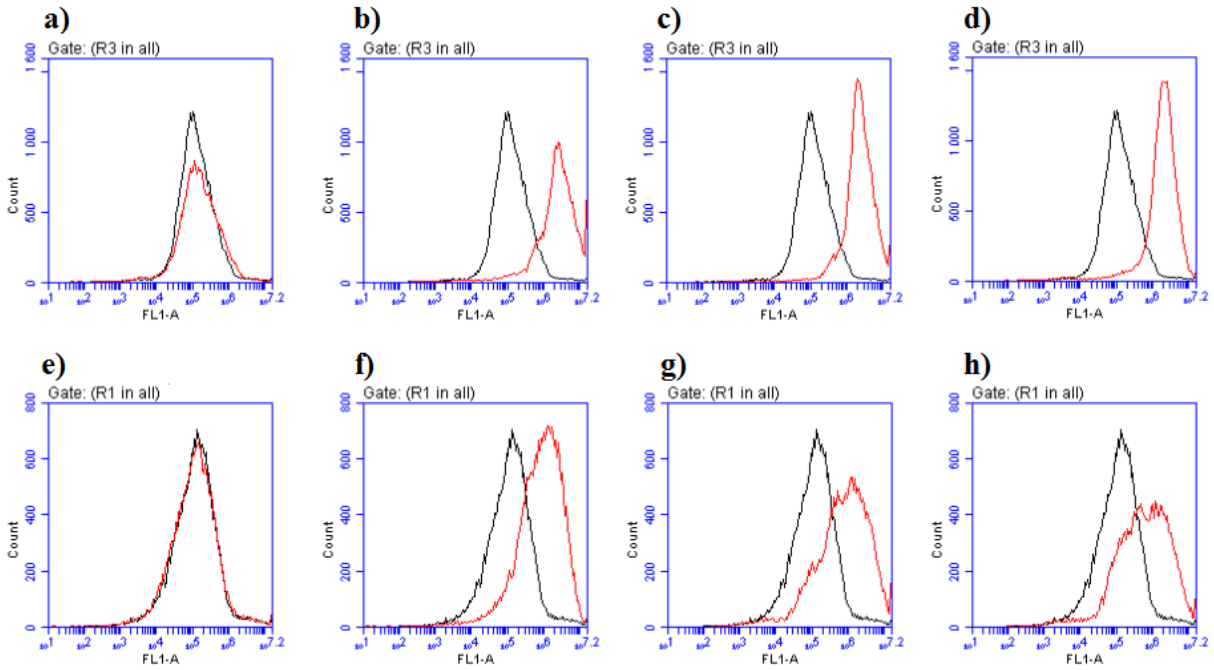

Figure 4.35. Overlay histograms for Raw264.7 (**a-d**) and HepG2 (**e-h**) cells, incubated with **a, e)** bare NPs, **b, f)** PEG6-9 coated NPs, **c, g)** PEG21 coated NPs and **d, h)** PEG44 coated NPs. In all histograms (**a-h**), the black histogram corresponds to the background cell population (no NP incubation), whereas the red histogram corresponds to the cell population following NP incubation.

4.4.4.2 Effect of coating length on uptake by Raw264.7 and HepG2 cells

In the flow cytometry experiments, Raw264.7 and HepG2 cells were incubated with NPs, coated with PEG of three different lengths; PEG6-9, PEG21 and PEG44. A high percentage of FL1-A positive cells was interpreted as that a large number of cells had taken up the particles. I found that for Raw264.7 cells, a higher PEG precursor length gave a lower cellular uptake (see Figure 4.36, Figure 4.37 and Table 4.12). For HepG2 cells, NPs coated with the longest coating precursor were also the ones taken up the least, whereas uptake of NPs coated with the two shorter PEG precursors was similar (see Figure 4.38 and Table 4.12).

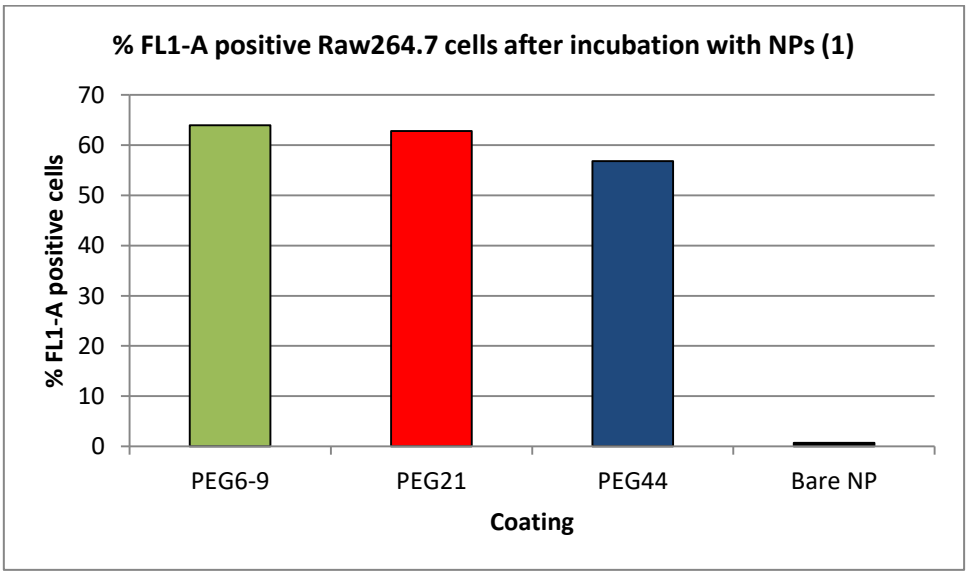

Figure 4.36. Percentage FL1-A positive Raw264.7 cells after incubation with 0.1 mM P NPs (Experiment 1).

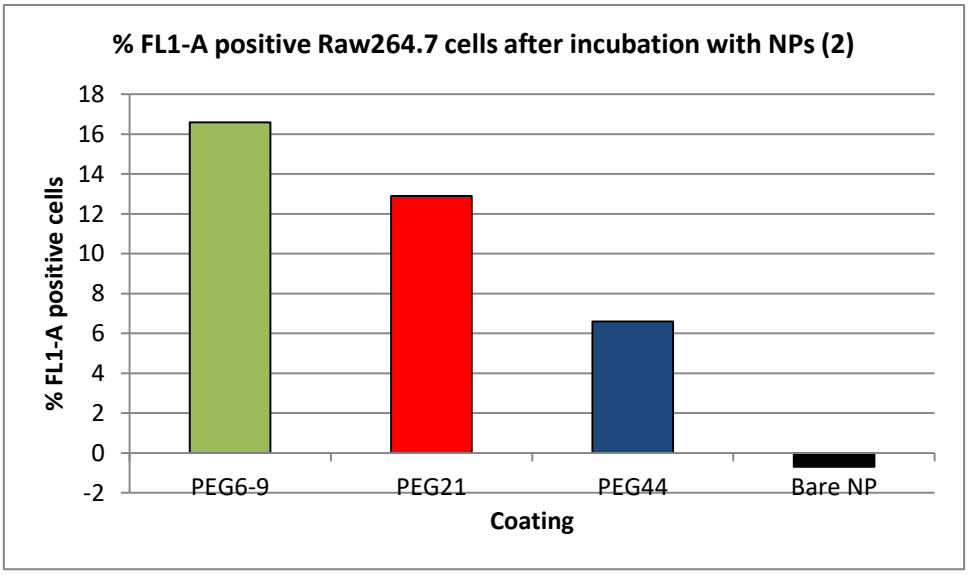

Figure 4.37. Percentage FL1-A positive Raw264.7 cells after incubation with 0.1 mM P NPs (Experiment 2).

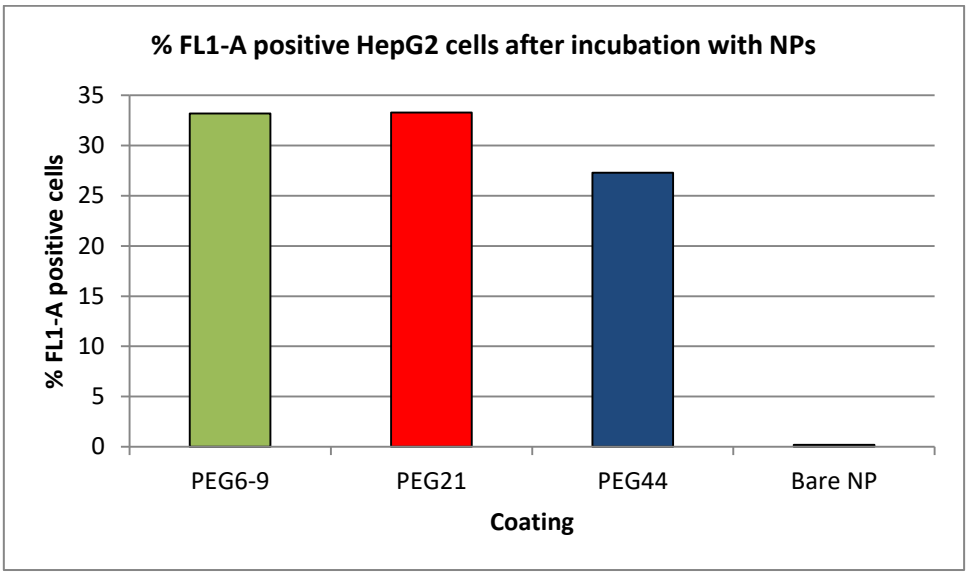

Figure 4.38. Percentage FL1-A positive HepG2 cells after incubation with 0.1 mM P NPs.

4.4.4.3 Flow cytometry discussion

When analyzed with flow cytometry, I found that NPs coated with high-length PEG (PEG44) showed a less efficient uptake than NPs coated with low- and medium-length PEG. This was consistent with results obtained with In-Cell ELISA, indicating that the results were reliable. However, conditions at which flow cytometry analysis was performed were not optimal and the method needs to be improved. Primary antibody concentration should be lowered to obtain lower FL1-A background. The percentage of viable cells, as well as the scatter intensity of the cells varied in between the experiments (see Figure IX.I, Figure IX.II and Figure IX.III in Appendix IX), indicating that cells were easily affected by the physical treatment (scraping, fixation etc.) performed during cell culture and staining procedure, preceding analysis. Results presented in this section are just indicative and more experiments should be performed.

4.5 Qualitative analysis of cellular uptake of nanoparticles

In-Cell ELISA, as well as flow cytometry experiments, allowed me to quantify the relative uptake of NPs by Raw264.7 and HepG2 cells. These experiments did, however, not allow me to determine the location of the NPs in cells. For this qualitative analysis I used fluorescence microscopy (see section 3.11). Only high-amount PEG coated NPs (100 mol% PEG6-9, 100 mol% PEG21 and 100 mol% PEG44 coated NPs) were included in fluorescence microscopy experiments, due to time limitations. Uptake of high-amount PEG coated 0.1 mM P NPs by Raw264.7 cells was studied in two experiments (pictures from Experiment 1 are the only ones presented in this thesis). No experiment was performed for HepG2 cells, due to time limitation.

4.5.1 Method development: antibody specificity

For staining of NPs taken up by cells, an anti-PEG primary antibody and a FITC-labeled secondary antibody were used (see section 3.11). Since a reliable detection of PEG coated NPs taken up by cells was dependent on the specificity of the primary antibody for these NPs, I included bare NPs as a negative control throughout the experiments. I also wanted to evaluate the specificity of the secondary antibody. Therefore, cells incubated with PEG coated NPs, but without primary antibody, were also included as a negative control in the experiments. Compared to Raw264.7 cells incubated with PEG coated NPs and both primary and secondary antibodies (see Figure 4.39c), FITC fluorescence was low for both of the negative controls (see Figure 4.39a-b). Low FITC fluorescence for the negative controls indicated that both antibodies were specific.

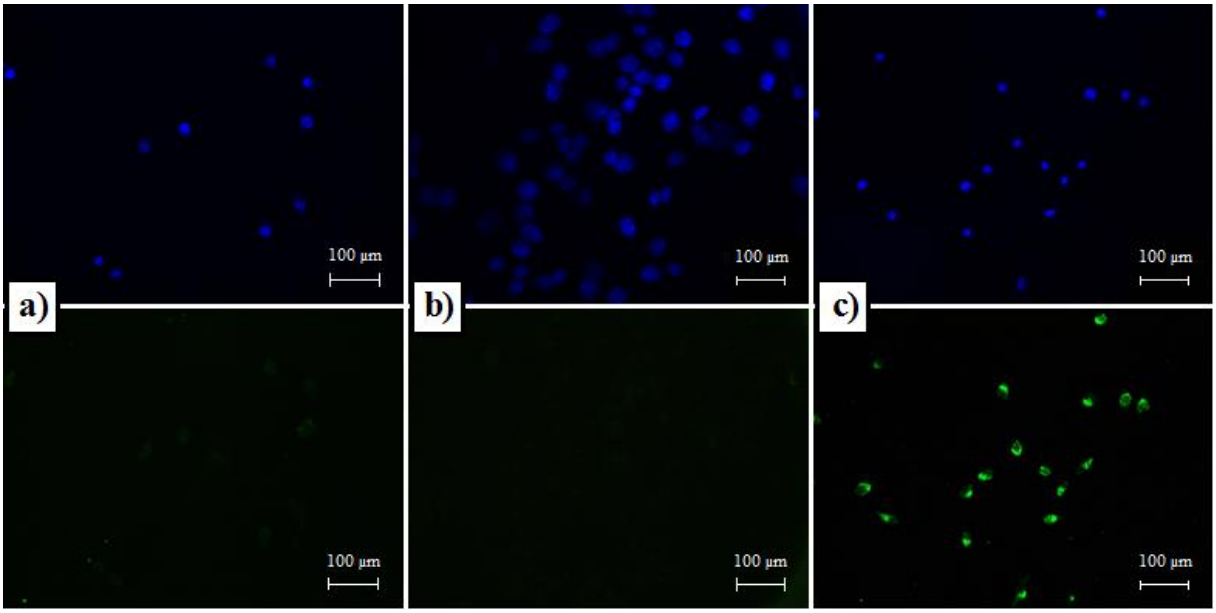

Figure 4.39. Raw264.7 cells incubated with **a)** bare NPs, primary antibody and secondary antibody, **b)** 100 mol% PEG6-9 coated NPs and secondary antibody, **c)** 100 mol% PEG44 coated NPs, primary antibody and secondary antibody. Upper pictures: fluorescence at 461 nm (DAPI staining = cell nucleus). Lower pictures: fluorescence at 519 nm (FITC staining = NPs). Light exposure times (t_E): DAPI = 1/20 s, FITC = 1/10 s

4.5.2 Cellular location of PEG coated NPs taken up by Raw264.7 cells

DAPI was used for staining of the nucleus of the Raw264.7 cells (see **a** in Figure 4.40-4.42), whereas a FITC conjugated antibody was used for staining of PEGylated NPs (see **b** in Figure 4.40-4.42). To make it easier to draw conclusions regarding the intracellular distribution of the NPs, I also stained the cells with LysoTracker Deep red (see **c** in Figure 4.40-4.42). Staining with LysoTracker Deep red allowed me to track acidic organelles, such as lysosomes, which I expected to be involved in the uptake of NPs. By overlaying the pictures (see **d** in Figure 4.40-4.42) I was able to see the distribution of the NPs, relative to the nucleus and acidic compartments.

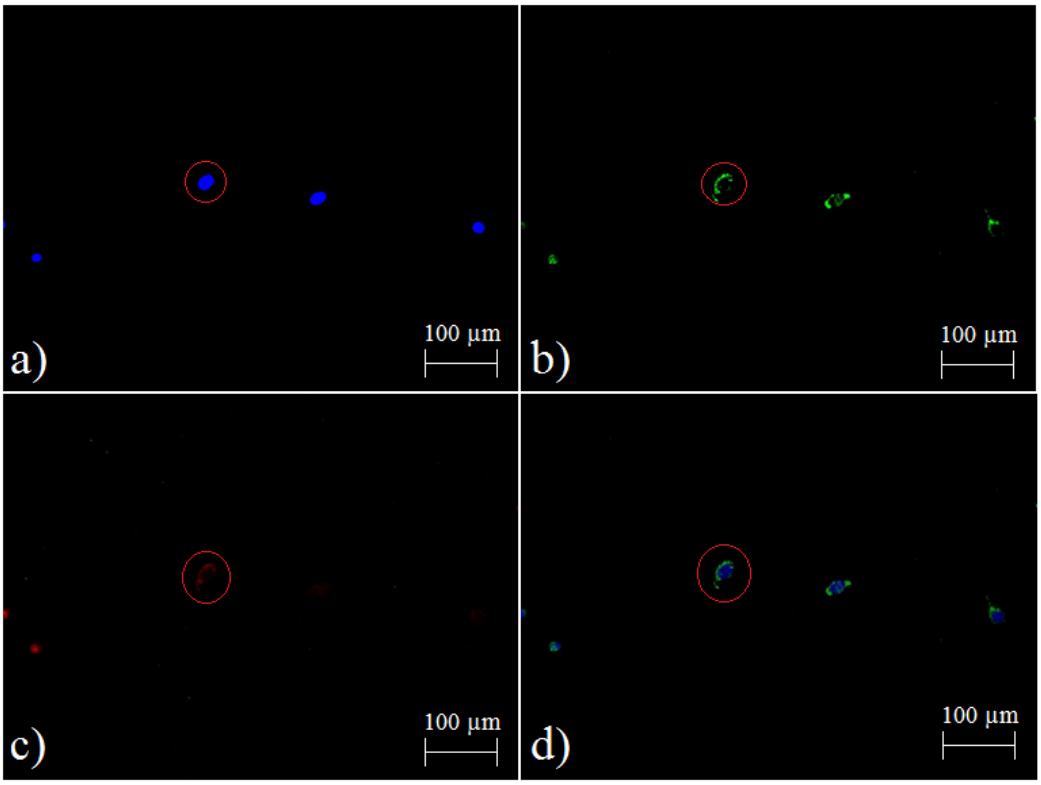

Figure 4.40. Fluorescence microscopy pictures for Raw264.7 cells incubated with 100 mol% PEG6-9 coated NPs (Experiment 1), **a)** fluorescence at 461 nm (DAPI staining), **b)** fluorescence at 519 nm (FITC staining), **c)** fluorescence at 668 nm (LysoTracker staining) and **d)** merging of **a-b** (enlarged in Figure XI.I in Appendix XI).
Light exposure times (t_E): DAPI = 1/20 s, FITC = 1/10 s, LysoTracker Deep red = 1 s

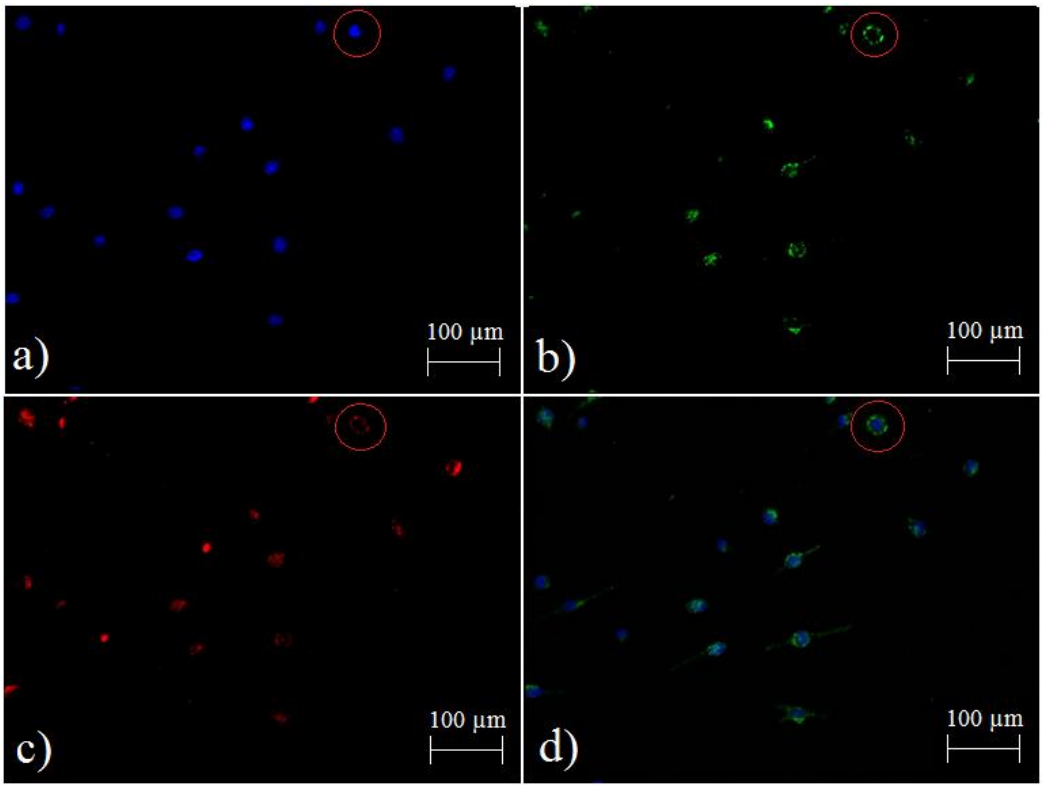

Figure 4.41. Fluorescence microscopy pictures for Raw264.7 cells incubated with 100 mol% PEG21 coated NPs (Experiment 1), **a)** fluorescence at 461 nm (DAPI staining), **b)** fluorescence at 519 nm (FITC staining), **c)** fluorescence at 668 nm (LysoTracker staining) and **d)** merging of **a-b** (enlarged in Figure XI.II in Appendix XI).
Light exposure times (t_E): DAPI = 1/20 s, FITC = 1/10 s, LysoTracker Deep red = 1 s

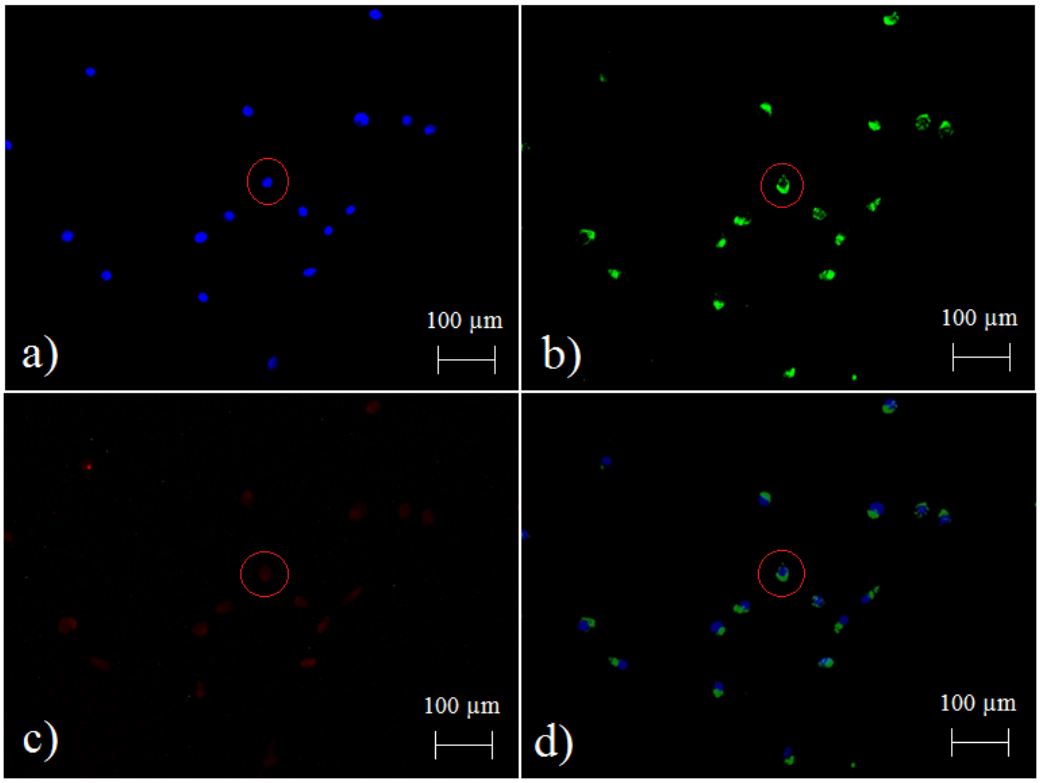

Figure 4.42. Fluorescence microscopy pictures for Raw264.7 cells incubated with 100 mol% PEG44 coated NPs (Experiment 1), **a)** fluorescence at 461 nm (DAPI staining), **b)** fluorescence at 519 nm (FITC staining), **c)** fluorescence at 668 nm (LysoTracker staining), and **d)** merging of **a-b** (enlarged in Figure XI.III in Appendix XI).
Light exposure times (t_E): DAPI = 1/20 s, FITC = 1/10 s, LysoTracker Deep red = 1 s

A general trend seen in both experiments was that the NPs tended to concentrate in the periphery of the cells (see encircled cell in **b** and **d**, Figure 4.40-4.42). I could see that acidic organelles were present in these regions as well (see encircled cell in **c** and **d**, Figure 4.40-4.42), indicating that the NPs had been internalized into the endocytic pathway. Since LysoTracker Deep red stained all endosomes of the endocytic pathway, I was however not able to determine the precise stage (early or late endosomal, lysosomal), at which NPs were at the time for the fixation of cells. For this analysis, a more detailed staining of e.g. Rab5 in EEs, Rab7 in LEs and LAMP-1 in lysosomes, would have been required. However, at the time for fixation, the cells had been incubated with NPs for 2 hours (1 hour with NPs only and 1 hour with NPs and LysoTracker Deep red). According to literature, endocytosed material should be able to reach the lysosomes within this time [18].

Longer light exposure time was needed for LysoTracker Deep red (1 s), compared to this time for FITC (1/10 s) (see Figure 4.40-4.42). When exposed to light for the same duration of time, fluorescence intensity was considerably lower for LysoTracker Deep red, than for FITC, possibly indicating that the amount of acidic organelles was low (in relation to the amount of NPs), or that staining with LysoTracker Deep red was not very successful.

Vague indications on differences in intracellular distribution of NPs coated with different coatings were seen. Indicatively, the location of PEG44 coated NPs was a bit more cytoplasmic, compared to for PEG6-9 and PEG21 coated NPs, which were located closer to the membrane. Clear differences were however hard to see. This could be due to that the magnification of the images was too low. However, there is a possibility that all internalized particles ended up in the same organelles, regardless of the coating, and that the only difference was the amount of NPs taken up by the cells during this time. Such differences were studied in the In-Cell ELISA (see section 4.4.2) and flow cytometry (see section 4.4.4) experiments.

5. CONCLUSIONS

The main goal of this project was to study whether coating degree and PEG precursor length of NPs had an impact on the uptake of these particles by Raw264.7 and HepG2 cells. The quantitative uptake of NPs was studied with In-Cell ELISA and flow cytometry. For both cell lines I found indications of that coating degree and PEG length had an impact on the uptake of NPs. The uptake of high-amount PEG coated NPs was lower than the uptake of low-amount PEG coated NPs, whereas NPs coated with long-length PEG showed a lower uptake compared to particles coated with short-length PEG. PEG21 seemed to be a critical coating length for this particle size. With the shorter coating (PEG6-9), the uptake was high regardless of coating degree, whereas with the longer coating (PEG44), the uptake was low regardless of coating degree. This indicated that PEG length affected cell uptake more than the coating degree. Fluorescence microscopy showed that NPs with a high coating degree were internalized into Raw264.7 cells' endocytic pathway after two hours of incubation. Preliminary indications of differences in intracellular distribution of the different particles were also seen. Overall, additional experiments need to be performed in order to confirm all these results. More experiments are also needed in order to further develop and optimize the methods used for quantitative and qualitative analysis of the cell uptake.

6. FUTURE WORK

During this Master's project, the initial steps in the development of a method for quantification of PEGylated NPs in Raw264.7 and HepG2 cells were taken. Experimental results obtained during the course of the project indicate that the method is promising. However, much more work still needs to be performed in order for the method to be fully developed and validated.

For the method to work in its current form, NPs have to be PEGylated, because an anti-PEG antibody is used for detection and quantification of NPs taken up by the cells. This is a drawback since it is not possible to quantify bare NPs and NPs coated with other coatings than PEG. For the quantification method to become more general, usage of an antibody that detects and quantifies all these particles is necessary.

Aggregation of NPs in culture medium was probably one of the reasons why standard curves for ELISA could not be developed. Compatibility of NPs with culture medium should therefore be improved. For this, a more comprehensive study investigating the effect of culture medium on aggregation of NPs should be performed. A possible way to do this would be to incubate NPs with culture medium as described in section 3.6, but in addition to the analysis that was performed in the experiments in this project (this analysis only defined particles as precipitated or non-precipitated), NPs still remaining in solution should be analyzed with DLS. Aggregation of NPs would be characterized by a shift in the size distribution of the NP population towards bigger size. For DLS analysis, the medium most likely has to be serum free, since serum proteins otherwise affect the DLS results. Incubating NPs in serum free medium is, however, a bit of drawback since this excludes one of the parameters (the serum proteins) that could have an impact on the aggregation of the particles. A more comprehensive study on the aggregating behavior of NPs in culture medium could also, theoretically, give indications on which endocytic mechanisms that are involved in the cellular uptake of the NPs, since these mechanisms are highly dependent on the size of the particles. Fluorescence microscopy on cells incubated with NPs and stained for different endocytic uptake mechanisms would be needed for full determination of uptake routes. A way to perform such an experiment would be to incubate cells with NPs of different concentrations and then stain for the uptake mechanisms. Variations in uptake mechanisms for different NP concentrations would be an indication of that aggregation of NPs occurs.

Overall, more In-Cell ELISA, flow cytometry and fluorescence microscopy experiments should be performed in order to verify that trends seen in the initial experiments are valid. Parameters such as NP concentration and incubation time should be varied. Changing the latter parameter would provide information on how different coatings affect cellular uptake of NPs over time. Having information about this is important when developing NPs for applications where long circulation times are needed.

In order to increase the quality and reproducibility of the results, optimization of current experimental procedures should also be performed. This should include optimization of antibody and NP concentrations, as well as of practical procedures. The coating procedures should also be optimized. Following optimization and validation of experimental procedures, the quantification method should be expanded to include quantification of NPs in cells other than the ones tested here. Cells of interest would be different types of cancer cells.

7. ACKNOWLEDGEMENTS

This thesis marks the end of my time as a Master's student in Biotechnology at LTH and I would like to express my sincerest gratitude to Spago Nanomedical AB and Malmö Högskola for giving me the opportunity to perform this Master's thesis project.

First of all, I would like to thank my **super**visors Sania, Tove and Anette, who have supported and encouraged me from the very first day of this project. Sania, thank you for always being there for me, for all the hours you have spent reading my texts and for your very professional way of guiding me through this project. Not least, thank you for all the laughs and endless discussions about life and wellbeing. Tove, thank you so much for sharing your office with me, for guiding me through the world of cell cultures and antibodies and not least for being so patient with me, even in days when my laboratory skills were not the best and the experiments kept failing over and over again. Anette, thank you for your guidance at Malmö Högskola and for giving me the opportunity to perform experiments that would not have been possible without this collaboration. Thank you for always giving me advices on how to proceed with my experiments and for guiding me in the lab, even at eight p.m. when everybody else had left. I am so grateful to all of you!

Furthermore, I would like to thank all you employees at Spago Nanomedical AB, who have encouraged and helped me during my Master's project. I would like to thank Oskar and Emil, who were the ones that invited me for my very first interview in November, 2014. Thank you for giving me the opportunity to do an internship at Spago in 2015. This was an experience that really opened my eyes for the world of nanomedicine and I am pretty sure that I would not have ended up doing my Master's thesis here if it was not for this internship. Moreover, thank you Oskar for always having the time to come with good advices whatever was the problem and for encouraging me to fulfill my dreams. I will not make you or myself disappointed. Emil, thank you for all your advices during the biological parts of my project and for the time you spent helping me with the calcium aggregation studies. Most of all, I would like to thank you for being so encouraging during the final months of my project. That really kept me going. Nooshin and Olof, thank you for all the hours you spent analyzing my countless number of samples. I felt a bit guilty every time I knocked your door with tube racks full of samples, but you just smiled, took my samples and the following day I got the results. Just like magic! Also, I would like to thank Andreas and Rodrigo for helping me whenever any machine was fighting with me. Having you there certainly saved me a lot of time and I am so grateful. Gabriel, Petter and Angelo, thank you for being so patient with me in the synthesis lab and for always giving me advices on how to proceed with my coating experiments. I certainly could not have had better organic chemistry teachers. Also, thank you Mats for always being interested in the progress of my project, even though I know you had enough to do with just being the CEO. Your interest really made me happy. Finally, Iliana, even though you did not arrive until I was finished with the experimental part of my project, you have played a big role in the progress of my thesis compilation. Thank you for all your kind and encouraging words and for always being so happy in the lab.

At last, I would like to thank Gema, former Master's thesis student at Spago Nanomedical AB. Thank you for taking such a good care of me during my internship in 2015, for teaching me about life as a Master's thesis student and most of all for being such an amazing friend. You were the biggest reason why I also wanted to do my Master's thesis at Spago. Thank you!

8. REFERENCES

1. World Health Organization (2016). Cancer. WHO. Available from: http://www.who.int/cancer/en/ (Accessed: 2016-09-10)
2. Wicki, A., Witzigmann, D., Balasubramanian, V., Huwyler, J. Nanomedicine in cancer therapy: Challenges, opportunities, and clinical applications. *J. Control. Release*. **200**, 138-157 (2014).
3. Bazak, R., Houri, M., Elachy, S., Hussein, W., Refaat, T. Passive targeting of nanoparticles to cancer: A comprehensive review of the literature. *Mol. Clin. Oncol.* **2**, 904-908
4. Oh, N., Park., J-H. Endocytosis and exocytosis of nanoparticles in mammalian cells. *Int. J. Nanomedicine*. **9(1)**, 51-63 (2014)
5. Dawidczyk, C., Russell, L., Searson, P. Nanomedicine for cancer therapy: state-of-the-art and limitations to the pre-clinical studies that hinder future developments. *Front. Chem.* **2(69)** (2014)
6. Eriksson, P-O., Aaltonen, E., Petoral Jr., R., Lauritzson, P., Miyazaki, H.,Pietras, K., Månsson, S., Hansson, L., Leander, P., Axelsson, O. Novel nano-sized MR contrast agent mediates strong tumor contrast enhancement in an oncogene-driven Breast Cancer Model. *PLoS ONE*. **9(10)** (2014)
7. Fang, J., Nakamura, H., Maeda, H. The EPR effect: unique features of tumor blood vessels for drug delivery, factors involved, and limitations and augmentation of the effect. *Adv. Drug Deliv. Rev.* **63,** 136–151 (2011).
8. Spago Nanomedical AB (2015). Passive tumor targeting. Spago Nanomedical AB. Available from: http://spagonanomedical.se/technology/passive-tumor-targeting/ (Accessed: 2016-05-01)
9. Liu, W., Rose, J., Plantevin, S., Aúffan, M., Botteroab, J-Y., Vidaud, C. Protein corona formation for nanomaterials and proteins of a similar size: hard or soft corona? *Nanoscale*. **5**, 1658-1668 (2013)
10. Owens, D., Peppas, N. Opsonization, biodistribution, and pharmacokinetics of polymeric nanoparticles. *Int. J. Pharm.* **307**, 93-102 (2005)
11. Dieni, C (2015). Nanoparticles and proteins, Part I. Benchfly. Available from: http://www.benchfly.com/blog/nanoparticles-and-proteins-part-i/ (Accessed: 2016-09-11)
12. Aggarwal, P., Hall, J., McLeland, C., Dobrovolskaia, M., McNeil, S. Nanoparticle interaction with plasma proteins as it relates to particle biodistribution, biocompatibility and therapeutic efficacy. *Adv. Drug Deliv. Rev*. **61**, 428-437 (2009)
13. Jokerst, J., Lobovkina, T., Zare, R., Gambhir, S. Nanoparticle PEGylation for imaging and therapy. *Nanomedicine (Lond).* **6(4)**, 715-728 (2011)
14. Zhang, Y-N., Poon, W., Tavares, A., McGilvray, I., Chan, W. Nanoparticle-liver interactions: Cellular uptake and hepatobiliary elimination. *J. Control. Release* (2016)
15. Kou, L., Sun, J., Z, Y., He, Z. The endocytosis and intracellular fate of nanomedicines: Implication for rational design. *AJPS*. **8**, 1-10 (2013)
16. Khandare, J., Calderón, M., Dagia, Nilesh., Haag, R. Multifunctional dendritic polymers in nanomedicine: opportunities and challenges. *Chem. Soc. Rev*. **41**, 2824-2848 (2012)
17. Juling, S., David, J., Lalkowski, G., Lichtenstein, D., Böhmert, L., Rozycki, C., Braeuning, A., Lampen, A. Protein corona analysis indicates clathrin-mediated endocytosis of carboxydextran-coated nanoparticles in HepG2 cells. *Toxicol. Let*. **258**, 263 (2016)
18. Huotari, J., Helenius, A. Endosome maturation. *EMBO J*. **30**, 3481-3500 (2011)
19. Amin, L., Joo, J Y., Yi, D K., An, S S. Surface modification and local orientations of durface molecules in nanotherapeutics. *J. Control. Release*. **207**, 131-142 (2015)
20. Pitkänen, L., Striegel, A. Size-exclusion chromatography of metal nanoparticles and quantum dots. TrAC. **80**, 311-320 (2016)
21. Cho, E., Holback, H., Liu, Karen C., Abouelmagd, S., Park, J., Yeo, Y. Nanoparticle Characterization: State of the Art, Challenges, and Emerging Technologies. *Mol. Pharm*. **10**, 2093-2110 (2013)
22. Malvern Instruments. Zetasizer Nano user manual. Malvern Instruments (2013)

23. Millipore. Protein Concentration and Diafiltration by Tangential Flow Filtration. Millipore Corporation (2003)
24. Houp, R. Ultrafiltration and Diafiltration. *JVT*. **15(4)** (2009)
25. Evans Analytical Group. ICP-OES and ICP-MS Detection Limit Guidance. **5(14)** (2014)
26. Stewart, I., Olesik, J. Steady state acid effects in ICP-MS. *J. Anal. At. Spectrom*. **13(12)**, 1313-1320 (1998)
27. Hunter, R. Zeta Potential in Colloids Science. Academic Press. New York (1981)
28. Nanocomposix (2016). Characterization Techniques. Nanocomposix Europe. Available from: http://nanocomposix.eu/pages/characterization-techniques (Accessed: 2016-05-21)
29. The Interdepartmental Equipment Facility (2009). The Zetasizer. The Hebrew University of Jerusalem. Available from: http://departments.agri.huji.ac.il/zabam/zetasizer.html (Accessed 2016-05-21)
30. Lonza. Technical Reference Guide Cell Counting and Determination of Viability via Hemocytometer. Lonza Cologne AG (2009)
31. Kim, Oliver (2016). The hemocytometer (counting chamber). MicrobeHunter Microscopy Magazine. Available from: http://www.microbehunter.com/the-hemocytometer-counting-chamber/ (Accessed: 2016-05-19)
32. Mather, J., Roberts, P. Introduction to Cell and Tissue Culture. 1st edition. New York: Plenum Press (1998)
33. Thermo Fisher Scientific (2016). Cell culture basics. Thermo Fisher Scientific Available from: https://www.thermofisher.com/se/en/home/references/gibco-cell-culture-basics/cell-culture (Accessed: 2016-05-24)
34. Expression Technologies Inc (2003). Bacterial E. coli growth media. Expression Technologies Inc. Available from: http://www.exptec.com/Expression%20Technologies/Bacteria%20growth%20media.htm Accessed: 2016-05-19
35. ATCC®. Animal cell culture guide. ATCC (2014)
36. Thermo Fisher Scientific (2015). Overview ELISA. Thermo Fisher Scientific. Available from: https://www.thermofisher.com/se/en/home/life-science/protein-biology/protein-biology-learning-center/protein-biology-resource-library/pierce-protein-methods/overview-elisa.htm (Accessed: 2016-05-25)
37. Boster (2016). ELISA Kits, ELISA Principle – Immunoassays. Boster. Available from: https://www.bosterbio.com/protocol-and-troubleshooting/elisa-principle (Accessed: 2016-05-25)
38. Storey, M., Jordan, S. An overview of the immune system. *Nurs. Stand*. **23(15-17)**, 47-56 (2008)
39. Liu, J. The history of monoclonal antibody development - Progress, remaining challenges and future innovations. *Ann. Med. Surg. (Lond)*. **3**, 113-116 (2014)
40. MitoSciences. In-Cell ELISA Protocol. MitoSciences. (2016)
41. Azevedo, A., Martins, V., Prazeres, D., Vojinovic, V., Cabral, J., Fonesca, L. Horseradish peroxidase: a valuable tool in biotechnology. *Biotechnol. Annu. Rev*. **9**, 199-247 (2003)
42. ThermoFisher Scientific (2015). In-Cell ELISA Colorimetric Detection Kit. ThermoFisher Scientific. Available from: https://www.thermofisher.com/order/catalog/product/62200 (Accessed: 2016-05-11)
43. Bio-Rad Laboraties. Flow Cytometry Basics Guide. Bio-Rad Laboraties. (2016)
BD Biosciences (2014). BD Accuri™ C6 Flow Cytometer. BD Biosciences. Available from: https://www.bdbiosciences.com/documents/BD_Accuri_Optical_Filter_Guide.pdf (Accessed: 2016-05-24)
44. Abcam (2016). Introduction to Flow Cytometry. Abcam. Available from: http://www.abcam.com/protocols/introduction-to-flow-cytometry (Accessed: 2016-05-29)
45. Nobel Media AB (2016).The Fluorescence Microscope. Nobel Media AB. Available from: http://www.nobelprize.org/educational/physics/microscopes/fluorescence/ (Accessed: 2016-05-23)
46. Kubitscheck, Ulrich. Fluorescence Microscopy: From Principles to Biological Applications. Wiley-Blackwell. New Jersey. (2013)

APPENDICES

Appendix I

SOP for DLS size measurements of nanoparticles

- **Sample**
  - Material: silica
    Refractive index (RI): 1.450
    Absorption: 0.001
  - Dispersant: water* OR ethylene glycol 80 %, H_2O 20 %**
    Temperature: 25 °C
    Viscosity: 0.8872 centipoise (cP)* OR see Table A.1**
    Refractive index (RI): 1.330* OR 1.346**
    General options: Use dispersant viscosity as sample viscosity
  - Temperature: 25 °C
  - Equilibration time (seconds): 180
  - Cell type: Disposable cuvettes (ZEN0040)
  - Volume: 250 µL
- **Measurement**
  - Measurement angle: 173° Backscatter (NIBS default)
  - Measurement duration: Automatic
  - Measurements:
    Number of measurements: 10
    Delay between measurements (seconds): 0
  - Measurement settings: Automatic attenuation selection
    Positioning method: Seek for optimum position
- **Data processing**
    Analysis model: Multiple narrow modes (high resolution)

* For NP samples before coating and after filtration
** For NP samples during the course of and right after coating (48h). For these samples, the viscosity has been calculated using the following relationship (Eq. AI), where x is the percentage of water in the sample. 1,4-dioxane has here been assumed having the same viscosity as water.

$$\mu = 5.087x^2 - 19.637x + 15.35 \qquad \text{(Eq. AI)}$$

Table I.I. Viscosities for coating solutions during coating. Viscosity changes due to the injection of coating monomer.

	Viscosity (cP) at:									
	3h	**6h**	**18h**	**21h**	**24h**	**27h**	**30h**	**42h**	**45h**	**48h**
PEG6-9	11.7395	11.8462	12.2166	12.2973	12.3291	12.3291	12.3291	12.3291	12.3291	12.3291
PEG21	11.7395	11.8462	12.2166	12.2973	12.3291	12.3291	12.3291	12.3291	12.3291	12.3291
PEG44	11.457	11.299	10.761	10.761	10.601	10.601	10.601	10.601	10.601	10.601
CC	11.7395	11.8462	12.2166	12.2973	12.3291	12.3291	12.3291	12.3291	12.3291	12.3291

Measurements were evaluated and NP size was determined using the criteria below.

- Measurements were aborted if the shape of the correlogram was non-sigmoidal.
- Measurements deviating from the average were excluded. This exclusion was based on the appearance of the size distribution by volume graph in the Volume PSD (M) window.

NP size was obtained from the Volume stats table (M) window and reported as the mode (highest bar) and size range (sizes for which the mean volume percent ≥ 5).

Appendix II

SOP for zeta potential measurements of nanoparticles

- **Sample**
  - Material: silica
    Refractive index (RI): 1.450
    Absorption: 0.001
  - Dispersant: water
    Temperature: 25 °C
    Viscosity: 0.8872 centipoise (cP)
    Refractive index (RI): 1.330
    Dielectric constant: 78.5
- **General options**
  - F(Ka) selection
    Model: Smoluchowski
    Sample viscosity options: Use dispersant viscosity as sample viscosity

Measurements were evaluated and NP zeta potential was determined using the criteria below.

- Measurements were aborted if the conductivity was deviating from the rest of the measurements.
- Measurements were aborted if the phase plot of the measurement was deviating from the rest of the measurements.
- For each NP batch, the zeta potential was reported as the zeta potential of the main peak in the zeta potential distribution diagram. For some NP batches, more than one such peak was present. A maximum of three peaks were reported.

Appendix III
Plate layouts

	1	2	3	4	5	6	7	8	9	10	11	12
A	PEG6-9, 20 % 0.1 µM P	PEG6-9, 20 % 0.1 µM P	PEG6-9, 100 % 0.1 µM P	PEG6-9, 100 % 0.1 µM P	PEG21, 20 % 0.1 µM P	PEG21, 20 % 0.1 µM P	PEG21, 100 % 0.1 µM P	PEG21, 100 % 0.1 µM P	PEG44, 20 % 0.1 µM P	PEG44, 20 % 0.1 µM P	PEG44, 100 % 0.1 µM P	PEG44, 100 % 0.1 µM P
B	PEG6-9, 20 % 1.0 µM P	PEG6-9, 20 % 1.0 µM P	PEG6-9, 100 % 1.0 µM P	PEG6-9, 100 % 1.0 µM P	PEG21, 20 % 1.0 µM P	PEG21, 20 % 1.0 µM P	PEG21, 100 % 1.0 µM P	PEG21, 100 % 1.0 µM P	PEG44, 20 % 1.0 µM P	PEG44, 20 % 1.0 µM P	PEG44, 100 % 1.0 µM P	PEG44, 100 % 1.0 µM P
C	PEG6-9, 20 % 10 µM P	PEG6-9, 20 % 10 µM P	PEG6-9, 100 % 10 µM P	PEG6-9, 100 % 10 µM P	PEG21, 20 % 10 µM P	PEG21, 20 % 10 µM P	PEG21, 100 % 10 µM P	PEG21, 100 % 10 µM P	PEG44, 20 % 10 µM P	PEG44, 20 % 10 µM P	PEG44, 100 % 10 µM P	PEG44, 100 % 10 µM P
D	PEG6-9, 20 % 100 µM P	PEG6-9, 20 % 100 µM P	PEG6-9, 100 % 100 µM P	PEG6-9, 100 % 100 µM P	PEG21, 20 % 100 µM P	PEG21, 20 % 100 µM P	PEG21, 100 % 100 µM P	PEG21, 100 % 100 µM P	PEG44, 20 % 100 µM P	PEG44, 20 % 100 µM P	PEG44, 100 % 100 µM P	PEG44, 100 % 100 µM P
E	PEG6-9, 20 % 100 µM P *	PEG6-9, 20 % 100 µM P *	PEG6-9, 100 % 100 µM P *	PEG6-9, 100 % 100 µM P *	PEG21, 20 % 100 µM P *	PEG21, 20 % 100 µM P *	PEG21, 100 % 100 µM P *	PEG21, 100 % 100 µM P *	PEG44, 20 % 100 µM P *	PEG44, 20 % 100 µM P *	PEG44, 100 % 100 µM P *	PEG44, 100 % 100 µM P *
F	CC, 100 % 0.1 µM P	CC, 100 % 0.1 µM P	CC, 100 % 100 µM P	CC, 100 % 100 µM P	Bare NP 100 µM P	Bare NP 100 µM P	No NP	No NP	Free PEG 0.1 µM	Free PEG 0.1 µM	Free PEG 100 µM	Free PEG 100 µM
G	CC, 100 % 1.0 µM P	CC, 100 % 1.0 µM P	CC, 100 % 100 µM P *	CC, 100 % 100 µM P *	Bare NP * 100 µM P	Bare NP * 100 µM P	No NP *	No NP *	Free PEG 1.0 µM	Free PEG 1.0 µM	Free PEG 100 µM *	Free PEG 100 µM *
H	CC, 100 % 10 µM P	CC, 100 % 10 µM P							Free PEG 10 µM	Free PEG 10 µM		

Figure III.I. Plate layout for ELISA, where * marks the absence of primary antibody. The same plate layout was used for both culture media (RPMI and DMEM).

	1	2	3	4	5	6	7	8	9	10	11	12
A	PEG6-9, 20 % 10 µM P	PEG6-9, 20 % 10 µM P	PEG6-9, 100 % 10 µM P	PEG6-9, 100 % 10 µM P	PEG21, 20 % 10 µM P	PEG21, 20 % 10 µM P	PEG21, 100 % 10 µM P	PEG21, 100 % 10 µM P	PEG44, 20 % 10 µM P	PEG44, 20 % 10 µM P	PEG44, 100 % 10 µM P	PEG44, 100 % 10 µM P
B	PEG6-9, 20 % 100 µM P	PEG6-9, 20 % 100 µM P	PEG6-9, 100 % 100 µM P	PEG6-9, 100 % 100 µM P	PEG21, 20 % 100 µM P	PEG21, 20 % 100 µM P	PEG21, 100 % 100 µM P	PEG21, 100 % 100 µM P	PEG44, 20 % 100 µM P	PEG44, 20 % 100 µM P	PEG44, 100 % 100 µM P	PEG44, 100 % 100 µM P
C	PEG6-9, 20 % 100 µM P *	PEG6-9, 20 % 100 µM P *	PEG6-9, 100 % 100 µM P *	PEG6-9, 100 % 100 µM P *	PEG21, 20 % 100 µM P *	PEG21, 20 % 100 µM P *	PEG21, 100 % 100 µM P *	PEG21, 100 % 100 µM P *	PEG44, 20 % 100 µM P *	PEG44, 20 % 100 µM P *	PEG44, 100 % 100 µM P *	PEG44, 100 % 100 µM P *
D	CC, 100 % 10 µM P	CC, 100 % 10 µM P	Bare NP 100 µM P	Bare NP 100 µM P	No NP	No NP						
E	CC, 100 % 100 µM P	CC, 100 % 100 µM P	Bare NP * 100 µM P	Bare NP * 100 µM P	No NP *	No NP *						
F	CC, 100 % 100 µM P *	CC, 100 % 100 µM P *										

Figure III.II. Plate layout for In-Cell ELISA, where * marks the absence of primary antibody. The same plate layout was used for both cell lines.

Appendix IV

GPC chromatograms for NPs during coating

Peaks in the ELSD curves have been labeled 1-5, and correspond to **1)** NPs, **2)** coating oligomers, **3)** coating monomer, **4)** ethylene glycol and **5)** salts. Each one of the ELSD curves corresponds to a unique sample, taken out at time points presented with different colors. The standard proteins, BSA (**A**) and myoglobin (**B**) correspond to the peaks in the curve for UV signal (black).

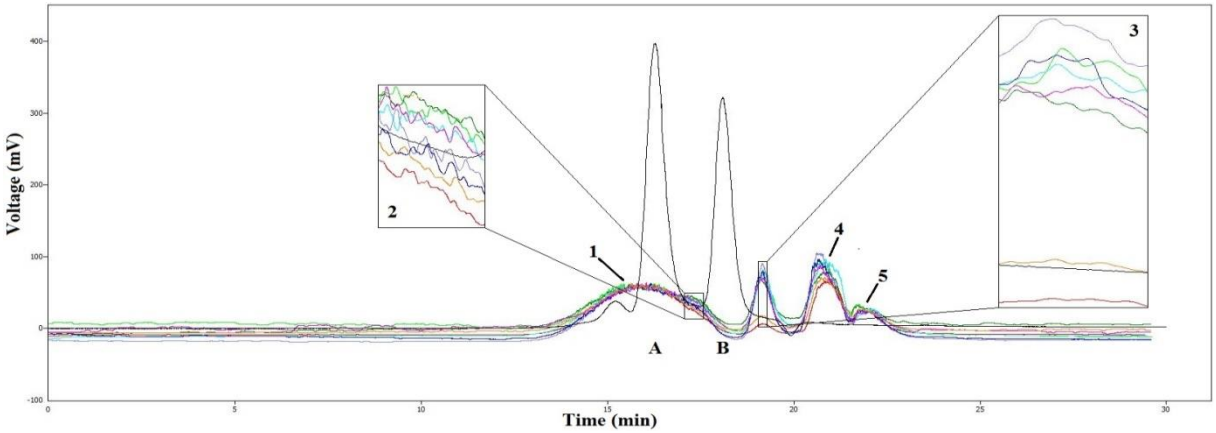

Figure IV.I. Chromatogram for coating of NPs with 20 mol% PEG6-9. Color codes: red = 3h, orange = 6h, pink = 21h, blue = 24h, purple = 27h, turquoise = 30h, dark green = 45h, and light green = 48h.

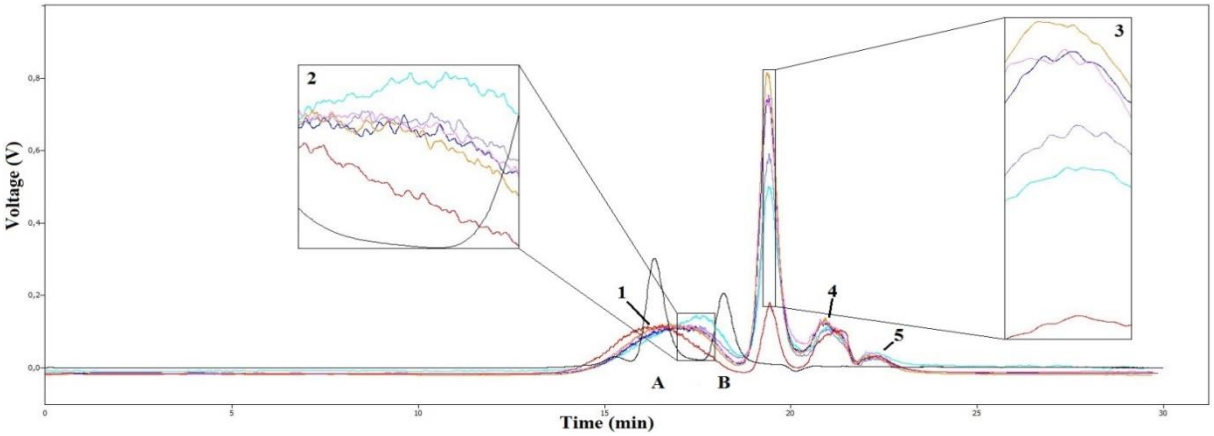

Figure IV.II. Chromatogram for coating of NPs with 100 mol% PEG6-9. Color codes: red = 3h, orange = 18h, pink = 21h, blue = 24h, purple = 27h and, turquoise = 48h.

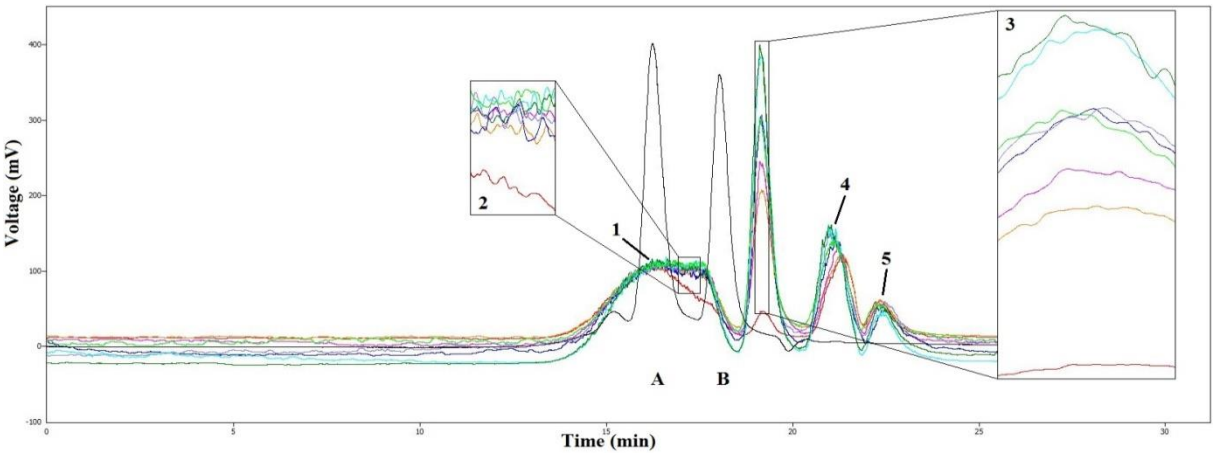

Figure IV.III. Chromatogram for coating of NPs with 20 mol% PEG21. Color codes: red = 3h, orange = 18h, pink = 21h, blue = 24h, purple = 27h, turquoise = 42h, dark green = 45h, and light green = 48h.

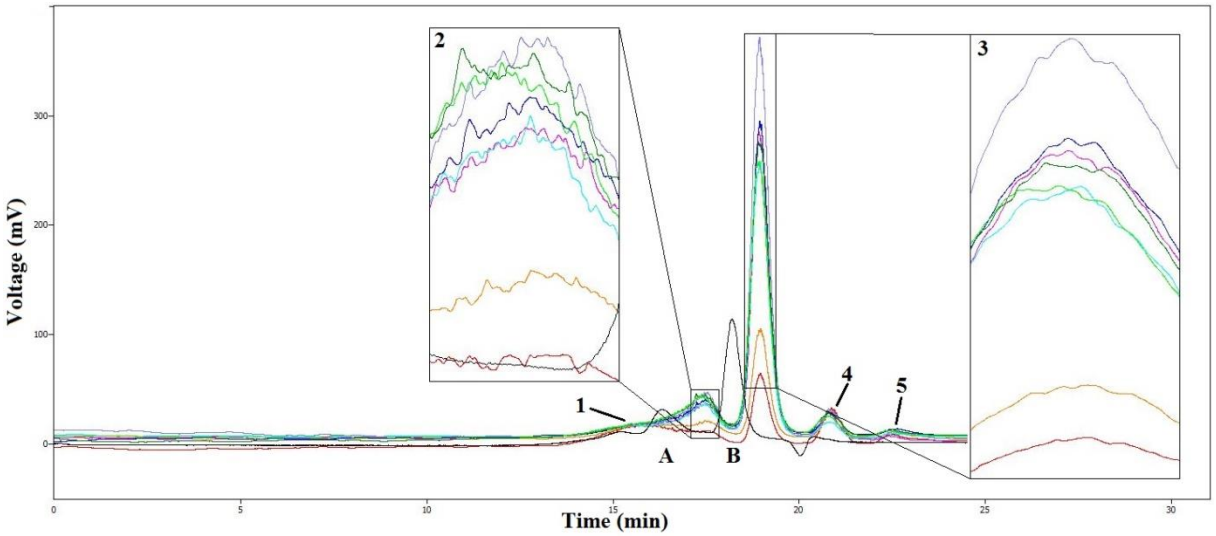

Figure IV.IV. Chromatogram for coating of NPs with 100 mol% PEG21. Color codes: red = 3h, orange = 6h, pink = 21h, blue = 24h, purple = 27h, turquoise = 30h, dark green = 45h, and light green = 48h.

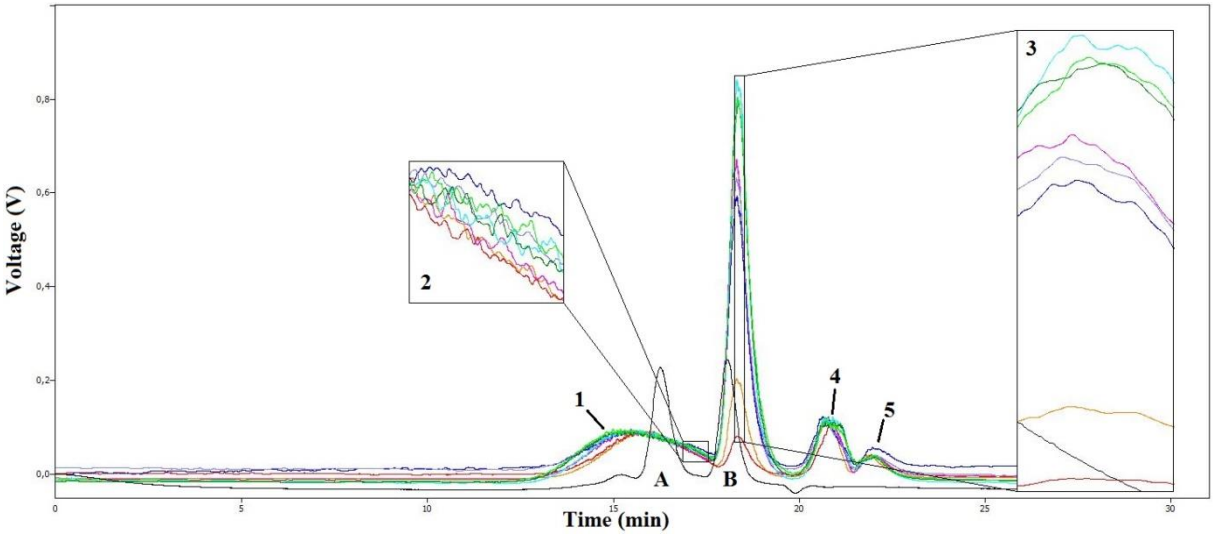

Figure IV.V. Chromatogram for coating of NPs with 20 mol% PEG44. Color codes: red = 3h, orange = 6h, pink = 21h, blue = 24h, purple = 27h, turquoise = 30h, dark green = 45h, and light green = 48h.

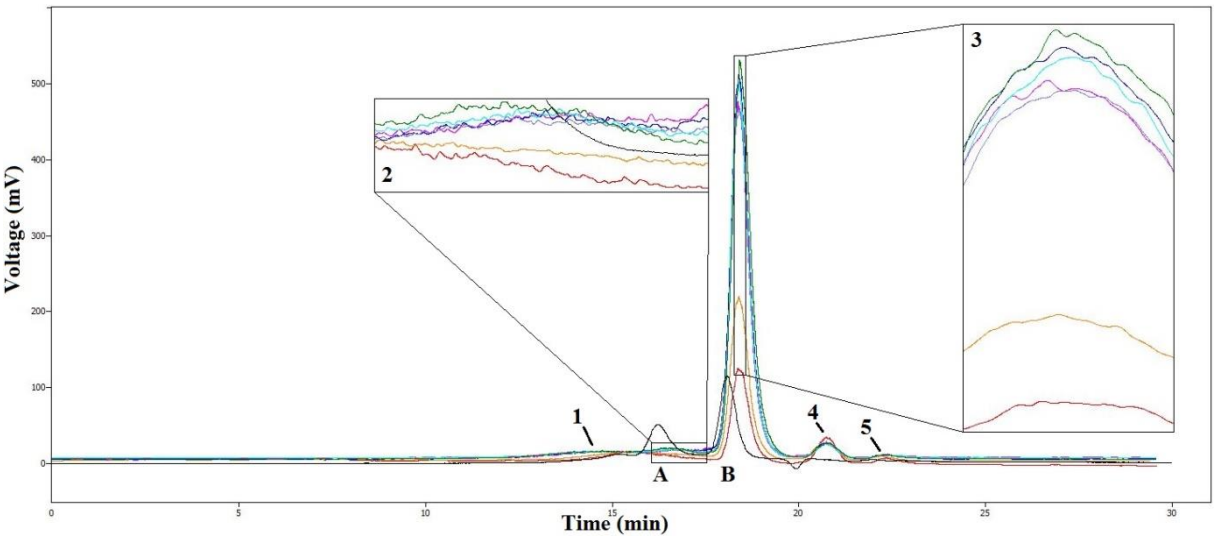

Figure IV.VI. Chromatogram for coating of NPs with 100 mol% PEG44. Color codes: red = 3h, orange = 6h, pink = 21h, blue = 24h, purple = 27h, turquoise = 30h, and dark green = 48h.

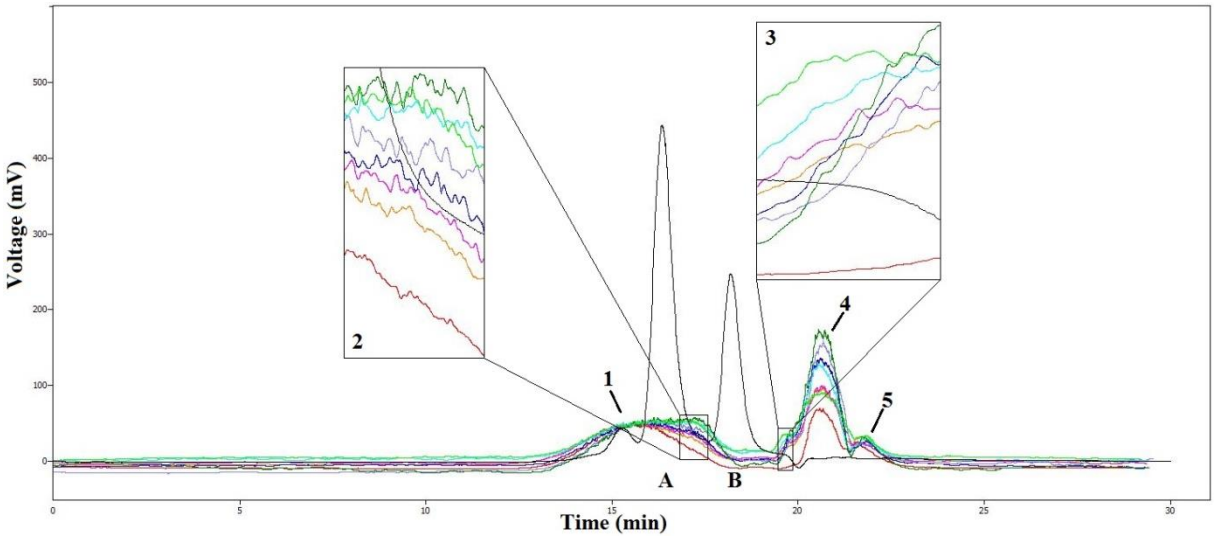

Figure IV.VII. Chromatogram for coating of NPs with 100 mol% CC. Color codes: red = 3h, orange = 6h, pink = 21h, blue = 24h, purple = 27h, turquoise = 30h, dark green = 45h, and light green = 48h.

Appendix V

GPC chromatograms for coated NPs after filtration

NP peaks in the ELSD curves have been labeled **1** and **2**, corresponding to **1)** NPs in the unfiltered batch (red curve) and **2)** NPs in the 100 kDa retentate of the filtered NP batch (green curve). The blue curve corresponds to the 100 kDa permeate (not collected for 100 mol% PEG21 coated NPs). The standard proteins, BSA (**A**) and myoglobin (**B**) correspond to the peaks in the curve for UV signal (black).

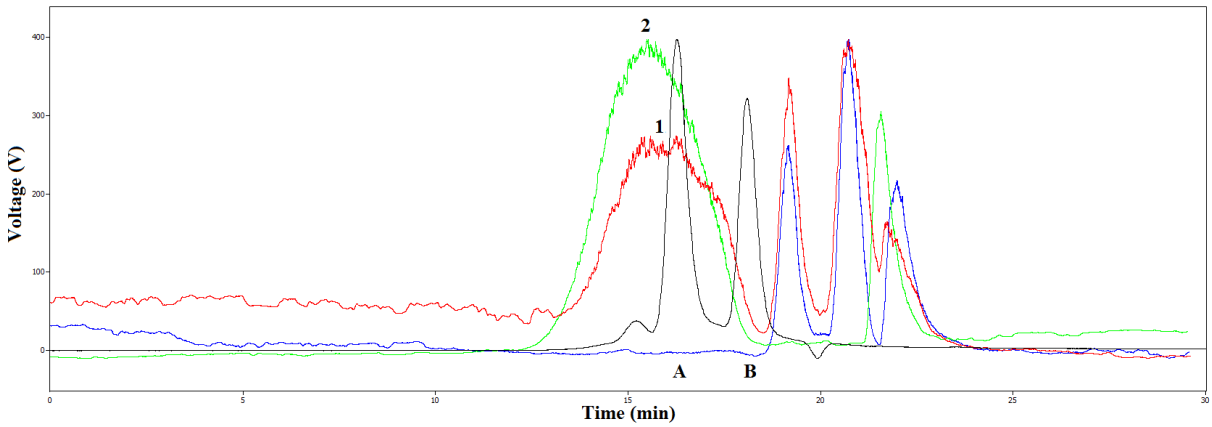

Figure V.I. Chromatogram for 20 mol% PEG6-9 coated NPs after 100 kDa filtration.

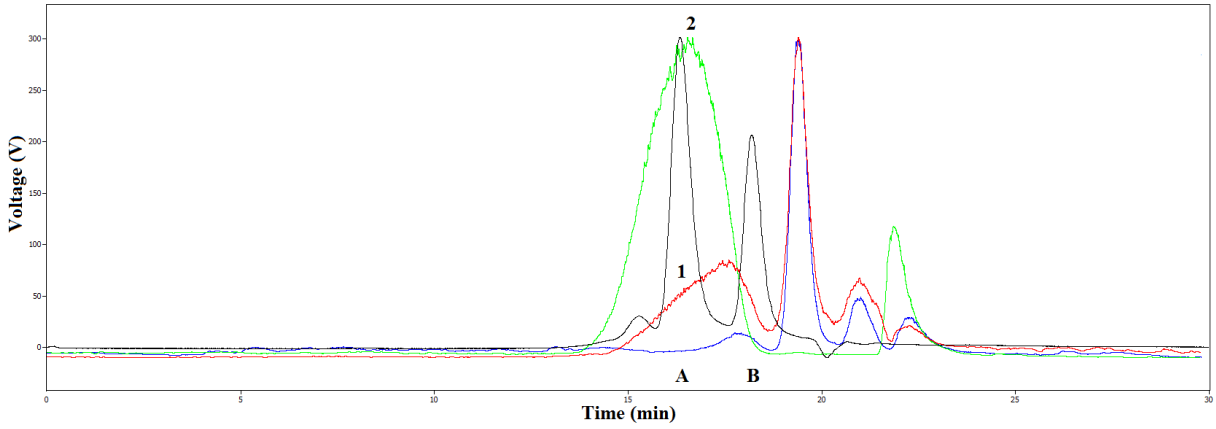

Figure V.II. Chromatogram for 100 mol% PEG6-9 coated NPs after 100 kDa filtration.

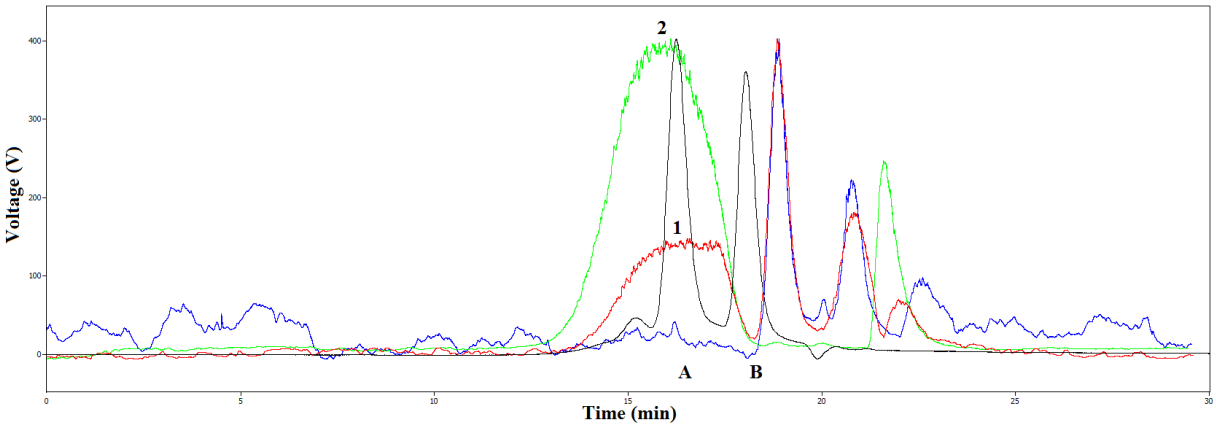

Figure V.III. Chromatogram for 20 mol% PEG21 coated NPs after 100 kDa filtration.

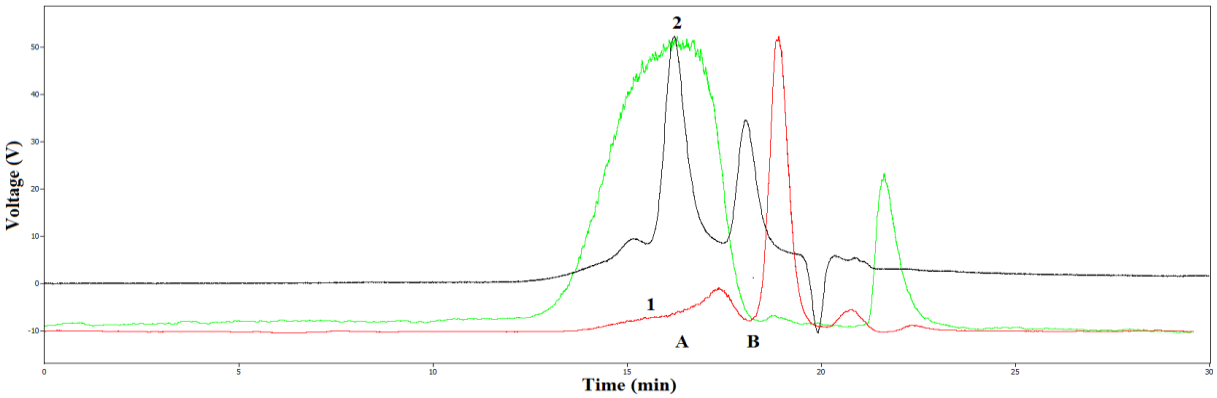

Figure V.IV. Chromatogram for 100 mol% PEG21 coated NPs after 100 kDa filtration.

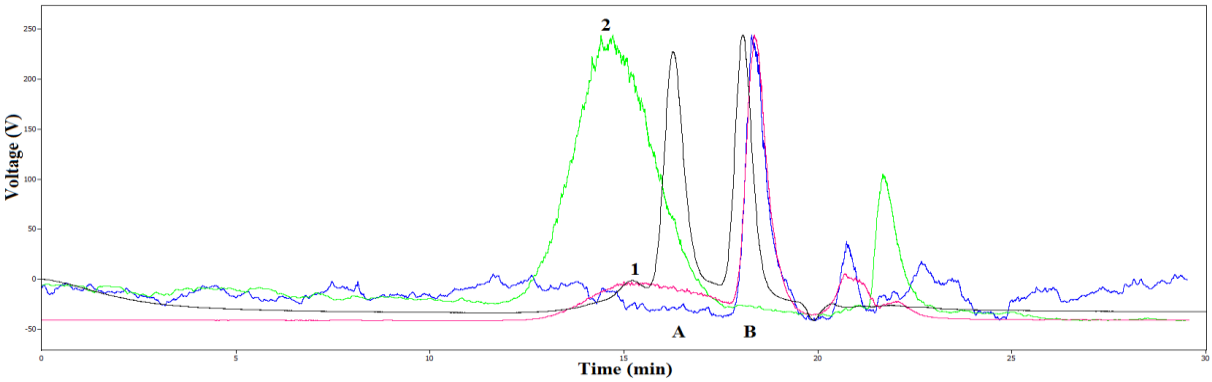

Figure V.V. Chromatogram for 20 mol% PEG44 coated NPs after 100 kDa filtration.

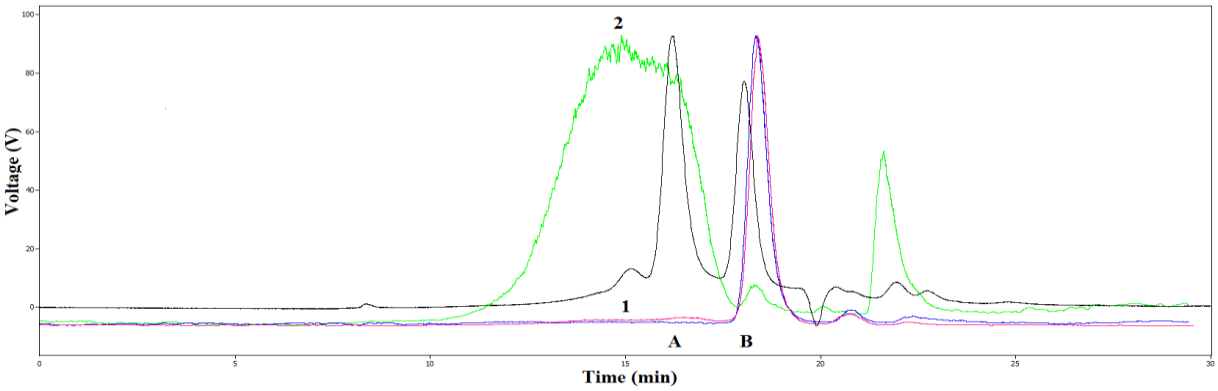

Figure V.VI. Chromatogram for 100 mol% PEG44 coated NPs after 100 kDa filtration.

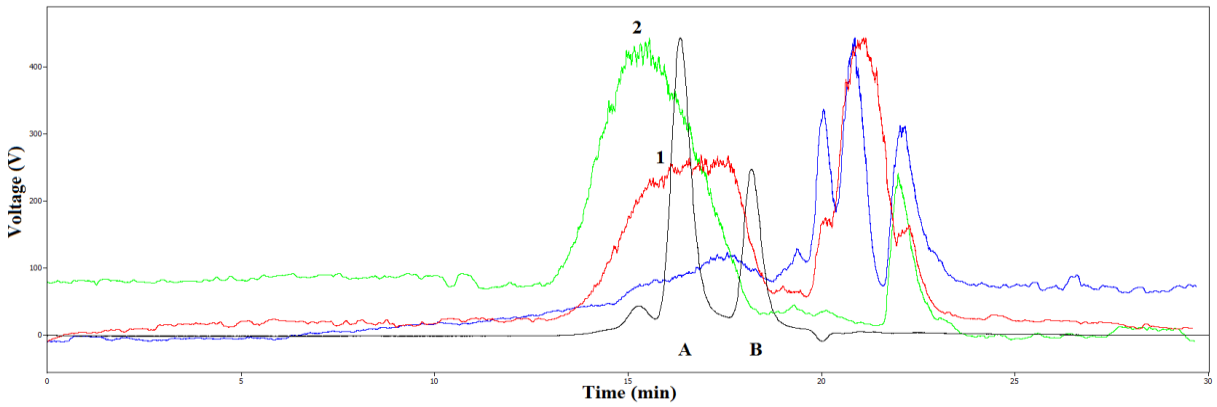

Figure V.VII. Chromatogram for 100 mol% CC coated NPs after 100 kDa filtration.

Appendix VI

GPC chromatograms for coated NPs after one month of storage

In each chromatogram, the black curve corresponds to the 100 kDa retentate, right after filtration, while the red curve corresponds to this retentate after one month of storage at room temperature. In the latter of these two curves, the very small peak to the right of the NP peak (marked with an arrow), corresponds to free coating monomers.

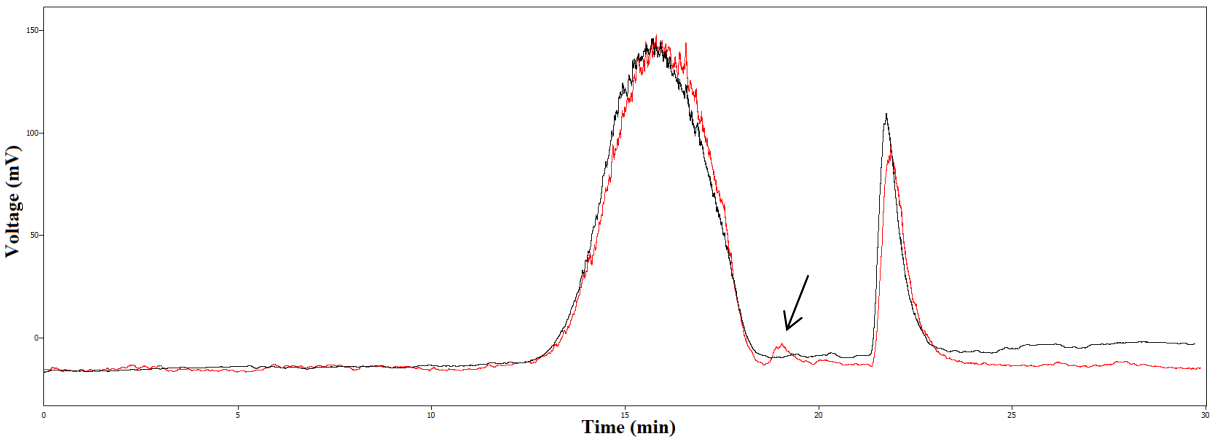

Figure VI.I. Chromatogram for 20 mol% PEG6-9 coated NPs after one month of storage.

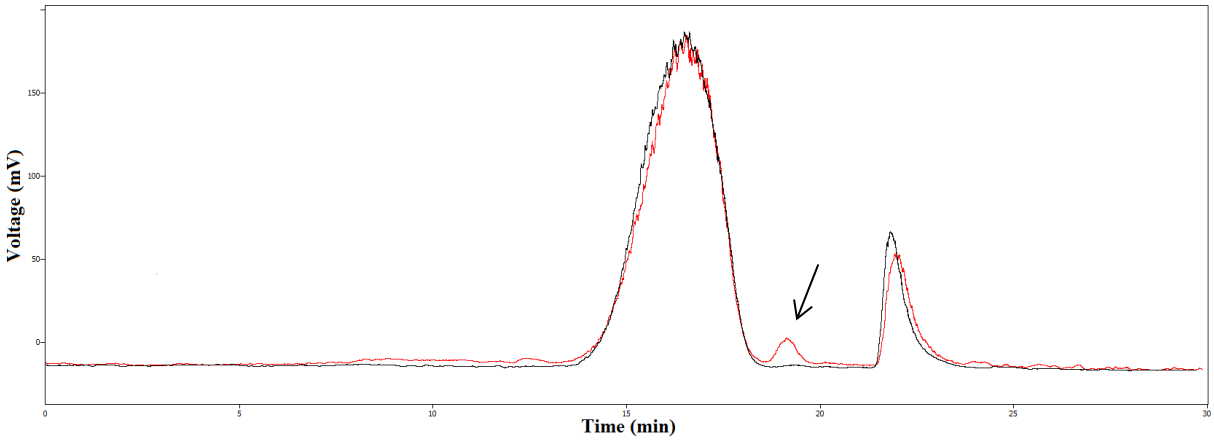

Figure VI.II. Chromatogram for 100 mol% PEG6-9 coated NPs after one month of storage.

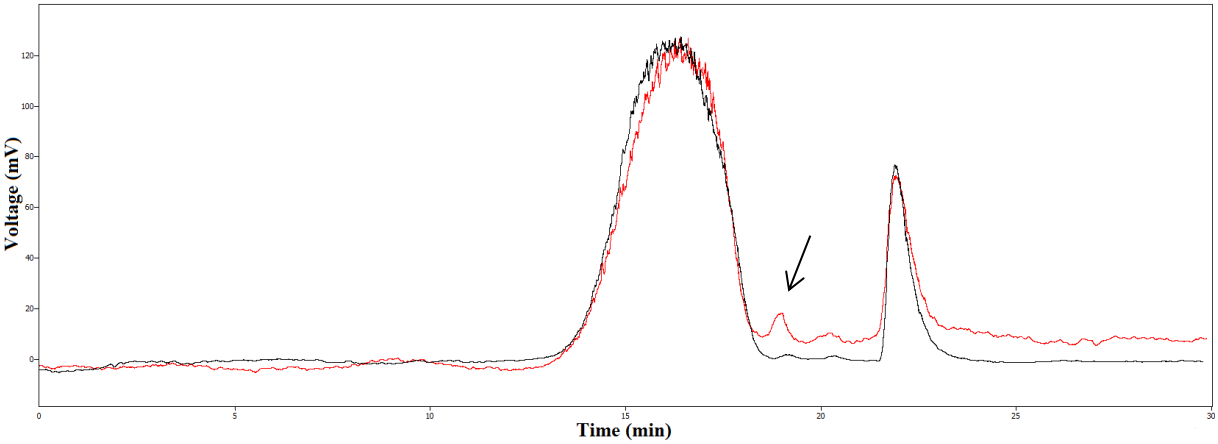

Figure VI.III. Chromatogram for 20 mol% PEG21 coated NPs after one month of storage.

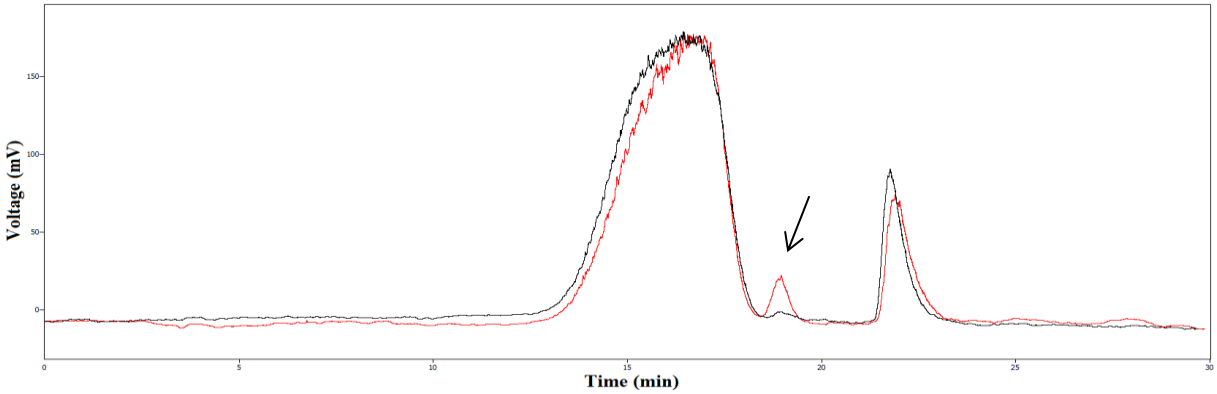

Figure VI.IV. Chromatogram for 100 mol% PEG21 coated NPs after one month of storage.

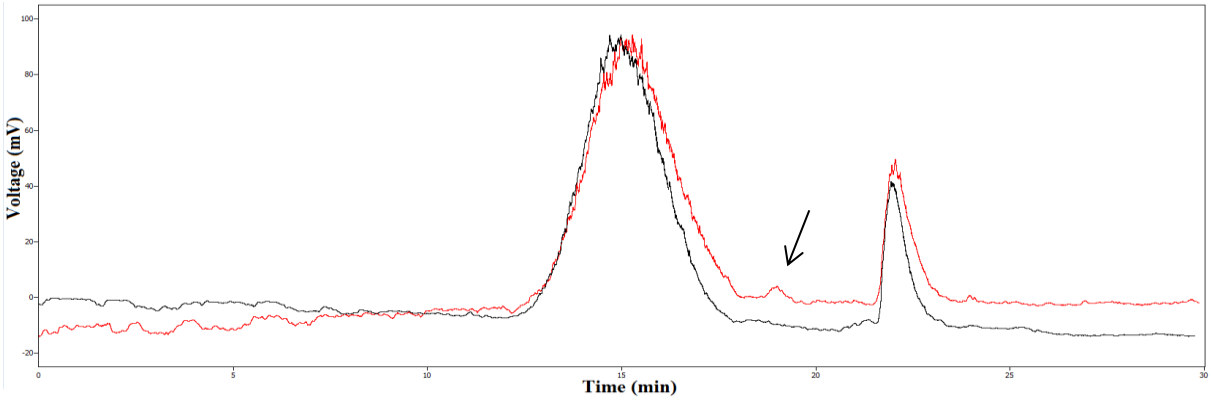

Figure VI.V. Chromatogram for 20 mol% PEG44 coated NPs after one month of storage.

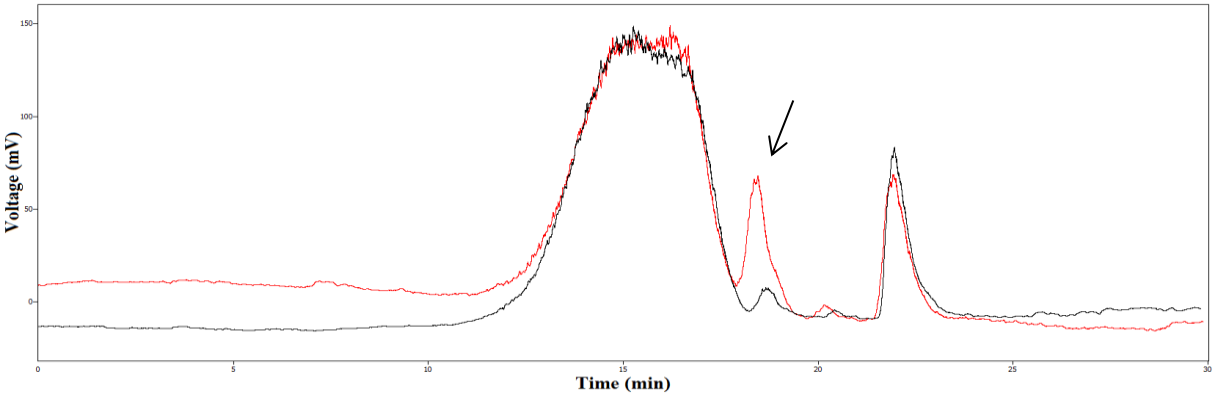

Figure VI.VI. Chromatogram for 100 mol% PEG44 coated NPs after one month of storage.

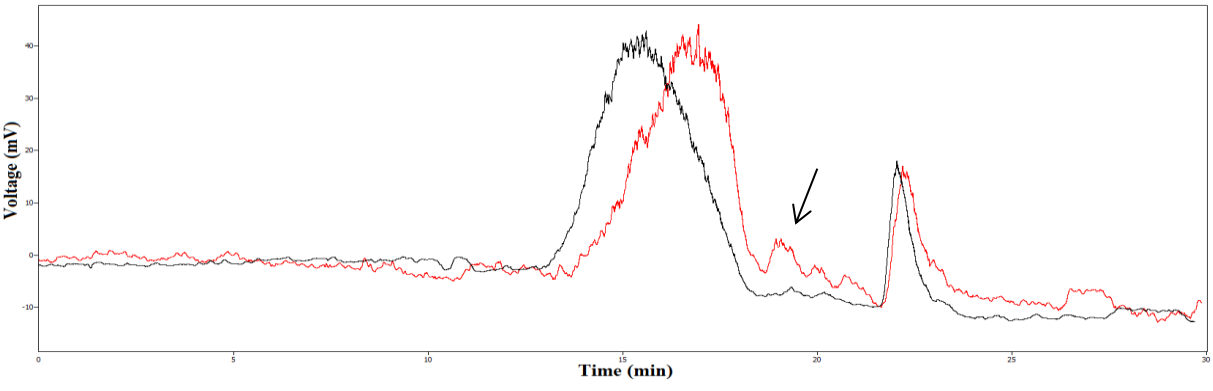

Figure VI.VII. Chromatogram for 100 mol% CC coated NPs after one month of storage.

Appendix VII

Hydrodynamic diameter (d_H) for NPs during coating and after filtration

d_H (measured with DLS) of each NP at each sampling time has been reported as the mode (highest bar) with a size range including size bars for which the mean volume percent ≥ 5.

Table VII.I. DLS results for 20 mol% PEG6-9 coated NPs.

	0h	3h	6h	21h	24h	27h	30h	45h	48h	After filtration
$d_{H.\ max}$ (nm)	10.1	7.5	10.1	8.7	13.5	10.1	8.7	8.7	11.7	10.1
$d_{H.\ min}$ (nm)	4.8	4.2	4.8	4.2	5.6	4.8	4.8	4.2	4.8	4.2
$d_{H.\ mode}$ (nm)	6.5	5.6	6.5	5.6	7.5	6.5	6.5	5.6	7.5	5.6

Table VII.II. DLS results for 100 mol% PEG6-9 coated NPs.

	0h	3h	18h	21h	24h	27h	48h	After filtration
$d_{H.\ max}$ (nm)	10.1	10.1	11.7	10.1	11.7	11.7	11.7	13.5
$d_{H.\ min}$ (nm)	4.8	4.8	4.8	4.8	5.6	4.8	4.8	5.6
$d_{H.\ mode}$ (nm)	6.5	6.5	7.5	6.5	7.5	6.5	6.5	8.7

Table VII.III. DLS results for 20 mol% PEG21 coated NPs.

	0h	3h	18h	21h	24h	27h	42h	45h	48h	After filtration
$d_{H.\ max}$ (nm)	10.1	10.1	10.1	8.7	8.7	7.5	7.5	8.7	10.1	11.7
$d_{H.\ min}$ (nm)	4.8	4.8	4.8	4.2	4.2	4.2	4.2	4.8	4.8	5.6
$d_{H.\ mode}$ (nm)	6.5	6.5	6.5	5.6	5.6	5.6	5.6	5.6	6.5	7.5

Table VII.IV. DLS results for 100 mol% PEG21 coated NPs.

	0h	6h	21h	24h	27h	30h	45h	48h	After filtration
$d_{H.\ max}$ (nm)	10.1	8.7	11.7	10.1	8.7	10.1	8.7	11.7	10.1
$d_{H.\ min}$ (nm)	4.8	4.2	4.8	4.8	4.2	4.2	3.6	4.8	4.2
$d_{H.\ mode}$ (nm)	6.5	5.6	7.0	6.5	5.6	5.6	5.6	6.5	6.5

Table VII.V. DLS results for 20 mol% PEG44 coated NPs.

	0h	3h	6h	21h	24h	27h	30h	45h	48h	After filtration
$d_{H.\ max}$ (nm)	10.1	8.7	8.7	7.5	8.7	11.7	8.7	10.1	11.7	11.7
$d_{H.\ min}$ (nm)	4.8	4.2	4.2	3.6	4.2	4.8	4.2	4.2	4.8	5.6
$d_{H.\ mode}$ (nm)	6.5	5.6	5.6	4.8	5.6	6.5	5.6	6.5	6.5	7.5

Table VII.VI. DLS results for 100 mol% PEG44 coated NPs.

	0h	3h	6h	21h	24h	27h	30h	48h	After filtration
$d_{H.\ max}$ (nm)	10.1	7.5	10.1	11.7	8.7	10.1	11.7	15.7	13.5
$d_{H.\ min}$ (nm)	4.8	3.6	4.2	4.8	4.2	4.8	4.2	4.2	6.5
$d_{H.\ mode}$ (nm)	6.5	4.8	6.5	7.0	5.6	6.5	6.5	7.5	8.7

Table VII.VII. DLS results for 100 mol% CC coated NPs.

	0h	3h	6h	21h	24h	27h	30h	45h	48h	After filtration
$d_{H.\ max}$ (nm)	10.1	8.7	8.7	13.5	11.7	11.7	13.5	8.7	8.7	21.04
$d_{H.\ min}$ (nm)	4.8	4.2	4.2	5.6	4.8	4.8	4.8	3.6	3.6	8.7
$d_{H.\ mode}$ (nm)	6.5	5.6	5.6	8.1	7.5	7.5	7.5	5.6	5.6	11.7

Appendix VIII

Coating degree

Derivation of equation for coating degree determination

$$[Si]_{PEG} = [Si]_{coated} - [Si]_{core}$$

$$\leftrightarrow$$

$$[Si]_{PEG} = [Si]_{coated} - \frac{[Si]_{bare}}{[P]_{bare}} \cdot [P]_{coated}$$

$$\leftrightarrow$$

$$\frac{[Si]_{PEG}}{[P]_{coated}} = \frac{[Si]_{coated}}{[P]_{coated}} - \frac{[Si]_{bare}}{[P]_{bare}}$$

$$\% \, coating = \frac{[Si]_{PEG}}{[NP \, monomer]} \cdot 100 \, \%$$

$$\leftrightarrow$$

$$\% \, coating = \frac{[Si]_{PEG}}{\frac{1}{2} \cdot [P]_{coated}} \cdot 100 \, \%$$

$$\leftrightarrow$$

$$\% \, coating = \frac{[Si]_{PEG}}{[P]_{coated}} \cdot 200 \, \%$$

$$\leftrightarrow$$

$$\% \, coating = \left(\frac{[Si]_{coated}}{[P]_{coated}} - \frac{[Si]_{bare}}{[P]_{bare}}\right) \cdot 200 \, \% \qquad \text{(Eq. A.II)}$$

where

$[Si]_{PEG}$ = Silicon from coating in coated nanoparticles
$[Si]_{core}$ = Silicon from core in coated nanoparticles
$[Si]_{coated}$ = Silicon from coating + core in coated nanoparticles
$[Si]_{bare}$ = Silicon in bare nanoparticles
$[P]_{coated}$ = Phosphorus from core in coated nanoparticles
$[P]_{bare}$ = Phosphorus from core in bare nanoparticles

Determination of real degree of coating

Table VIII.I. Concentrations of Si and P after 300 kDa ultrafiltration and 100 kDa diafiltration. For each NP batch, the coating degree has been calculated using Eq. A.II.

Nanoparticle	**$[Si]_{coated}$ (mM)**	**$[P]_{coated}$ (mM)**	**$[Si]_{bare}$ (mM)**	**$[P]_{bare}$ (mM)**	**Coating degree (mol%)**
$NP_{PEG6\text{-}9,\ 20\ mol\%}$	18.13	16.48	77.02	75.41	15.75
$NP_{PEG6\text{-}9,\ 100\ mol\%}$	15.53	13.42	77.02	75.41	27.18
$NP_{PEG21,\ 20\ mol\%}$	15.22	13.79	77.02	75.41	16.47
$NP_{PEG21,\ 100\ mol\%}$	18.94	15.88	77.02	75.41	34.27
$NP_{PEG44,\ 20\ mol\%}$	10.95	9.53	77.02	75.41	25.53
$NP_{PEG44,\ 100\ mol\%}$	22.47	15.08	77.02	75.41	93.74
$NP_{CC,\ 100\ mol\%}$	8.07	6.49	77.02	75.41	44.42

Appendix IX

Flow cytometry raw data

- **Scatter plots**

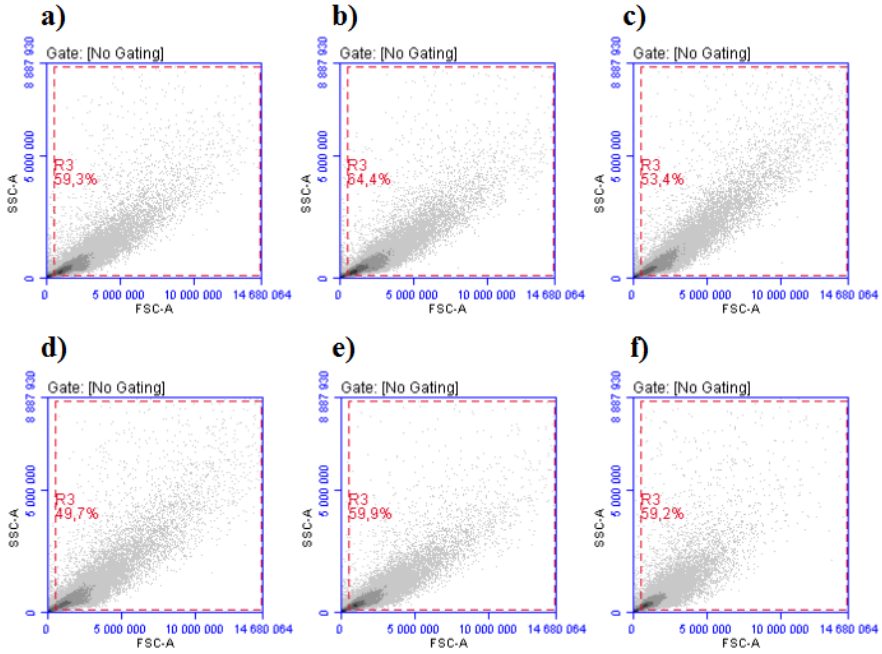

Figure IX.I. Scatter plots for Raw264.7 cells (Experiment 1) after incubation **a)** without NPs and without primary antibody, **b)** without NPs, but with primary antibody, **c)** with bare NPs, **d)** with 100 mol% PEG6-9 coated NPs, **e)** with 100 mol% PEG21 coated NPs and **f)** with 100 mol% PEG44 coated NPs. Primary antibody was included in **b-f**.

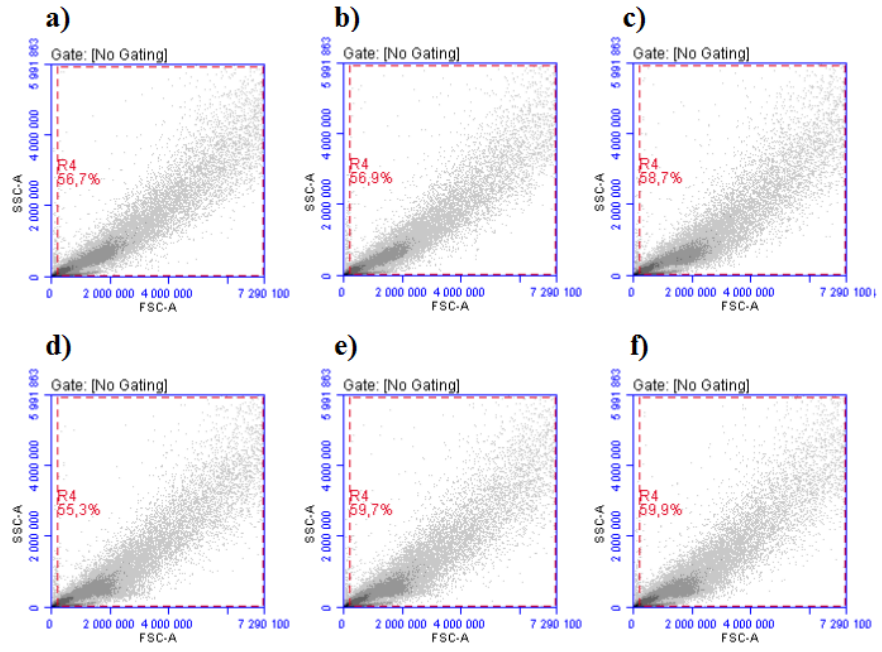

Figure IX.II. Scatter plots for Raw264.7 cells (Experiment 2) after incubation **a)** without NPs and without primary antibody, **b)** without NPs, but with primary antibody, **c)** with bare NPs, **d)** with 100 mol% PEG6-9 coated NPs, **e)** with 100 mol% PEG21 coated NPs and **f)** with 100 mol% PEG44 coated NPs. Primary antibody was included in **b-f**.

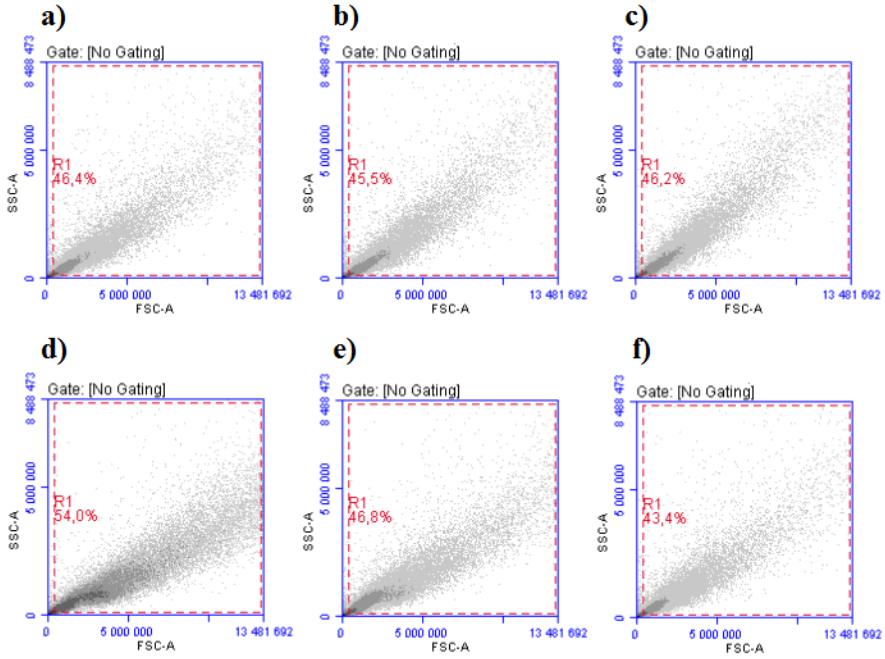

Figure IX.III. Scatter plots for HepG2 cells after incubation **a)** without NPs and without primary antibody, **b)** without NPs, but with primary antibody, **c)** with bare NPs, **d)** with 100 mol% PEG6-9 coated NPs, **e)** with 100 mol% PEG21 coated NPs and **f)** with 100 mol% PEG44 coated NPs. Primary antibody was included in **b-f**.

- **FL – plots**

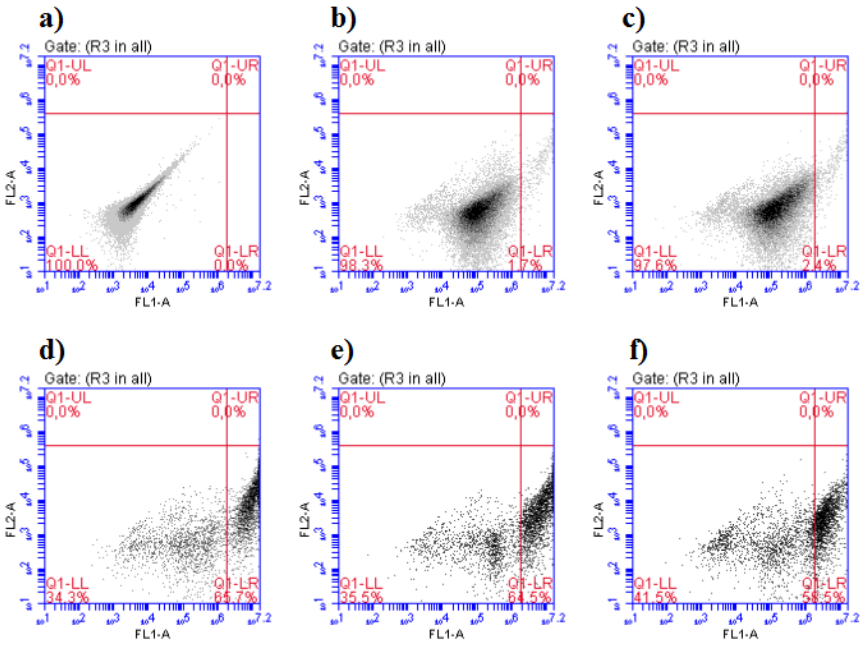

Figure IX.IV. FL-plots for Raw264.7 cells (Experiment 1) after incubation **a)** without NPs and without primary antibody, **b)** without NPs, but with primary antibody, **c)** with bare NPs, **d)** with 100 mol% PEG6-9 coated NPs, **e)** with 100 mol% PEG21 coated NPs and **f)** with 100 mol% PEG44 coated NPs. Primary antibody was included in **b-f**.

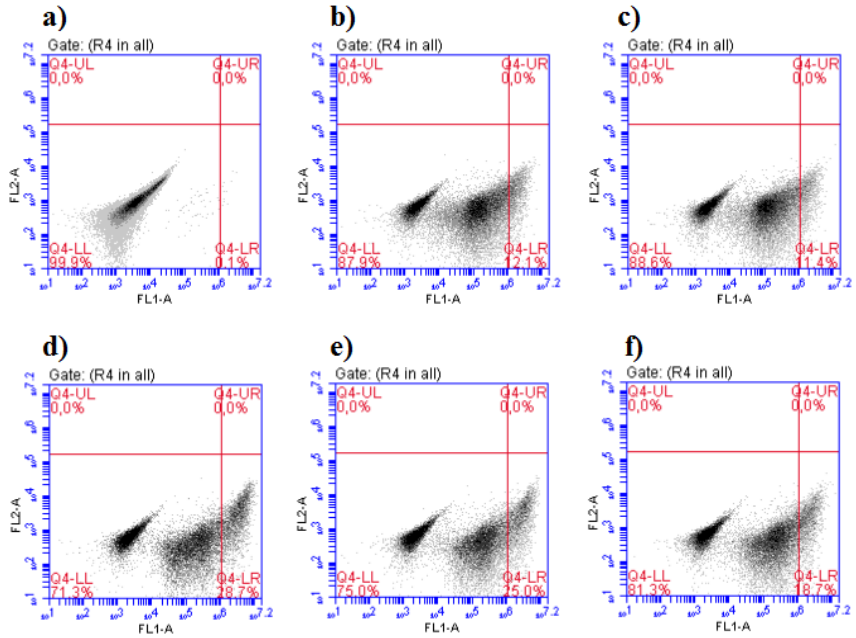

Figure IX.V. FL-plots for Raw264.7 cells (Experiment 2) after incubation **a)** without NPs and without primary antibody, **b)** without NPs, but with primary antibody, **c)** with bare NPs, **d)** with 100 mol% PEG6-9 coated NPs, **e)** with 100 mol% PEG21 coated NPs and **f)** with 100 mol% PEG44 coated NPs. Primary antibody was included in **b-f**.

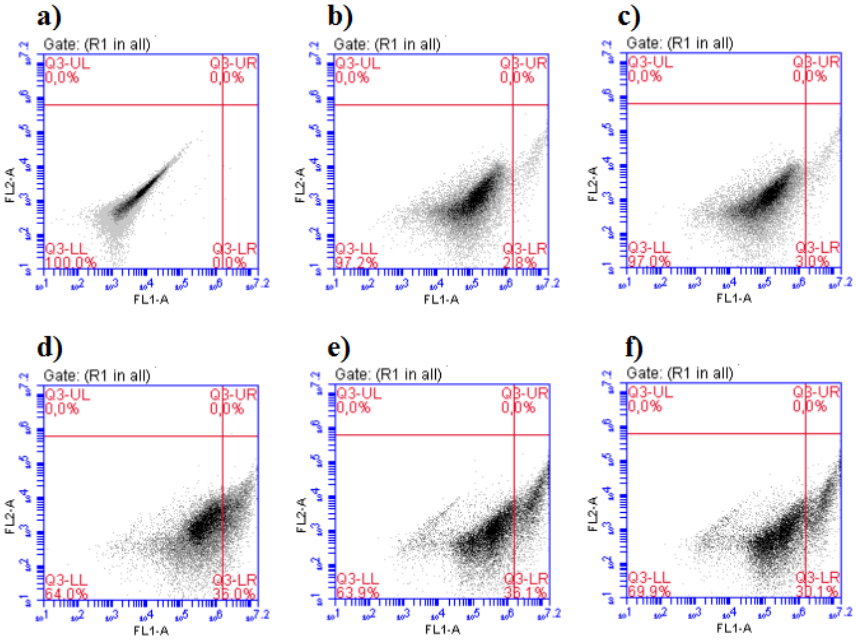

Figure IX.VI. FL-plots for HepG2 cells after incubation **a)** without NPs and without primary antibody, **b)** without NPs, but with primary antibody, **c)** with bare NPs, **d)** with 100 mol% PEG6-9 coated NPs, **e)** with 100 mol% PEG21 coated NPs and **f)** with 100 mol% PEG44 coated NPs. Primary antibody was included in **b-f**.

Table IX.I. % FL1-A positive cells in Figure IX.IV, Figure IX.V and Figure IX.VI. No subtraction of background.

% FL1-A positive cells in fig.	a	b	c	d	e	f
IX.IV	0.0	1.7	2.4	65.7	64.5	58.5
IX.V	0.1	12.1	11.4	28.7	25.0	18.7
IX.VI	0.0	2.8	3.0	36.0	36.1	30.1

Appendix X

Well saturation calculation

$Area_{well} = 0.32\ cm^2$

$d_{H,\ NP} = 6.5\ nm$

$Area_{NP} = (6.5 \cdot 10^{-7})^2\ cm^2 = 4.225 \cdot 10^{-13}\ cm^2/NP$

Maximum number of NPs/well = $0.32/4.225 \cdot 10^{-13} = 7.57 \cdot 10^{11}$ NPs

Number of NP monomers in a 6.5 nm NP = 306

Maximum number of NP monomers/well = $7.57 \cdot 10^{11} \cdot 306 = 2.32 \cdot 10^{14}$ NP monomers

Number of P/NP monomer = 2

Maximum number of P/well = $2 \cdot 2.32 \cdot 10^{14} = 4.64 \cdot 10^{14}$ P

$n_P = 4.64 \cdot 10^{14}/6.022 \cdot 10^{23} = 7.70 \cdot 10^{-10}$ mol

$V_{NP/well} = 100\ \mu l$

$c_{NP/well} = 7.70 \cdot 10^{-10}/10^{-4} = 7.7\ \mu M$

Above this concentration (at $V_{NP/well} = 100\ \mu l$), the surface will be saturated → response not linear

Appendix XI

Enlarged fluorescence microscopy pictures

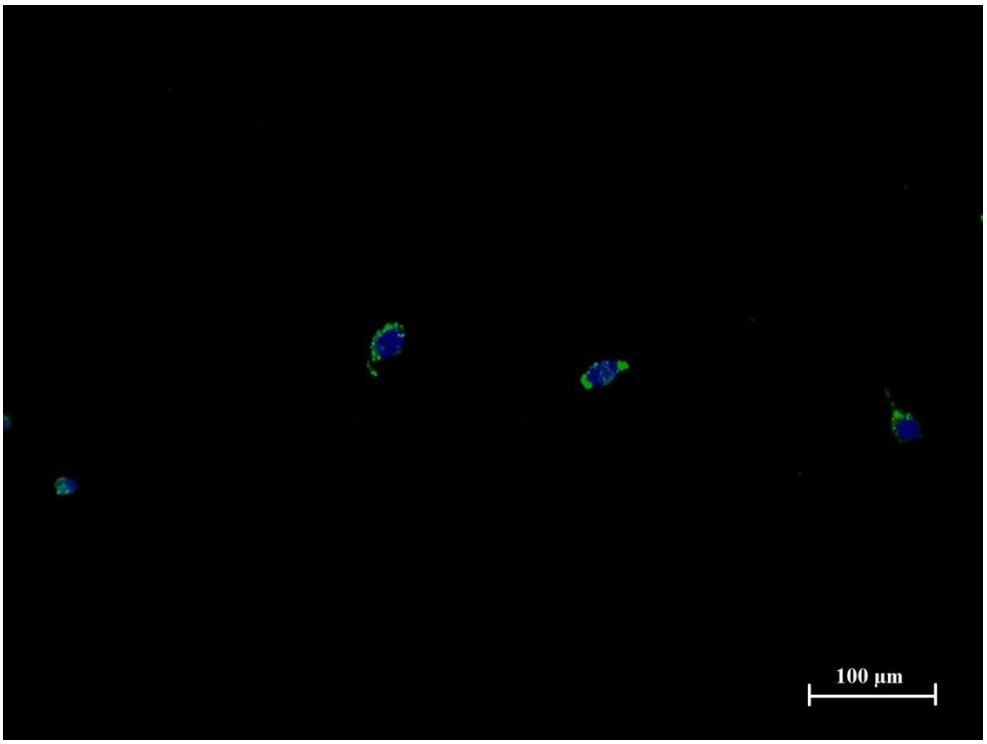

Figure XI.I. Merged picture for Raw264.7 cells incubated with 100 mol% PEG6-9 coated NPs (Experiment 1). Color codes: blue = fluorescence at 461 nm (DAPI staining), green = fluorescence at 519 nm (FITC staining). Light exposure times: DAPI = 1/20 s, FITC = 1/10 s

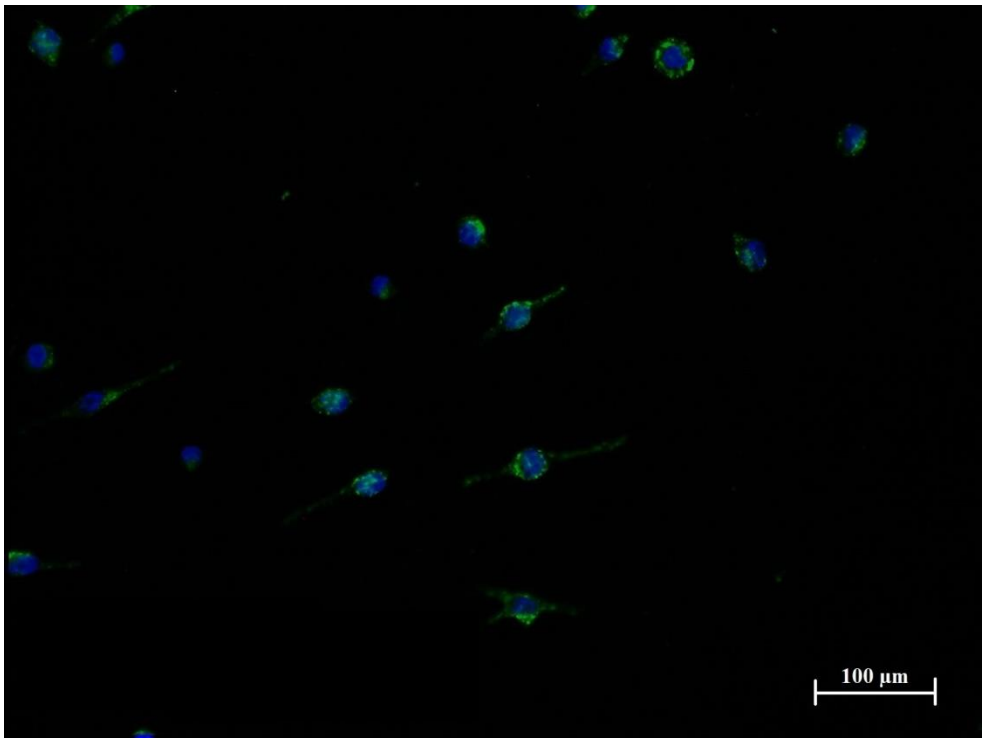

Figure XI.II. Merged picture for Raw264.7 cells incubated with 100 mol% PEG21 coated NPs (Experiment 1). Color codes: blue = fluorescence at 461 nm (DAPI staining), green = fluorescence at 519 nm (FITC staining). Light exposure times: DAPI = 1/20 s, FITC = 1/10 s

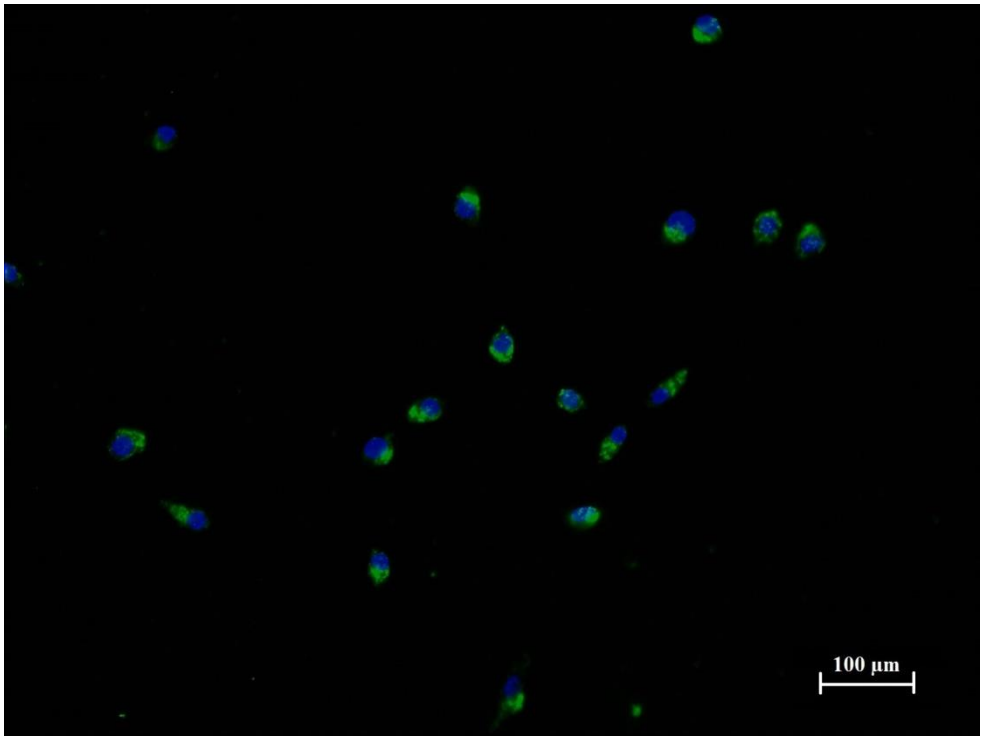

Figure XI.III. Merged picture for Raw264.7 cells incubated with 100 mol% PEG44 coated NPs (Experiment 1). Color codes: blue = fluorescence at 461 nm (DAPI staining), green = fluorescence at 519 nm (FITC staining). Light exposure times: DAPI = 1/20 s